2019-08-01

Computational Studies of High-Oxidation State Main-Group Metal Hydrocarbon C-H Functionalization

Clinton R. King
Brigham Young University

Computational Studies of High-Oxidation State Main-Group Metal Hydrocarbon C-H Functionalization

Clinton R. King

A dissertation submitted to the faculty of
Brigham Young University
in partial fulfillment of the requirements for the degree of

Doctor of Philosophy

Daniel H. Ess, Chair
Roger G. Harrison
David J. Michaelis
Kara J. Stowers

Department of Chemistry and Biochemistry

Brigham Young University

ABSTRACT

Computational Studies of High-Oxidation State Main-Group Metal Hydrocarbon C-H Functionalization

Clinton R. King
Department of Chemistry and Biochemistry, BYU
Doctor of Philosophy

High-oxidation state main-group metal complexes are potential alternatives to transition metals for electrophilic C-H functionalization reactions. However, there is little known about how selection of the p-block, main-group metal and ligand impact C-H activation and functionalization thermodynamics and reactivity. Chapter 2 reports density functional theory (DFT) calculations used to determine qualitative and quantitative features of C-H activation and metal-methyl functionalization energy landscapes for reaction between high-oxidation state $d^{10}s^0$ In^{III}, Tl^{III}, Sn^{IV}, and Pb^{IV} carboxylate complexes with methane. While the main-group metal influences the C-H activation barrier height in a periodic manner, the carboxylate ligand has a much larger quantitative impact on C-H activation with stabilized carboxylate anions inducing the lowest barriers. For metal-methyl reductive functionalization reactions, the barrier heights, are correlated to bond heterolysis energies as model two-electron reduction energies.

In Chapter 3, DFT calculations reveal that arene C-H functionalization by the p-block main-group metal complex $Tl^{III}(TFA)_3$ (TFA = trifluoroacetate) occurs by a C-H activation mechanism akin to transition metal-mediated C-H activation. For benzene, toluene, and xylenes a one-step C-H activation is preferred over electron transfer or proton-coupled electron transfer. The proposed C-H activation mechanism is consistent with calculation and comparison to experiment, of arene thallation rates, regioselectivity, and H/D kinetic isotope effects. For trimethyl and tetramethyl substituted arenes, electron transfer becomes the preferred pathway and thermodynamic and kinetic calculations correctly predict the experimentally reported electron transfer crossover region.

In Chapter 4, DFT calculations are used to understand the C-H oxidation reactions of methane and isobutane with Sb^VF_5. Sb^VF_5 is generally assumed to oxidize methane through a methanium-methyl cation mechanism. DFT calculations were used to examine methane oxidation by Sb^VF_5 in the presence of CO leading to the acylium cation, $[CH_3CO]^+$. While there is a low barrier for methane protonation by $[Sb^VF_6]^-[H]^+$ to give the $[Sb^VF_5]^-[CH_5]^+$ ion pair, H_2 dissociation is a relatively higher energy process, even with CO assistance, and so this protonation pathway is reversible. The C-H activation/σ-bond metathesis mechanism with formation of an Sb^V-Me intermediate is the lowest energy pathway examined. This pathway leads to $[CH_3CO]^+$ by functionalization of the Sb^V-Me intermediate by CO, and is consistent with no observation of H_2. In contrast to methane, due to the much lower carbocation hydride affinity, isobutane significantly favors hydride transfer to give *tert*-butyl carbocation with concomitant Sb^V to Sb^{III} reduction. In this mechanism, the resulting highly acidic Sb^V-H intermediate provides a route to H_2 through protonation of isobutane.

Keywords: main group, CH activation, indium, thallium, tin, lead, antimony

ACKNOWLEDGMENTS

The people that have helped me are almost too numerous to list here. I will focus on listing those people that have helped me in the last twelve years since I finished my master's thesis.

I would like to thank Nagwa Nahwar, a visiting scholar from Egypt, and Matthew Asplund for initially encouraging me to look into this program.

I would like to thank all the current and former members of the Ess research group including, but not limited to Deepa, Samantha, Jack, Doo, Ryan, Josh, Ashley, Ben, Nick, Steven, Madhu, Kyle, Jimmy, and many others.

I thank my collaborators at Hyconix and at the Scripps Research Institute.

I would like to thank my colleagues from my time at Snow College: Dan, Mark, Ted, Larry, Renee, Omel, Garth, Kevin, Scott, Kevin, and numerous others.

I would like to thank my current and former ecclesiastical leaders: Marlin, Brandon, Loren, Kim, and Troy.

I would also like to thank Scott, Logan, Ted, Jill, John, Sandy, Kris, and several other dear friends from the support group in Manti.

I would like to thank my parents, Robert and Renee King; and my in-laws, William and Diane Rosier, for their love and support. I would also like to thank mine and my wife's siblings and their spouses. (Thanks for the copy-editing, Dianna!) I would like to thank my children: Benjamin, Taylor, Alecia, and Samuel.

It is with strong emotions that I acknowledge my marvelously talented wife, April. She is the 'love of my life', and none of this would be possible without her prayers on my behalf.

I finally, gratefully, acknowledge my Savior, Jesus Christ, and my Heavenly Father.

TABLE OF CONTENTS

LIST OF FIGURES

LIST OF TABLES

LIST OF SCHEMES

Chapter 1:

A Brief Introduction to C-H Functionalization Reactions by Fifth and Sixth Period Main-Group Metal Complexes

1.1 Introduction

C-H functionalization occurs when a reaction or reaction sequence converts a carbon-hydrogen bond into a carbon-heteroatom bond, typically nitrogen, oxygen, or halogen. This term often describes a reaction where a transition metal center cleaves a hydrocarbon C-H bond (e.g. alkane, arene, or vinyl) resulting in organometallic M-C bond, rendering the carbon activated

(Scheme 1a).[1] The M-C bond is potentially more reactive than the C-H bond, which can be

subsequently functionalized into a carbon-heteroatom bond (Scheme 1-1a).

a) **C-H Functionalization by Organometallic Reactions**

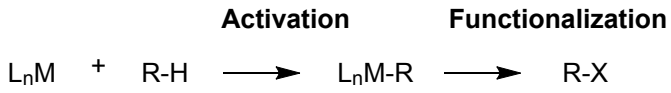

b) **Activation**

Oxidative Addition

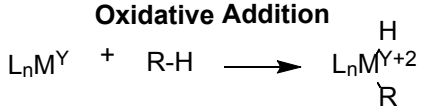

Electrophilic Activation

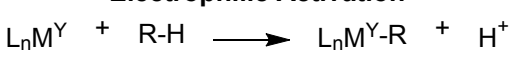

σ-Bond Metathesis

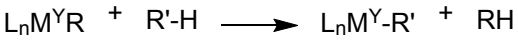

c) **Functionalization**

Functionalization by an External Nucleophile

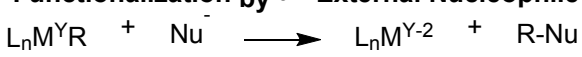

Elimination by an Internal Nucleophile

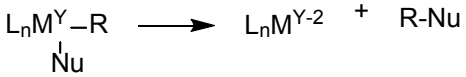

Scheme 1-1. a) C-H functionalization strategy by activation and M-R functionalization. b) Classes of metal-mediated C-H activation mechanisms. Oxidative addition is characterized by an increase in the formal oxidation state of the metal. Electrophilic activation is characterized by no change in the formal oxidation state, and by the deprotonation of the C-H bond. σ–Bond metathesis occurs when one M-R bond is exchanged for another.[1] c) Functionalization involves formal oxidation of the carbon, and can occur through nucleophilic displacement of the metal center. In this scheme, L represents a generic ligand, Y is the formal oxidation state of the metal, and R is a generic hydrocarbon.

There are several metal-mediated C-H activation mechanisms, and the most prominently described are oxidative addition (generally to low valent metals), electrophilic, and σ–bond metathesis. Scheme 1b illustrates that oxidative addition results in the formation M-C and M-H bond with a concomitant increase in the metal oxidation state by +2. In contrast, electrophilic C-H activation involves formation of a M-C bond and loss of a proton from the C-H bond, and typically there is no formal oxidation state change of the metal center. A σ-bond metathesis mechanism involves M-C bond exchange for the incoming C-H bond, and similar to electrophilic activation there is generally no change in the metal oxidation state.[1,2]

Metal-carbon functionalization (M-R functionalization, Scheme 1c) occurs when the metal center is displaced by a strong or weak heteroatom nucleophile. Similar to C-H activation, M-R functionalization can occur through a variety of mechanisms, but when coupled to organometallic C-H activation, this typically occurs through nucleophilic displacement of the metal where the nucleophile originates either from the metal coordination sphere or from the solution.[2]

C-H functionalization involving C-H activation and M-R functionalization (both stoichiometric and catalytic) are most prominent with transition-metal complexes that have $<d^{10}$ metal electron occupation. For example, Shilov described methane conversion to a mixture of methanol and methyl chloride.[3] The established mechanism is outlined in Scheme 1-2 for the

$[Pt^{II}Cl_4]^{-2}$ complex. First, the methane C-H bond undergoes electrophilic activation to generate a Pt-CH_3 intermediate. Second, $[Pt^{IV}Cl_6]^{-2}$ oxidizes the Pt^{II}-methyl complex to a Pt^{IV}-CH_3 complex. Third, the Pt^{IV}-CH_3 intermediate undergoes M-C bond functionalization.[1a,3]

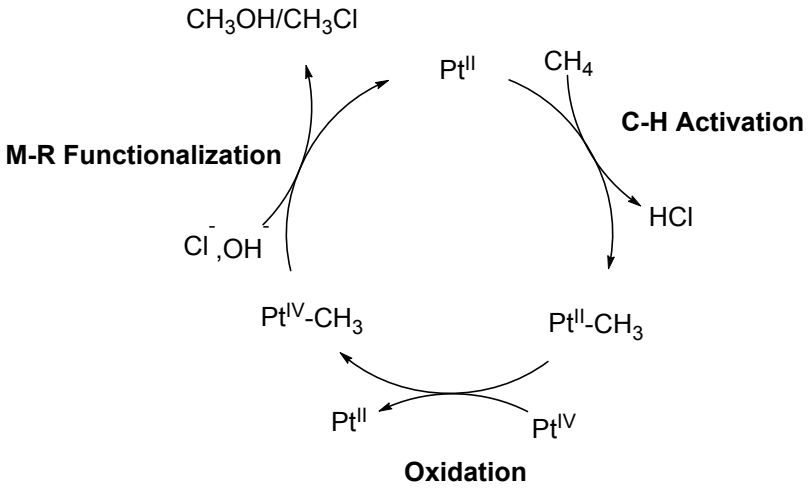

Scheme 1-2. The Shilov cycle, which selectively oxidizes methane to a mixture of methanol and methyl chloride. The exact coordination sphere of the Pt complexes are unknown, but in water the possible ligands are Cl^-, OH^-, and H_2O.[1a,3]

The Shilov reaction requires stoichiometric Pt^{IV} oxidant, and Periana[4] later developed a bipyridine Pt^{II} catalyst that efficiently and selectively oxidizes methane to methyl bisulfate in concentrated sulfuric acid using the sulfuric acid as the stoichiometric oxidant (Scheme 1-3). The bipyridine ligand stabilizes the catalyst against deactivation and maintains its solubility in concentrated sulfuric acid. Based on computations and experiments, Scheme 1-3b presents details of intermediates in the methane to methyl bisulfate catalytic cycle.[4a] While there are key differences of this catalytic cycle compared to the Shilov reaction, the basic C-H activation and M-R functionalization steps are similar.

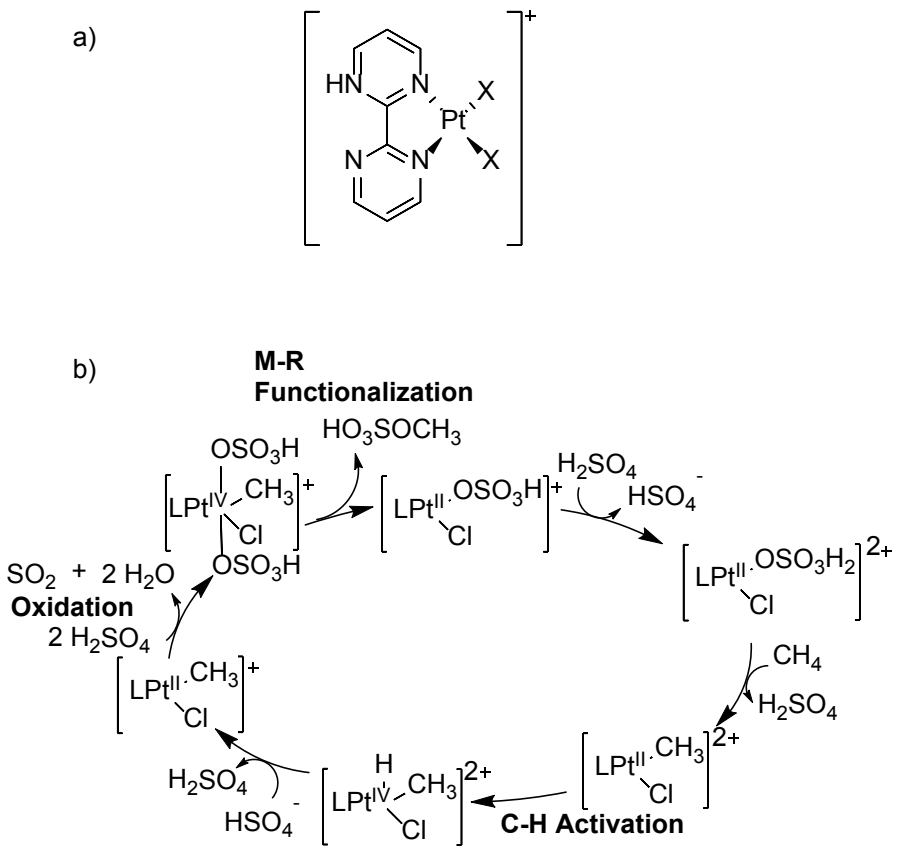

Scheme 1-3. a) Periana's methane C-H functionalization catalyst.[4b] b) Generalized catalytic cycle for the Periana Pt catalyst.[4a]

While the majority of C-H bond functionalization promoters and catalysts developed use transition-metal centers, as exemplified by the Shilov and Periana reactions, an alternative strategy that is the subject of this computational chemistry dissertation is the use of fifth and sixth period main-group metals to induce C-H activation and M-R functionalization. While fifth and sixth period main-group metals with d^{10} or $d^{10}s^2$ metal electron occupation (e.g. Ag-I and Au-Bi) are typically viewed as Lewis acids, oxidants, additives, and transmetalation reagents, they are not commonly proposed to be involved in reactions forming organometallic intermediates with M-C bonds. While it has previously been proposed that fifth and sixth period main-group metals can mechanistically act similar to transition metals, these reactions generally involve low oxidation

states (e.g. Sn^{II}).[5] This dissertation is concerned with high oxidation state main-group metal reactions, in particular reactions that involve C-H activation and M-R functionalization.

1 H																	2 He
3 Li	4 Be											5 B	6 C	7 N	8 O	9 F	10 Ne
11 Na	12 Mg											13 Al	14 Si	15 P	16 S	17 Cl	18 Ar
19 K	20 Ca	21 Sc	22 Ti	23 V	24 Cr	25 Mn	26 Fe	27 Co	28 Ni	29 Cu	30 Zn	31 Ga	32 Ge	33 As	34 Se	35 Br	36 Kr
37 Rb	38 Sr	39 Y	40 Zr	41 Nb	42 Mo	43 Tc	44 Ru	45 Rh	46 Pd	47 Ag	48 Cd	49 In	50 Sn	51 Sb	52 Te	53 I	54 Xe
55 Cs	56 Ba	57-71	72 Hf	73 Ta	74 W	75 Re	76 Os	77 Ir	78 Pt	79 Au	80 Hg	81 Tl	82 Pb	83 Bi	84 Po	85 At	86 Rn
87 Fr	88 Ra	89-103	104 Rf	105 Db	106 Sg	107 Bh	108 Hs	109 Mt	110 Ds	111 Rg	112 Cn	113 Nh	114 Fl	115 Mc	116 Lv	117 Ts	118 Og

57 La	58 Ce	59 Pr	60 Nd	61 Pm	62 Sm	63 Eu	64 Gd	65 Tb	66 Dy	67 Ho	68 Er	69 Tm	70 Yb	71 Lu
89 Ac	90 Th	91 Pa	92 U	93 Np	94 Pu	95 Am	96 Cm	97 Bk	98 Cf	99 Es	100 Fm	101 Md	102 No	103 Lr

Figure 1-1. The elements discussed in this work are outlined in red.

1.2 Brief Overview of Some Experimental and Computational Studies of Main-Group Metal C-H Activation and Functionalization.

In 1993, Periana reported that mercuric bisulfate (Hg^{II} has d^{10} electronic occupation) in concentrated sulfuric acid catalyzes the functionalization of methane to methyl bisulfate.[6] Scheme 1-4 shows the originally proposed catalytic cycle, which consists of electrophilic C-H activation followed by M-R functionalization and then SO_3-induced Hg oxidation. Consistent with the electrophilic activation description, experiments with methyl bisulfate showed that the rate of its oxidation is significantly slower than the rate of reaction with methane.

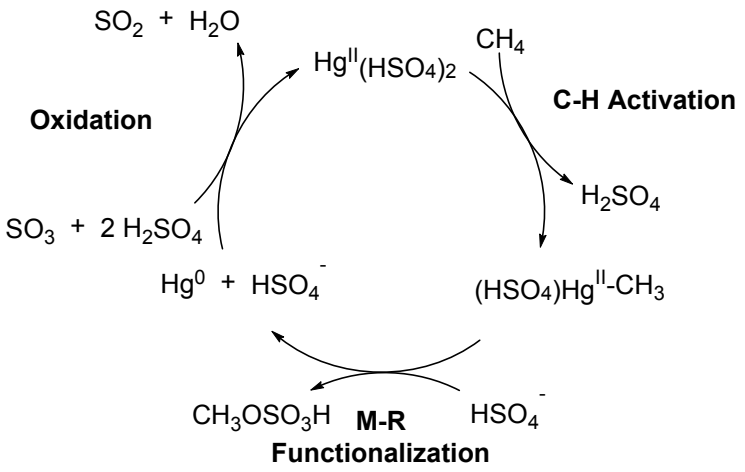

Scheme 1-4. Proposed catalytic cycle for mercury catalyzed oxidation of methane in sulfuric acid.

Our group recently examined this Hg-catalyzed methane C-H functionalization reaction using a combination of continuum and explicit-continuum solvent methods.[6b] Calculation of the thermodynamics of several intermediates, including methyl radical, methane radical cation, and various mercury(I) structures, suggest that these intermediates are endergonic unlikely to induce C-H functionalization. Overall, this DFT study provided evidence that mercury catalyzes methane C-H functionalization through an electrophilic C-H activation step rather than an open-shell radical mechanism.

While the ability of gold to activate the C-H bonds in arenes was reported as early as the 1930's, in 2004, Periana described methane to methyl bisulfate C-H functionalization using a gold catalyst in concentrated sulfuric acid.[7] NMR experiments demonstrated that hydrogen/deuterium (H/D) exchange between methane and solvent occurs, which is consistent with a reversible C-H activation step. Calculations by Goddard suggests that both Au^{I} and Au^{III} can induce methane C-H activation. The d^{10} Au^{I} C-H activation route was proposed to occur through an oxidative addition transition state while the Au^{III} d^{8} C-H activation was proposed to occur through an electrophilic activation transition state (Scheme 1-5). While Au^{I} can induce C-H activation, M-R

functionalization was proposed to occur after oxidation through an Au^{III}-CH_3 intermediate, which occurs through an external nucleophilic substitution mechanism.

Oxidative Addition to Au^{I}

a) 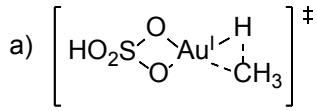

Electrophilic Activation by Au^{III}

b) 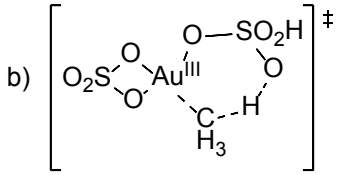

Functionalization of Au^{III}-CH_3

c) 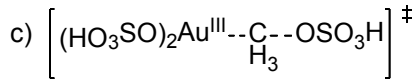

Scheme 1-5. a) Oxidative addition transitions state between methane to $Au^{I}(HSO_4)$. b) Electrophilic activation transition state between methane and $Au^{III}(SO_4)(HSO_4)$. c) Au^{III}-CH_3 functionalization transition state.[7]

Periana and co-workers reported that the main-group element iodine catalyzes conversion of methane to methyl bisulfate in 2% oleum at 195 °C with sulfur trioxide as the terminal oxidant.[8a] It was demonstrated that $I_2^+[Sb_2F_{11}]^-$ reacts stoichiometrically with methane at 50 °C while other oxidized iodine compounds (e.g. $I^{III}O(HSO_4)$, $I^{V}O_2(HSO_4)$, and $I^{III}(HSO_4)_3$) do not. Because experiments with radical scavengers and initiators demonstrated that radical pathways are unlikely, the proposed catalytic cycle is shown in Scheme 1-6. In this cycle, the I_2^+ cation is assumed to react with methane through an electrophilic step, although it is unclear if this involves C-H activation. Related to the Periana reaction, in 65% oleum, Gang et al.[8b] found that KI, NaI, CH_3I, I_2O_5, KIO_3, and KIO_4 were also able to catalyze methane C-H functionalization to methyl bisulfate. Their study, along with a later study by Jarosińska et al.,[8c] in 25% oleum, which determined an

initial rate dependence of ½ for I_2, suggests that the active catalyst is mononuclear in iodine. Davico reported gas phase experiments and gas-phase electronic structure calculations that indicated that I^+ reacts more readily with methane than I_2^+,[8d] which led to the proposal of an I^I cation as the active catalyst.

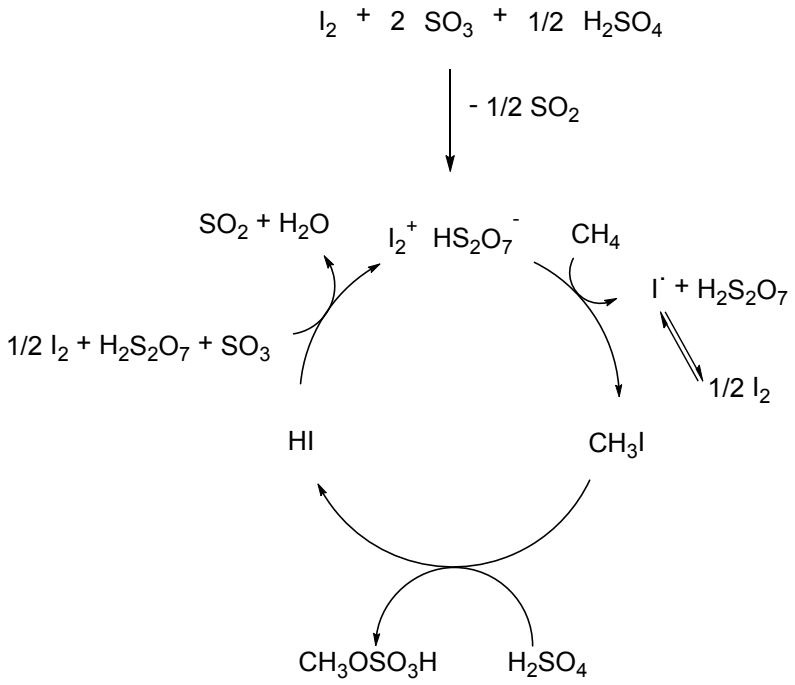

Scheme 1-6. Catalytic cycle proposed by Periana et al for the iodine catalyzed oxidation of methane to methyl bisulfate in 2% oleum.[8a]

Tl^{III} salts have been used to promote several different types of organic transformations,[9] and one of the most prominent uses is to electrophilically activate arenes. Tl^{III} carboxylates were first reported to react regioselectively with arenes in 1969 by McKillop et al. (Scheme 1-7a,b) (see also chapter 3 and the references therein).[10] The thallated arenes are typically iodo-substituted in a subsequent step for use in aryl coupling reactions often catalyzed by palladium.[11] McKillop suggested that $Tl^{III}(TFA)_3$ (TFA = trifluoroacetate) in trifluoroacetic acid (TFAH) reacts by the classic two step S_EAr mechanism (Scheme 7c), but Kochi[12] proposed that Tl^{III} oxidizes arenes

through an open-shell charge transfer complex (Scheme 1-7d) which can either collapse to a Wheland intermediate or dissociate fully. This open-shell mechanism rationalized EPR observation of certain arene radicals in reactions with Tl^{III} and the formation of bi-aryl products from the same arene reactants. However, until recently, the mechanism of Tl^{III} carboxylates with arenes had not been examined computationally, and this is the subject of Chapter 3.

Thallium-mediated Functionalization of Benzene

a) 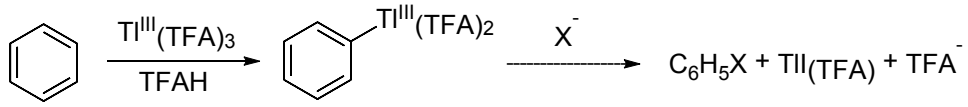

Results reported by McKillop et al[10]

b) 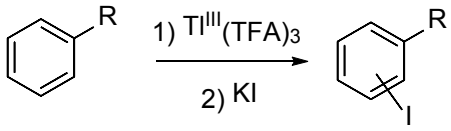

R = Me; o : m : p = 9% : 4% : 87%
R = CO_2H; o : m : p = 95% : 5% : 0%
R = CO_2Me; o : m : p = 95% : 5% : 0%

Proposed S_EAr Mechanism for Arene Thallation

c) 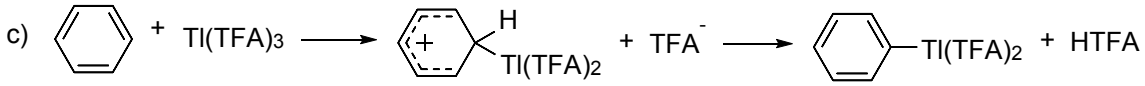

Wheland intermediate

Mechanism for Arene Thallation Proposed by Lau and Kochi[12]

d) 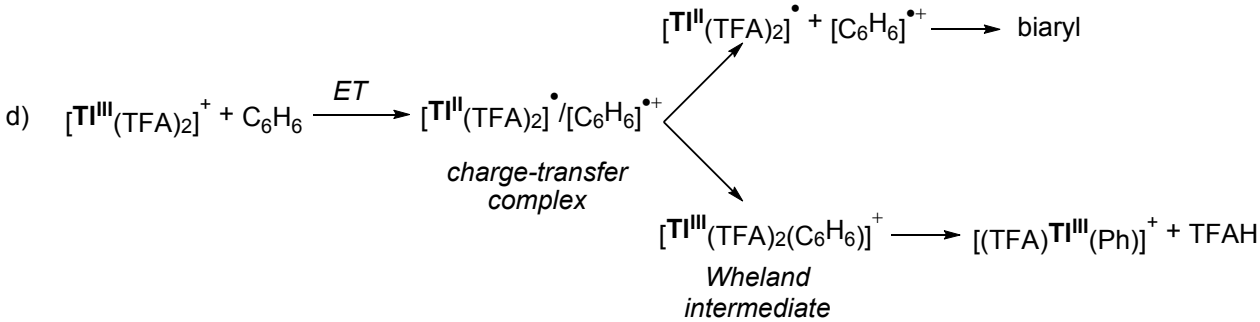

Scheme 1-7. a) $Tl^{III}(TFA)_3$ mediated C-H functionalization of arenes. b) McKillop[10] reported the regioselectivity of this reaction. c) S_EAr mechanism for arene thallation. d) Mechanism proposed by Kochi.[12]

Similar to the reaction of Tl^{III} with arenes discussed above, in 2001 Grushin[13] reported that $Sn^{IV}(TFA)_4$ reacts with arenes to form stable stannylated aryl compounds. Upon oxidation of $Sn^{II}O$ in trifluoroacetic acid and hydrogen peroxide, the presumably Sn^{IV} containing mixture was allowed to react with benzene or *p*-xylene. X-ray structures of the resulting Sn-aryl products revealed a tetranuclear Sn trifluoroacetate complex with two oxo bridges and two aryl groups. The Sn^{IV} mixture was able to catalyze rapid H/D exchange in deuterated toluene and TFAH at the meta and para positions, but only slowly at the ortho position, and not at all at the methyl position.

Recently, experiments by the Periana group and DFT calculations by the Ess group demonstrated that main-group Tl^{III} and Pb^{IV} carboxylates in carboxylic acids can induce alkane C-H functionalization through an electrophilic C-H activation and M-R functionalization mechanism.[14] While Periana had previously reported that Tl^{III} was capable of methane C-H functionalization in sulfuric acid,[6a] this recent study showed that $Tl^{III}(TFA)_3$ and $Pb^{IV}(TFA)_4$ both selectively induce C-H functionalization of methane, ethane, and propane to their corresponding esters in trifluoroacetic acid (Scheme 1-8a). Experiments suggest radical pathways are not likely, and DFT calculations strongly support the operation of a closed shell C-H activation and M-R functionalization mechanism. In contrast to reactions of transition metals with alkanes, with main group metals, the rate limiting step appears to be C-H bond cleavage, not alkane coordination.

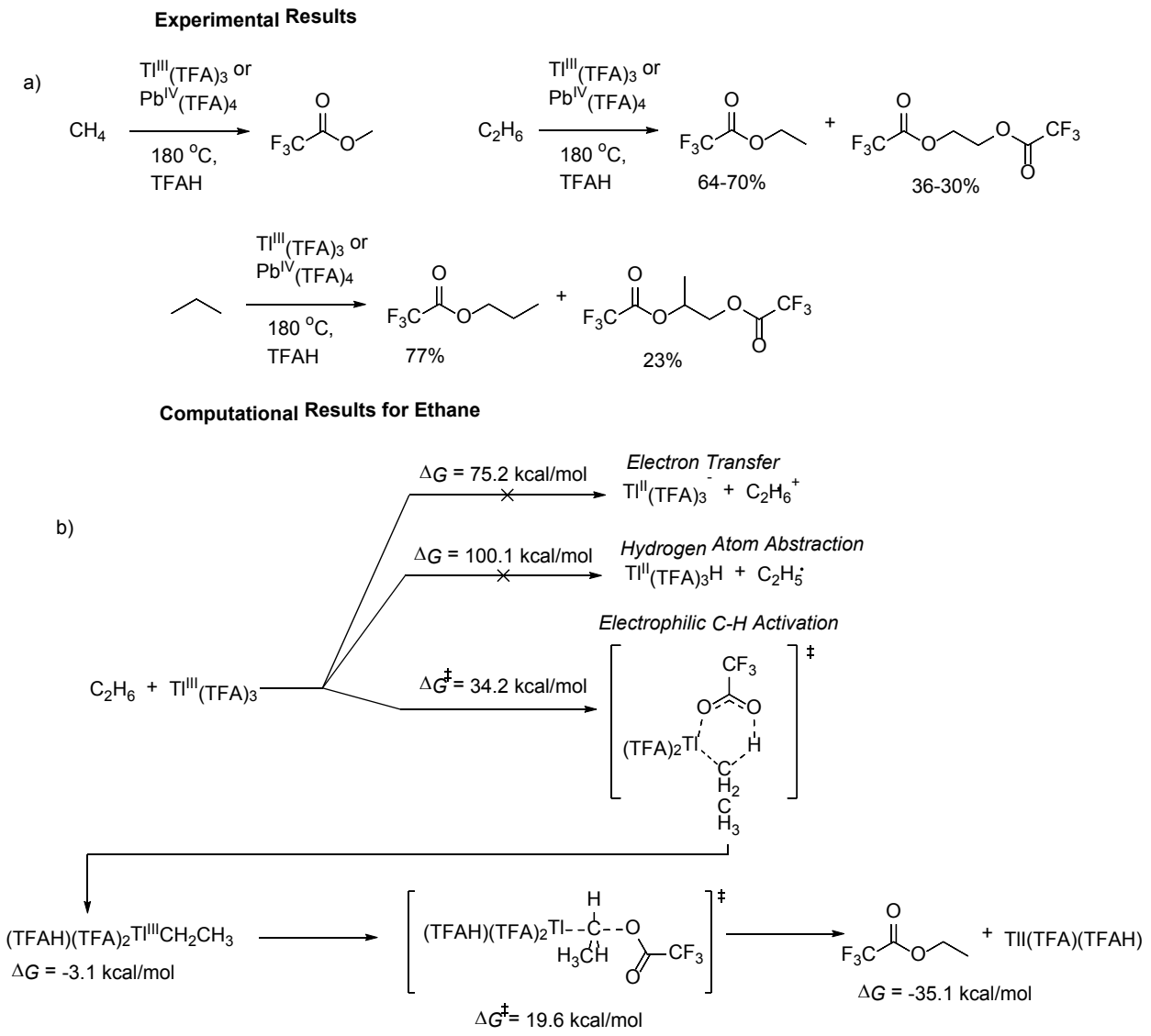

Scheme 1-8. a) Overview of experimental results for the reactions of propane, ethane, and methane with $Tl^{III}(TFA)_3$ or $Pb^{IV}(TFA)_4$. Overall reaction yields ranged between 55% and 95%. b) Computational analysis of possible reactions of $Tl^{III}(TFA)_3$ with ethane. Outline of the proposed electrophilic C-H transition state follow by S_N2-type functionalization.[14]

Scheme 1-8b shows some of the results of the computational analysis of the reaction of methane with $Tl(TFA)_3$ in TFAH. The open-shell pathways of electron transfer (ET) and hydrogen atom abstraction (HAT) were ruled out due to unfavorable thermodynamics. While a direct functionalization/oxidation pathway through a concerted hydride abstraction/methyl cation

capture transition state was examined, it was found to be much higher barrier in energy than that computed for electrophilic C-H activation . Calculations also showed that methyl trifluoroacetate is kinetically protected from reacting with $Tl^{III}(TFA)_3$, since the barrier for a second C-H activation step of the methyl group is >10 kcal/mol higher that the initial C-H activation barrier. The barrier to functionalization, modeled through an S_N2-type transition state was significantly lower than the initial C-H activation step, which potentially explains the lack of observed H/D exchange.

1.3 Computational Methods

In this work, density functional theory (DFT) as implemented in Gaussian 09[15] was used to find and compute the energies of structures that correspond to stationary points (local energy minima or transition states) for possible reaction pathways.

In DFT,[16] energies are derived as eigenvalues of a 'functional', F, that acts on the electron density, ρ. The functional can be split into kinetic energy (T_S), nuclear-electron potential energy (E_{NE}), electron-electron potential (J), and an electron exchange-correlation term (E_{XC}):

$$E_{DFT}[\rho] = F[\rho] = T_S[\rho] + E_{NE}[\rho] + J[\rho] + E_{XC}[\rho]$$

Within the Born-Oppenheimer approximation, E_{NE} is a constant. In order to simplify the computations, Kohn-Sham theory uses a Hamiltonian operator for a fictitious system of non-interacting electrons which has a density identical to the real system. T_S and J may be calculated exactly for the non-interacting system by representing the electrons as occupying orbitals. E_{XC} then contains terms that describe corrections to the kinetic energy due to the interaction of the electrons in the real system and non-classical corrections to the electron-electron potential energy. The exact form of E_{XC} remains unknown, but numerous approximate forms have been proposed. The DFT energy may be solved for iteratively, in a manner similar to Hartree-Fock theory.

In this work, the Minnesota 06 functional,[17] developed by the Truhlar group of the University of Minnesota, is primarily used to approximate E_{XC}. It is a hybrid meta-GGA (generalized gradient approximation) functional with 35 parameters and 27% HF exchange. This functional was parametrized for main-group thermochemistry, transition metal thermochemistry, organometallics, and non-covalent interactions.

In Gaussian 09, the Kohn-Sham orbitals are computed using Gaussian basis sets. For structure optimization and vibrational frequency calculations, the 6-31G(d,p) and 6-31+G(d,p) basis sets of Pople[18] were used for atoms in rows 1-3, and the basis sets of Hay and Wadt,[19] combined with a larger ECP, were used for the heavier elements (In, Sn, Sb, Tl, and Pb). Based on these smaller basis set geometries, SCF energies were calculated with the Def2TZVPpd basis sets developed by the Ahlrichs group.[20] These basis sets contain a triple zeta expansion for valance orbitals, and incorporate diffuse and polarization functions and have seen extensive use in both wave-function and DFT methods. For the atoms of the fifth and sixth periods, these basis sets have been augmented with an effective core potential (ECP) that replaces electrons up through the *n-2* principle quantum number with analytic functions.[21] The effective core potential takes into account scalar relativistic effects on the core electrons and transmits them, through orthogonality requirements, to the valance electrons. The primary effect is to contract the valance *s* orbitals, making them of significantly lower energy than might otherwise be expected.

Throughout the succeeding chapters, both enthalpy (*H*) and Gibbs free energy (*G*) are computed according to the following formulae:

$$G = E + E_{ZPE} + U + nRT - TS + \Delta G_{solv}$$

$$H = E + E_{ZPE} + U + nRT + \Delta G_{solv}$$

The first term, E, is the electronic energy determined from the electron density through an SCF (self-consistent field) process; E_{ZPE}, U, nRT, and TS terms were calculated within Gaussian 09 using the standard ideal gas partition functions for system translations and rotations and using the harmonic oscillator partition function for internal motions as determined from a frequency calculation at the given stationary state.[22] The solvation terms were determined using the self-consistent reaction field method which surrounds the system in a polarizable dielectric medium. The solvent model[23] was parameterized to reproduce free energies of solvation, hence the solvation term is given as a free energy of solvation.

1.4 Overview of Chapters

Chapters 2-4 are computational chemistry studies using DFT calculations to examine the reaction mechanisms and reactivity of main-group metals with alkanes and arenes leading to C-H functionalization. Chapter 2 discusses reactivity predictions using the electrophilic C-H activation and M-R functionalization for high oxidations state In^{III}, Sn^{IV}, Tl^{III}, and Pb^{IV} carboxylate complexes. Chapter 2 was previously published as doi: 10.1021/acs.organomet.8b00418.[24] Chapter 3 provides computational evidence that benzene undergoes an electrophilic C-H activation mechanism for reaction with Tl^{III} carboxylates. Chapter 3 was previously published as doi: 10.1021/acs.organomet.6b00475.[25] Chapter 4 uses DFT calculations to examine the possibility that SbF_5 induces electrophilic C-H activation with light alkanes.

1.5 References

1. a) Shilov, A. E.; Shul'pin, G. B. "Activation of C-H Bonds by Metal Complexes." *Chem. Rev.* **1997**, *97*, 2879-2932. b) Goldman, A. S.; Goldberg, K. I. ACS Symposium Series 885, Activation and Functionalization of C-H Bonds, Organometallic C-H Bond Activation: An

Introduction, **2004**, 1-43. c) Bates, R. Introduction. In Organic Synthesis Using Transition Metals, Second Edition. Wiley: **2012**; pg 1-20.

2. a) Hashiguchi, B. G.; Bischof, S. M.; Konnick, M. M.; Periana, R. A. "Designing Catalysts for Functionalization of Unactivated C–H Bonds Based on the CH Activation Reaction." *Acc. Chem. Res.* **2012,** *45*, 885–898. b) Crabtree, R. H. "Organometallic alkane C-H activation." *J. Organomet. Chem.* **2004,** *689,* 4083–4091. c) Crabtree, R. H. "Alkane C–H activation and functionalization with homogeneous transition metal catalysts: a century of progress – a new millennium in prospect." *J. Chem. Soc., Dalton Trans.* **2001** *17* 2437–2450. d) Wencel-Delord, J.; Dröge, T.; Liu, F.; Glorius, F. "Towards Mild Metal-Catalyzed C–H Bond Activation." *Chem. Soc. Rev.* **2011** *40* 4740–4761.
3. Lersch, M.; Tilset, M. "Mechanistic Aspects of C-H Activation by Pt Complexes.", *Chem. Rev*. **2005**, *105,* 2471-2526.
4. a) Mironov, O. A.; Bischof, S. M.; Konnick, M. M.; Hashiguchi, B. G.; Ziatdinov, V. R.; Goddard, W. A.; Ahlquist, M.; Periana, R. A., "Using Reduced Catalysts for Oxidation Reactions: Mechanistic Studies of the "Periana-Catalytica" System for CH_4 Oxidation." *J. Am. Chem. Soc.* **2013**, *135*, 14644-14658. b) Periana, R. A.; Taube, D. J.; Gamble, S.; Taube, H.; Satoh, T.; Fujii, H. "Platinum Catalysts for the High-Yield Oxidation of Methane to a Methanol Derivative." *Science* **1998**, *280*, 560–564.
5. a) Chu, T. Nikonov, G. I. "Oxidative Addition and Reductive Elimination at Main-Group Element Centers." *Chem Rev* **2018**, *118*, 3608-3680. b) Power, P. P. "Main-group elements as transition metals." *Nature* **2010** *463*, 171-177.
6. a) Periana, R. A.; Taube, D. J.; Evitt, E. R.; Loffler, D. G.; Wentrcek, P. R.; Voss, G.; Masuda, T., "A mercury-catalyzed, high-yield system for the oxidation of methane to methanol." *Science* **1993**, *259*, 340-343. b) Fuller, J. T.; Butler, S.; Devarajan, D.; Jacobs, A.; Hashiguchi, B. G.; Konnick, M. M.; Goddard, W. A.; Gonzales, J.; Periana, R. A.; Ess, D. H., "Catalytic Mechanism and Efficiency of Methane Oxidation by Hg(II) in Sulfuric Acid and Comparison to Radical Initiated Conditions." *ACS Catal.* **2016**, *6*, 4312-4322. c) Gunsalus, N. J.; Koppaka, A.; Park, S. H.; Bischof, S. M.; Hashiguchi, B. G.; Periana, R. A., "Homogeneous Functionalization of Methane." *Chem. Rev.* **2017**, *117*, 8521-8573.
7. a) Kharasch, M. S.; Isbell, H. S., "The Chemistry of Organic Gold Compounds. III. Direct Introduction of Gold Into The Aromatic Nucleus (Preliminary Communication)." *J. Am. Chem. Soc.* **1931**, *53*, 3053-3059. b) Jones, C. J.; Taube, D.; Ziatdinov, V. R.; Periana, R. A.; Nielsen, R. J.; Oxgaard, J.; Goddard, W. A., III, "Selective oxidation of methane to methanol catalyzed,

with C-H activation, by homogeneous, cationic gold." *Angew. Chem., Int. Ed.* **2004**, *43*, 4626-4629. c) Boorman, T. C.; Larrosa, I., "Gold-mediated C-H bond functionalization." *Chem. Soc. Rev.* **2011**, *40*, 1910-1925.

8. a) Periana, R. A.; Mirinov, O.; Taube, D. J.; Gamble, S., "High yield conversion of methane to methyl bisulfate catalyzed by iodine cations." *Chem. Comm.* **2002**, 2376-2377. b) Gang, X.; Zhu, Y.; Birch, H.; Hjuler, H. A.; Bjerrum, N. J., "Iodine as catalyst for the direct oxidation of methane to methyl sulfates in oleum." *App. Catal. A* **2004**, *261*, 91-98. c) Jarosińska, M.; Lubkowski, K.; Sośnicki, J. G.; Michalkiewicz, B., "Application of Halogens as Catalysts of CH_4 Esterification." *Catal. Let.* **2008**, *126*, 407-412. d) Davico, G. E., "The Conversion of Methane to Methanol: A Reaction Catalyzed by I^+ or I_2^+?" *J. Phys. Chem. A* **2005**, *109*, 3433-3437.

9. Dagorne, S.; Bellemin-Laponnaz, S.: Group 13 Metal-Mediated Organic Reactions. In The Group 13 Metals Aluminium, Gallium, Indium and Thallium: Chemical Patterns and Peculiarities; John Wiley & Sons, Ltd, **2011**; pp 654-700.

10. a) McKillop, A.; Fowler, J. S.; Zelesko, M. J.; Hunt, J. D.; Taylor, E. C.; McGillivray, G., "Thallium in organic synthesis. IX. Facile thallation of aromatic compounds with thallium(III) trifluoroacetate (1, 2)." *Tet. Lett.* **1969**, *10*, 2423-2426. b) McKillop, A.; Hunt, J. D.; Zelesko, M. J.; Fowler, J. S.; Taylor, E. C.; McGillivray, G.; Kienzle, F., "Thallium in organic synthesis. XXII. Electrophilic aromatic thallation using thallium(III) trifluoroacetate. Simple synthesis of aromatic iodides." *J. Am. Chem. Soc.* **1971**, *93*, 4841-4844. Taylor, E. C.; Kienzle, F.; Robey, R. L.; McKillop, A.; Hunt, J. D., "Thallium in organic synthesis. XXIII. Electrophilic aromatic thallation. Kinetics and applications to orientation control in the synthesis of aromatic iodides." *J. Am. Chem. Soc.* **1971**, *93*, 4845-4850.

11. Bates, R., Coupling Reactions. In Organic Synthesis Using Transition Metals, Second Edition. Wiley: **2012**; pg 37-40.

12. Lau, W.; Kochi, J. K., "Kinetics and mechanism of aromatic thallation. Identification and proof of competing electrophilic and electron-transfer pathways." *J. Am. Chem. Soc.* **1984**, *106*, 7100-12. Lau, W.; Kochi, J. K., "Arene activation with mercury(II) and thallium(III) electrophiles. Mechanistic relevance of charge-transfer transitions in π-complexes as intermediates." *J. Am. Chem. Soc.* **1986**, *108*, 6720-32.

13. Grushin, Vladimir V.; Marshall, William J.; Thorn, David L., "Electrophilic Stannylation of Arenes: A New S_EAr Reaction." *Adv. Synth. & Catal.* **2001**, *343*, 433-438.

14. a) Hashiguchi, B. G.; Konnick, M. M.; Bischof, S. M.; Gustafson, S. J.; Devarajan, D.; Gunsalus, N.; Ess, D. H.; Periana, R. A., "Main-Group Compounds Selectively Oxidize Mixtures of Methane, Ethane, and Propane to Alcohol Esters." *Science* **2014**, *343*, 1232. b) Konnick, M. M.; Bischof, S. M.; Yousufuddin, M.; Hashiguchi, B. G.; Ess, D. H.; Periana, R. A., "A Mechanistic Change Results in 100 Times Faster CH Functionalization for Ethane versus Methane by a Homogeneous Pt Catalyst." *J. Am. Chem. Soc.* **2014**, *136*, 10085-10094. c) Gustafson, S. J.; Fuller, J. T.; Devarajan, D.; Snyder, J.; Periana, R. A.; Hashiguchi, B. G.; Konnick, M. M.; Ess, D. H., "Contrasting Mechanisms and Reactivity of Tl(III), Hg(II), and Co(III) for Alkane C-H Functionalization." *Organometallics* **2015**, *34*, 5485-5495. d) Gustafson, S. J.; Konnick, M. M.; Periana, R. A.; Ess, D. H., "Mechanisms and Reactivity of Tl(III) Main-Group-Metal-Alkyl Functionalization in Water." *Organometallics* **2018**, *37*, 2723-2731.

15. Frisch, M. J.; Trucks, G. W.; Schlegel, H. B.; Scuseria, G. E.; Robb, M. A.; Cheeseman, J. R.; Scalmani, G.; Barone, V.; Mennucci, B.; Petersson, G. A.; Nakatsuji, H.; Caricato, M.; Li, X.; Hratchian, H. P.; Izmaylov, A. F.; Bloino, J.; Zheng, G.; Sonnenberg, J. L.; Hada, M.; Ehara, M.; Toyota, K.; Fukuda, R.; Hasegawa, J.; Ishida, M.; Nakajima, T.; Honda, Y.; Kitao, O.; Nakai, H.; Vreven, T.; Montgomery Jr., J. A.; Peralta, J. E.; Ogliaro, F.; Bearpark, M. J.; Heyd, J.; Brothers, E. N.; Kudin, K. N.; Staroverov, V. N.; Kobayashi, R.; Normand, J.; Raghavachari, K.; Rendell, A. P.; Burant, J. C.; Iyengar, S. S.; Tomasi, J.; Cossi, M.; Rega, N.; Millam, N. J.; Klene, M.; Knox, J. E.; Cross, J. B.; Bakken, V.; Adamo, C.; Jaramillo, J.; Gomperts, R.; Stratmann, R. E.; Yazyev, O.; Austin, A. J.; Cammi, R.; Pomelli, C.; Ochterski, J. W.; Martin, R. L.; Morokuma, K.; Zakrzewski, V. G.; Voth, G. A.; Salvador, P.; Dannenberg, J. J.; Dapprich, S.; Daniels, A. D.; Farkas, Ö.; Foresman, J. B.; Ortiz, J. V.; Cioslowski, J.; Fox, D. J. Gaussian 09, Gaussian, Inc.: Wallingford, CT, USA, **2009**.

16. a) Cramer, C. J., Chapter 8: Density Functional Theory, in Essentials of Computational Chemistry: Theories and Models. 2nd ed.; J. Wiley: Hoboken, NJ, **2004**; pp 596. b) Jensen, F., Chapter 6: Density Functional Methods, in Introduction to Computational Chemistry. 3rd ed.; John Wiley & Sons, Ltd.: Hoboken, NJ, **2017**; pp 638.

17. Zhao, Y.; Truhlar, D. G., "The M06 suite of density functionals for main group thermochemistry, thermochemical kinetics, noncovalent interactions, excited states, and transition elements: two new functionals and systematic testing of four M06-class functionals and 12 other functionals." *Theor. Chem. Acc.* **2007**, *120*, 215-241.

18. Metz, B.; Stoll, H.; Dolg, M., "Small-core multiconfiguration-Dirac-Hartree-Fock-adjusted pseudopotentials for post-d main group elements: Application to PbH and PbO." *J. Chem. Phys.* **2000**, *113*, 2563-2569.

19. a) Frisch, M. J.; Pople, J. A.; Binkley, J. S., "Self-consistent molecular orbital methods. 25. Supplementary functions for Gaussian basis sets." *J. Chem. Phys.* **1984**, *80*, 3265-9. b) Clark, T.; Chandrasekhar, J.; Spitznagel, G. W.; Schleyer, P. v. R., "Efficient diffuse function-augmented basis sets for anion calculations. III. The 3-21 + G basis set for first-row elements, lithium to fluorine." *J. Comp. Chem.* **1983**, *4*, 294-301. c) Krishnan, R.; Binkley, J. S.; Seeger, R.; Pople, J. A., "Self-consistent molecular orbital methods. XX. A basis set for correlated wave functions." *J. Chem. Phys.* **1980**, *72*, 650-654.

20. a) Rappoport, D.; Furche, F., "Property-optimized Gaussian basis sets for molecular response calculations." *J. Chem. Phys.* **2010**, *133*, 134105/1-134105/11. b) Weigend, F.; Ahlrichs, R., "Balanced basis sets of split valence, triple zeta valence and quadruple zeta valence quality for H to Rn: Design and assessment of accuracy." *Phys Chem Chem Phys* **2005**, *7*, 3297-305.

21. a) Check, C. E.; Faust, T. O.; Bailey, J. M.; Wright, B. J.; Gilbert, T. M.; Sunderlin, L. S., "Addition of Polarization and Diffuse Functions to the LANL2DZ Basis Set for P-Block Elements." *J. Phys. Chem. A* **2001**, *105*, 8111-8116. b) Wadt, W. R.; Hay, P. J., "Ab initio effective core potentials for molecular calculations. Potentials for main group elements Na to Bi." *J. Chem. Phys.* **1985**, *82*, 284-298.

22. a) Jensen, F., Chapter 14: Statistical Mechanics and Transition State Theory, in Introduction to Computational Chemistry. 3rd ed.; John Wiley & Sons, Ltd.: Hoboken, NJ, **2017**; pp 638. b) Cramer, C. J., Chapter 10: Thermodynamic Properties, in Essentials of computational chemistry: Theories and models. 2nd ed.; J. Wiley: Hoboken, NJ, **2004**; pp 596.

23. Marenich, A. V.; Cramer, C. J.; Truhlar, D. G., "Universal Solvation Model Based on Solute Electron Density and on a Continuum Model of the Solvent Defined by the Bulk Dielectric Constant and Atomic Surface Tensions." *J. Phys. Chem. B* **2009**, *113*, 6378-6396.

24. King, C. R.; Rollins, N.; Holdaway, A.; Konnick, M. M.; Periana, R. A.; Ess, D. H., "Electrophilic Impact of High-Oxidation State Main-Group Metal and Ligands on Alkane C–H Activation and Functionalization Reactions." *Organometallics* **2018**, *37*, 3045-3054.

25. King, C. R.; Gustafson, S. J.; Black, B. R.; Butler, S. K.; Konnick, M. M.; Periana, R. A.; Hashiguchi, B. M.; Ess, D. H., "Arene C–H Functionalization by p-Block Metal Tl(III) Occurs at the Borderline of C–H Activation and Electron Transfer." *Organometallics* **2017**, *36*, 109-113.

Chapter 2:

Electrophilic Impact of High-Oxidation State Main-Group Metal and Ligands on Alkane C-H Activation and Functionalization Reactions

2.1 Introduction

Metal complexes can mediate C-H functionalization of methane and other light alkanes by a C-H activation reaction to generate a metal-alkyl intermediate, which can then be functionalized to a carbon-oxygen bond (Scheme 2-1a).[1,2] This C-H functionalization strategy generally involves two-electron oxidation of the carbon and two-electron reduction of the metal center (e.g. M^{III} to M^{I}, Scheme 1a). Most catalysts that efficiently promote this type of two-electron methane C-H activation and metal-alkyl functionalization sequence involve 2nd-row and 3rd-row transition-metal complexes, such as Pd, Hg, and Pt.[3,4] Because progress developing new methane functionalization catalysts based on transition metals has plateaued, we have become interested in an alternative strategy using high oxidation state p-block, main-group metal complexes.

From the 1960s to the 1980s there were some reports of main-group hydrocarbon C-H functionalization reactions, but these reactions generally involved arene substrates and never emerged as a general strategy for oxyfunctionalization.[5] However, based on these previous uses of Tl^{III} as a two-electron oxidant, and the previous report of Tl^{III} to oxidize methane to methyl bisulfate in sulfuric acid,[6] it was recently reported that $Tl^{III}(TFA)_3$ (TFA = trifluoroacetate) promotes C-H oxygen functionalization of methane in trifluoroacetic acid (TFAH) solvent to methyl trifluoroacetate (MeTFA, Scheme 2-1b).[7] For example, with 0.25 M $Tl^{III}(TFA)_3$, 3.4 MPag of methane was oxidized to a 74% yield of methyl trifluoroacetate (MeTFA) at 180 °C in 3 hours (Scheme 2-1b).[7] Under similar conditions, $Pb^{IV}(TFA)_4$ also oxidizes methane to a nearly identical

MeTFA yield. It was also demonstrated that $Tl^{III}(OAc)_3$ (OAc = acetate) in acetic acid (AcOH) oxidizes alkanes, but with a significant decrease in product yield,[7] and the origin of this decrease in yield remains unexamined.

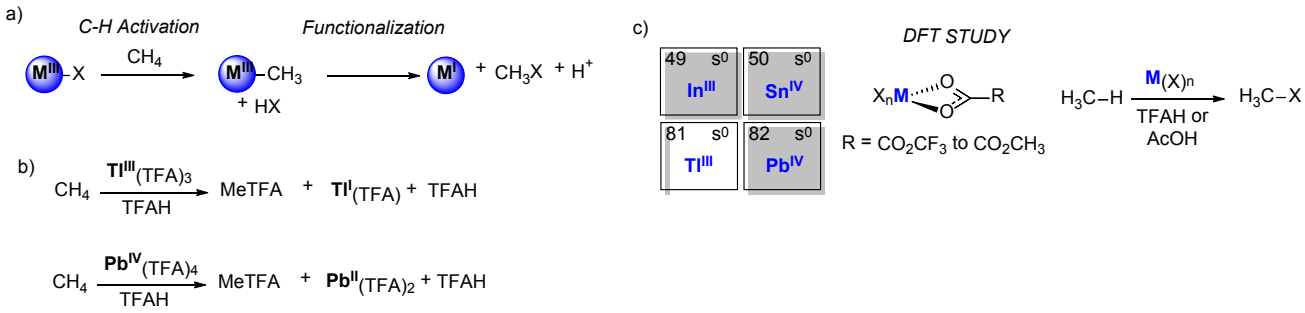

Scheme 2-1. a) Generalized electrophilic C-H activation and metal-methyl functionalization strategy for methane. b) Two examples of methane C-H functionalization with high-oxidation state p-block, main-group metals in TFAH solvent.[Error! Bookmark not defined.] c) This work examined In^{III}, Tl^{III}, Sn^{IV}, and Pb^{IV} C-H activation and metal-alkyl functionalization reactions for with carboxylate ligands in TFAH and AcOH solvents.

Because the similar transition-metal complex $Co^{III}(TFA)_3$ oxidizes alkanes by an open-shell mechanism,[8] and Tl^{III} can mediate electron transfer with hydrocarbons[9] (and potentially hydride transfer), we previously used density functional theory (DFT) calculations and experimental studies to examine the mechanism of ethane oxidation by $Tl^{III}(TFA)_3$. Our calculations suggest that $Tl^{III}(TFA)_3$ oxidizes ethane by a closed-shell electrophilic C-H activation and one-step metal-alkyl oxygen functionalization mechanism.[7,10] We have not reported calculations on methane oxidation by $Tl^{III}(TFA)_3$ or calculations on the thermodynamic and reactivity impact of the main-group metal center and surrounding acetate ligands. Therefore, in pursuit of evaluating possible C-H functionalization catalysts based on p-block, main-group metals, we used DFT calculations to compare the reactivity of methane C-H activation and metal-methyl functionalization reactions for 5th and 6th-row high-oxidation state ($d^{10}s^0$) In^{III}, Tl^{III}, Sn^{IV},

and Pb^{IV} with acetate ligands in carboxylic acid solvents. In this report we describe that C-H activation is electrophilically controlled, and correlated to 5s and 6s unoccupied orbital energies, but the range of C-H activation barriers for this set of main-group metals is relatively narrow. Unexpectedly, the carboxylate ligand has a much larger quantitative impact on C-H activation with stabilized carboxylate anions inducing the lowest barriers. In contrast, the stability of the metal-methyl intermediates and the reductive functionalization barriers are extremely sensitive to the main-group metal center and are correlated to reaction thermodynamics and bond heterolysis energies as a model two-electron reduction energies.

2.2 Results and Discussion

2.2.1 Computational Details

Gaussian 09 was used for optimization and normal-mode vibrational frequency analysis for minima or transition-state structures.[11] Structures were optimized with M06/6-31G**[LANL2DZdp for In, Tl, Sn, and Pb].[12] Electronic energies and orbital energies were calculated using M06/def2-TZVPPD//M06/6-31G**[LANL2DZdp].[13] This level of theory was chosen based on our previous assessment of p-block, main-group ionization energies.[10] For thermochemical corrections, temperature was set to 298 K and pressure to 1 atm. All calculations were performed with either an augmented TFAH or acetic acid SMD continuum model for estimates of the standard state solvation free energy change (ΔG_{solv}).[14] Similar to several previous studies, for TFAH solvent, the dielectric was set to 8.42 and the radii set to 2.479 (see Supporting Information (SI)).[7,10,15] All free energies and enthalpies reported include ΔG_{solv}. Free energies are the sum of $E_{(SCF,large)} + \Delta E_{ZPE(small)} + \Delta U_{(small)} + nRT - T\Delta S_{(small)} + \Delta G_{solv(large)}$ (Large = M06/def2-

TZVPPD; Small = M06/6-31G**[LANL2DZdp]. No concentrations corrections or scaling of vibrational frequencies were applied.

$Tl^{III}X_3$, $Sn^{IV}X_4$, $Pb^{IV}X_4$ (X = TFA or OAc), and similar main-group acetate complexes can be synthesized by dissolving the metal oxide in either TFAH or AcOH with an oxidant, such as a peracetic acid. For example, $Sn^{IV}(TFA)_4$ can be generated by SnO in trifluoroperacetic acid/trifluoroacetic anhydride or protonation of tetraphenyltin in TFAH.[16] In these carboxylic acid solvents there are a variety of possible mononuclear and polynuclear structures with several different ligand coordination environments possible. However, we chose to compare and analyze κ^2-type coordination main-group mononuclear models (Scheme 2-2a) for several reasons. 1) This κ^2 type model corresponds to the experimental x-ray structure of $Tl^{III}(OAc)_3$.[17] 2) While polynuclear main-group structures have been observed,[16,18] extensive kinetic studies of arene and cyclopropane oxidation by $Tl^{III}(TFA)_3$ showed first-order rate dependence on Tl^{III}.[5,19] 3) For $Tl^{III}(TFA)_3$, our previous study showed a relatively small difference between C-H activation barriers calculated with mononuclear and multinuclear models.[10] 4) While carboxylic acid solvent coordination to the main-group metal center is energetically favorable (e.g. $Tl^{III}(TFA)_3(TFAH)$), which likely facilitates fast proton transfer and ligand exchange with solvent, solvent-coordinated models and the κ^2 type model used here provide relatively similar calculated C-H activation barrier heights.[10]

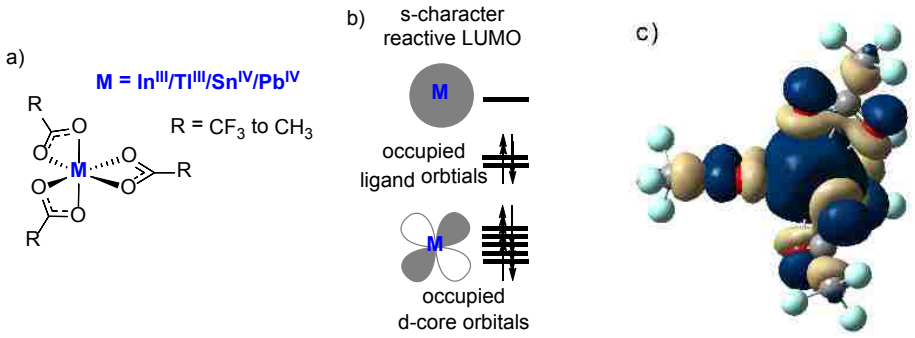

Scheme 2-2. a) Main-group metal acetate model used to explore relative reactivity trends. For $Tl^{III}X_3$ and $In^{III}X_3$ structures, the κ^2 metal-carboxylate coordination is equivalent for both metal-oxygen interactions. For $Sn^{IV}X4$ and $Pb^{IV}X_4$, the κ^2 metal-carboxylate coordination is not equivalent for both metal-oxygen interactions. For each carboxylate there is one shorter distance (~2.15 Å for Sn and Pb) and one longer distance (~2.40 Å for Pb and ~2.20 Å for Sn). b) Qualitative orbital level diagram for $d^{10}s^0$ main-group metal acetate complexes. c) Example of 3D-structure and LUMO orbital for $Pb(TFA)_4$.

2.2.2 Electronic Structure

For the κ^2 type metal acetate models, as expected, the $d^{10}s^0$ electronic structure gives a dominant low-spin singlet configuration with high spin states more than 30 kcal/mol higher in energy. Scheme 2b illustrates that these main-group complexes have a low-energy core set of d^{10} electrons that are ~6 eV lower in energy than the HOMO orbitals that are ligand centered. The reactive empty orbital is a 5s or 6s orbital that has antibonding interactions with the acetate ligands (Scheme 2-2c).

2.2.3 Mechanism

We previously used DFT and experiments to examine the mechanism for ethane C-H functionalization by $Tl^{III}(TFA)_3$.[10] Based on our calculated and experimental data,[7] we proposed that this neutral Tl^{III} complex reacts with alkanes rather than the monocationic structure $[Tl^{III}(TFA)_2]^+$. With the addition of one explicit TFAH solvent stabilization to both the metal and TFA anion we estimated ligand dissociation to be ~25 kcal/mol, which is likely too large for viable

reaction pathways emanating from this monocation in relatively non-polar, although hydrogen bonding, solvent. However, this estimate for TFA anion dissociation is potentially an upper bound with only one explicit solvent hydrogen bonding interaction stabilizing the cation and anion pair. Therefore, following the Strassner approach for Pd carboxylate complexes,[15] we calculated TFA dissociation for $In^{III}(TFA)_3$, $Tl^{III}(TFA)_3$, $Sn^{IV}(TFA)_4$, and $Pb^{IV}(TFA)_4$ using $M(TFA)_n + (TFAH)_5 \rightarrow [M(TFA)_{n-1}(TFAH)]^+ + [(TFAH)_4(TFA)]^-$. ΔG values are: In^{III} = 21.9 kcal/mol, Tl^{III} = 21.4 kcal/mol, Sn^{IV} = 27.6 kcal/mol, and Pb^{IV} = 23.3 kcal/mol. While inclusion of several explicit solvents stabilize the metal monocation and TFA anion, these dissociation energies are still too high to make the monocation a lower energy C-H activation pathway compared to the neutral C-H activation pathway.

The reaction pathway we used to evaluate the relative reactivity impact of main-group metals and acetate ligands is shown in Scheme 2-3. Here the C-H activation transition state for methane involves an electrophilic substitution,[20,21] which has also been called by several alternative names.[22,23] In this transition-state structure the metal-carbon bond is formed simultaneous to C-H bond cleavage and proton transfer to the acetate ligand. For the κ^2 type model the intrinsic reaction coordinate (IRC) leads directly from the metal complex and methane to the metal-methyl intermediate. At this intermediate, the formed carboxylic acid requires very little energy to dissociate from the now more electron rich metal-methyl intermediate. The mechanisms used to determine relative functionalization reactivity involve either an internal or external nucleophilic acetate functionalization transition state, which results in a methyl acetate or two electron metal reduction. The internal transition state involves transfer of the methyl group from the metal center to one of the acetate ligands without inversion of the carbon configuration and without acetate ligand dissociation. The external functionalization transition state first involves

acetate dissociation followed by nucleophilic substitution where the acetate is oriented in a co-linear arrangement with the metal-carbon bond and results in configuration inversion of the methyl group.

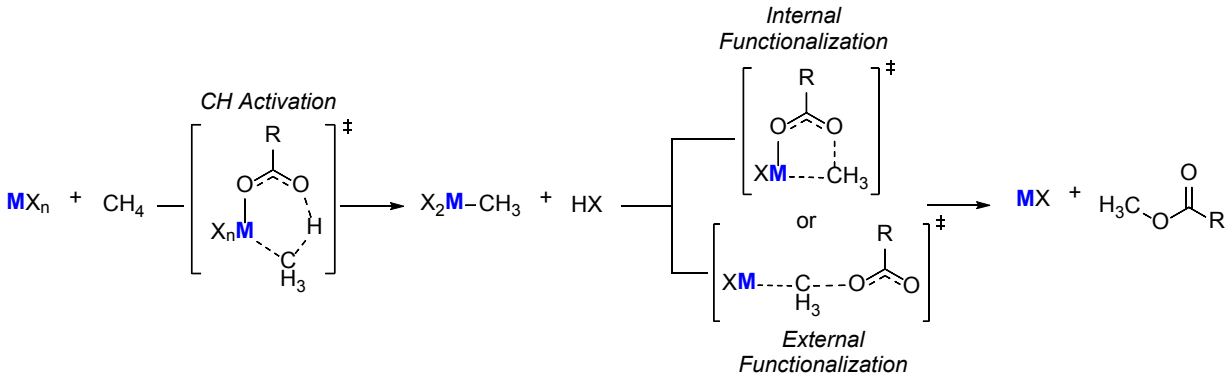

Scheme 2-3. Outline of C-H activation and metal-methyl functionalization mechanism used to examine metal, ligand, and solvent effects on reactivity.

2.2.4 Metal and Carboxylate Ligand Impact on C-H Activation Barriers and Thermodynamics

Scheme 2-4 illustrates and compares the thermodynamics and barriers for C-H activation reaction of methane with $In^{III}(TFA)_3$, $Tl^{III}(TFA)_3$, $Sn^{IV}(TFA)_4$, and $Pb^{IV}(TFA)_4$. The result of these reactions are the corresponding metal-methyl intermediates. Because these main-group TFA complexes occupy different periodic table rows, and have different oxidation states, we initially assumed they would have dramatically different C-H activation barriers. However, the smallest activation barrier ($\Delta G^{\ddagger}$) of 31.9 kcal/mol is for $Tl^{III}(TFA)_3$ and the largest is 34.3 kcal/mol for $Sn^{IV}(TFA)_4$. Interestingly, $Tl^{III}(TFA)_3$ and $In^{III}(TFA)_3$ have nearly identical barrier heights, despite 6s and 5s LUMO energies that differ by more than 1 eV,[24] and there is no linear correlation between the metal TFA complex LUMO energies and $\Delta G^{\ddagger}$ values. However, this suggests that In^{III} could be viable for alkane C-H activation chemistry by generation of an organometallic

intermediate rather than only act as a dative coordination-type Lewis acid, if it can be generated as species similar to $In^{III}(TFA)_3$. A slightly larger range in $\Delta G^{\ddagger}$ values (~7 kcal/mol) was found for the calculated C-H activation barriers of methane with $In^{III}(OAc)_3$, $Tl^{III}(OAc)_3$, $Sn^{IV}(OAc)_4$, and $Pb^{IV}(OAc)_4$ (Scheme 2-5).

In contrast to the C-H activation barriers, the reaction thermodynamics for forming the metal-methyl intermediates have a relatively large range in stability. For example, $(TFA)_3Pb^{IV}$-Me is exergonic by 18.8 kcal/mol while $(TFA)_2In^{III}$-Me is endergonic by 6.0 kcal/mol, which is an ~25 kcal/mol range in thermodynamic stability. Similarly, there is ~16 kcal/mol thermodynamics stability difference between $(OAc)_3Pb^{IV}$-Me and $(OAc)_2In^{III}$-Me. It is important to recognize that there is not a kinetic-thermodynamic relationship between the C-H activation barrier heights and the metal-methyl stabilities. However, the ordering of the metal-methyl stabilities is heavily influenced by the 5s and 6s LUMO orbital energies. The LUMO orbital energies range from -3 to -5 eV for TFA and OAc complexes of In^{III}, Tl^{III}, Sn^{IV}, and Pb^{IV} (see Appendix 1). Similar to the metal-methyl stabilities, the LUMO energies increase as $Pb^{IV} < Tl^{III} < Sn^{IV} < In^{III}$. This suggests that the stabilizing influence of the 5s and 6s unoccupied orbitals in the main-group metal complexes is significant when the metal-methyl bonds are fully formed and the pair of electrons are highly polarized towards the metal center.

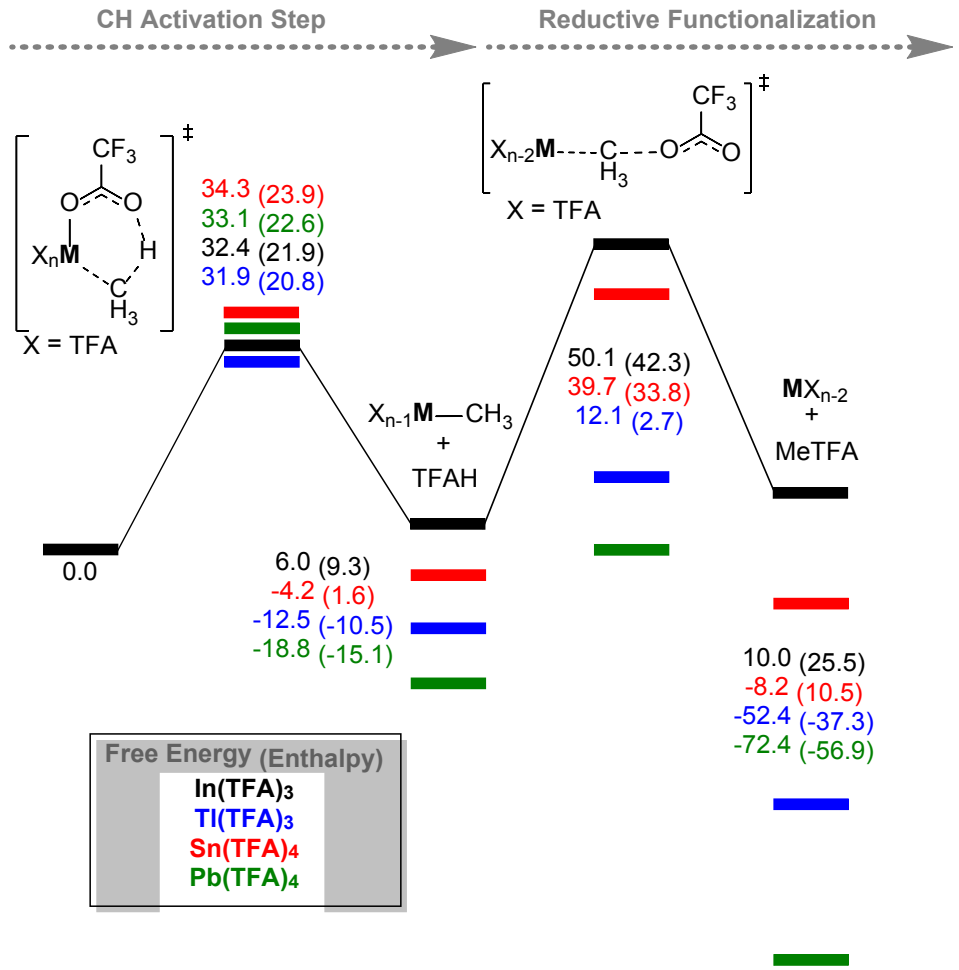

Scheme 2-4. Free energy landscapes for C-H activation of methane and external metal-methyl functionalization for main-group metal TFA complexes. Enthalpies are reported in parenthesis. No potential-energy barrier was found for $(TFA)_3Pb^{IV}$-Me external functionalization. See discussion. (kcal/mol)

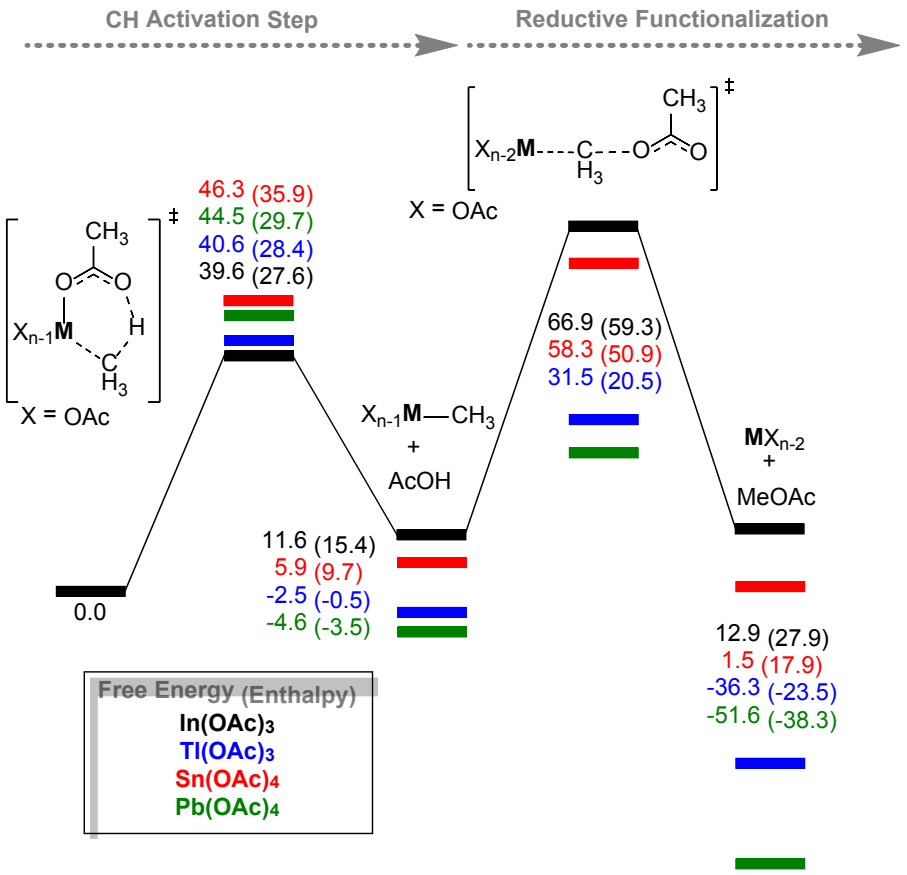

Scheme 2-5. Free energy landscapes for C-H activation of methane and external metal-methyl functionalization for main-group metal OAc complexes. Enthalpies are reported in parenthesis. No potential-energy barrier was found for $(TFA)_3Pb^{IV}$-Me external functionalization. See discussion. (kcal/mol)

While there is a relatively narrow range for C-H activation barriers by different metals with the same carboxylate ligand, the metal OAc complexes have ~8-10 kcal/mol larger free energy barriers than the metal TFA complexes (compare Schemes 2-4 and 2-5), and this can be correlated to higher energy LUMO orbitals of the metal OAc complexes as well as the ~5 unit pK_a difference between carboxylate ligands. While the C-H activation $\Delta G^{\ddagger}$ values for main-group metal TFA complexes are all below ~35 kcal/mol, and potentially thermally accessible, only $Tl^{III}(OAc)_3$ has a free energy barrier below 40 kcal/mol. This indicates that ligand influences, in particular for carboxylate complexes, are overall more impactful than the metal center for C-H activation.

However, the values in Scheme 2-4 values were calculated in TFAH and the values in Scheme 2-5 were calculated in AcOH. To more closely examine the effect of acetate ligands on C-H activation barriers for In^{III}, Tl^{III}, Sn^{IV}, and Pb^{IV} metals we also computed C-H barriers in TFAH solvent for the series OAc, monofluoroacetate, dichloroacetaete, difluoroacetate, trichloroacetate, to TFA (Scheme 2-6). This carboxylate ligand series was chosen because they represent the continuum between OAc and TFA.

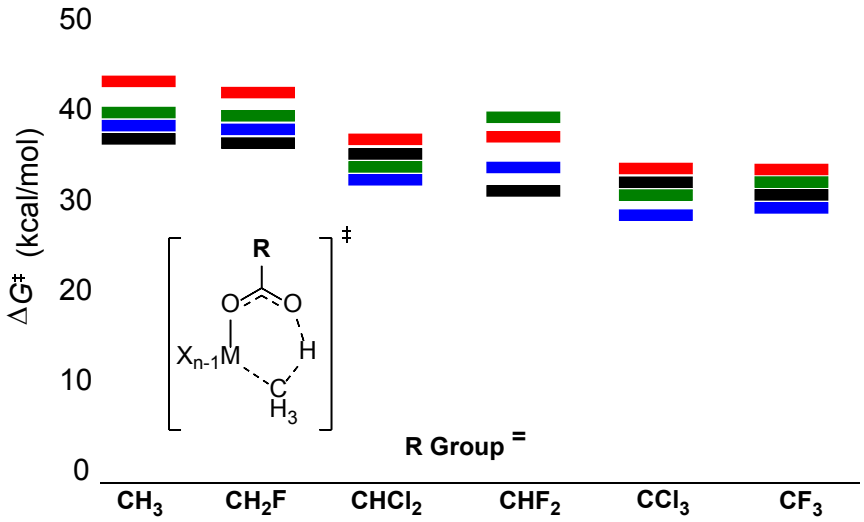

Scheme 2-6. Free energy barriers for methane C-H activation by In^{III} (black), Tl^{III} (blue), Sn^{IV} (red), and Pb^{IV} (green) with carboxylate ligands. (kcal/mol)

Similar to what we found for OAc and TFA, these mono-, di-, and tri-fluoro and chloro carboxylate ligands show a similar 5-7 range in C-H activation barriers for the four main-group metals, and all the barriers monotonically decrease as OAc methyl group C-H bonds are replaced by carbon-halogen electron withdrawing bonds. Inspection of the LUMO orbital energies shows that the carboxylate ligand can control the energy of the LUMO, and there is a high degree of linear correlation between the LUMO energies and C-H activation barriers for all these acetate ligands for each metal (see SI). For example, for Tl^{III}, $\Delta G^{\ddagger}$ = 7.0*LUMO + 60.9 kcal/mol with R^2

= 0.97. As expected, there is also a general qualitative correlation between the carboxylate conjugate acid pK_a value and barrier heights.

2.2.5 Metal and Carboxylate Ligand Impact on Metal-Methyl Functionalization Barriers and Thermodynamics

While there are several experimental and computational studies on the topic of metal-mediated C-H activation reactions, there are only a few studies that have examined mechanisms and reactivity trends of metal-alkyl oxygen functionalization reactions. Despite a limited number of functionalization studies, two bookend types of closed-shell metal-methyl functionalization reactions have emerged. The first of these reactions involves methyl anion transfer from the metal center to an electrophilic oxygen atom, usually an external oxidant. This type of mechanism has been proposed for functionalization of Re-methyl bonds with oxidants such as hydrogen peroxide and pyridine oxide, and is often referred to as an organometallic Bayer-Villiger reaction.[25,26] For this type of electrophilic functionalization reaction, Cundari and Gunnoe have surveyed the influence of the transition metal identity on (bpy)metal-methyl functionalization barriers.[27] A reasonable correlation was identified between functionalization barriers and reaction energies, which was attributed to lower metal-methyl bond strengths. There was also some correlation between the methyl group charge and functionalization barrier heights. Cundari has also compared organometallic Bayer-Villiger functionalization and oxygen atom transfer/methyl group migration for s-block to p-block 3d metal-methyl structures with β-diketiminate ligands using pyridine-*N*-oxide.[28]

At the other extreme, the second type of metal-methyl functionalization reaction involves nucleophilic oxygen attack of a polarized metal-methyl bond that results in two-electron reduction

of the metal center,[29,30] and is often referred to as an S_N2-like mechanism. As discussed above, Scheme 2-3 depicts this type of reductive functionalization pathway where a carboxylate nucleophile either migrates from the metal center to the methyl group (internal) or the carboxylate nucleophile leaves the metal coordination sphere and then induces substitution at the backside of the metal-methyl bond (external). The external nucleophilic reductive functionalization mechanism has been proposed in a variety of transition-metal-methyl intermediates, and generally requires a high oxidation state, presumably to substantially polarize the metal-methyl bond and to create a good metal leaving group. For example, Ziegler, Musgrave, and others have proposed that (bpym)Pt^{II}-methyl oxidation to (bpym)Pt^{IV}-methyl provides a route for reductive functionalization with extremely weak nucleophiles.[31-33] A similar functionalization mechanism was recently proposed based on experiments and computational studies for a diacetate Pt^{IV}-methyl complex.[34] This nucleophilic reductive mechanism has also been proposed for Pd-methyl functionalization, for example in the case of Pd-catalyzed methane oxidation to methyl bisulfate and to acetic acid.[35] Strassner also proposed this type of functionalization mechanism for bis(NHC)Pd catalyzed methane trifluoroacetoxylation.[36] Similarly, Vedernikov, Sanford, and others have also proposed nucleophilic reductive functionalization for Pd^{IV}-dimethyl functionalization reactions.[37] More related to main-group-methyl functionalization reactions, Periana and co-workers proposed that Au^{III}-methyl intermediates react by external reductive functionalization with bisulfate.[38] Interestingly, Labinger and Bercaw synthesized a N-heterocyclic carbene Au^{III}-methyl complex and kinetic studies suggest an internal reductive elimination mechanism for functionalization.[39] Very recently, we showed that Hg^{II}-methyl also undergoes reductive functionalization by an external bisulfate nucleophilic.[40]

Only a few DFT studies have explored the metal and ligand impact on functionalization barriers. In one example, Cundari used DFT calculations to explore functionalization of model group 9 bipyridine coordinated Rh^{III}-methyl complexes.[41] This study showed that substitution of the bipyridine ligand with electron withdrawing groups can lower functionalization barriers by greater than 10 kcal/mol, which was attributed to inducing a more electron poor metal center. Cundari and Gunnoe also examined terpyridine-coordinated Rh^{III}-methyl bond functionalization.[42,43] Cundari has also used DFT calculations to examine reductive functionalization of first-row transition-metal-methyl reactions.[44] It was found that d-electron occupation could not explain functionalization barrier heights, rather ligand size and electronics are more important.

To examine nucleophilic reductive functionalization for In^{III} Tl^{III}, Sn^{IV}, and Pb^{IV} main-group-methyl structures we first compared external and internal transition-state barriers (Scheme 2-3). We have previously reported both transition states for Tl^{III}-ethyl[7,10] and I^{III}-ethyl structures.[45] In these cases, internal and external functionalization transition states are close in energy. However, change from an ethyl group to a methyl group dramatically changes the preference for a lower energy external transition state. For example, $(TFA)_2Tl^{III}$-Me has an internal transition state barrier height of 34.7 kcal/mol and external barrier of 24.6 kcal/mol. Similarly, for $(TFA)_3Sn^{IV}$-Me the external barrier is 13.5 kcal/mol lower in energy than the internal barrier. This general preference for external functionalization results from less carbocation character required in the transition state, and is qualitatively consistent with relative methyl versus ethyl carbocation stabilities. The internal transition-state structures have highly elongated metal-carbon partial bond lengths with significant carbocation character that is not stabilized by a methyl group (see Appendix 1). Because of the external functionalization preference, Schemes 2-4 and 2-5 only

report external transition-state energies. However, despite significant searching, no external transition-state structure was located for functionalization of $(TFA)_3Pb^{IV}$-Me. In this case, when the TFA ligand dissociates and is oriented near the methyl group there is no potential energy barrier for collapse to form MeTFA. Therefore, we have estimated this barrier as the energy for ligand dissociation to create the $[(TFA)_3Pb^{IV}\text{-Me}]^+/[TFA]^-$ pair, which is 12.8 kcal/mol. This ion-pair energy is less than the internal functionalization with a barrier of 18.3 kcal/mol and was estimated using the equation $(TFA)_3Pb^{IV}\text{-Me} + (TFAH)_5 \rightarrow [(TFA)_2(TFAH)Pb^{IV}\text{-Me}]^+ + [(TFAH)_4(TFA)]^-$. For $(TFA)_2In^{III}$-Me, $(TFA)_2Tl^{III}$-Me, and $(TFA)_3Sn^{IV}$-Me the TFA dissociation energy estimates are 14.7, 7.3, and 20.3 kcal/mol. Importantly, our analysis of metal-dependent functionalization barrier trends is identical whether external or internal transition states are considered. Also important, for the purpose of comparing relative closed-shell functionalization reactivity we did not consider radical functionalization mechanisms.[46,47] While open-shell C-H functionalization mechanisms of alkanes by p-block elements have been proposed,[48,49] these reactions are unlikely to involve metal-methyl intermediates. Also, Goldberg and Ison have shown that open-shell transition-metal-methyl functionalization mechanisms are possible, but generally with O_2,[50-52] and previous experiments demonstrated that O_2 made no major impact on $Tl^{III}(TFA)_3$ alkane functionalization yields.[7]

The result of external functionalization is MeTFA and two-electron reduced metal complexes ($In^{I}(TFA)$, $Tl^{I}(TFA)$, $Sn^{II}(TFA)_2$, and $Pb^{II}(TFA)_2$). In contrast to the C-H activation barriers, there is a large range in barrier heights for In^{III}, Tl^{III}, Sn^{IV}, and Pb^{IV} metals. For example, $(TFA)_2Tl^{III}$-Me has a functionalization barrier of 24.6 kcal/mol while $(TFA)_2In^{III}$-Me has a barrier of 44.1 kcal/mol. In general, 6s Tl^{III} and Pb^{IV} have low functionalization barriers while 5s In^{III} and Sn^{IV} have large functionalization barriers. The $(TFA)_2Tl^{III}$-Me and $(TFA)_3Pb^{IV}$-Me

functionalization barriers are lower than the reverse barriers for TFAH protonolysis while $(TFA)_2In^{III}$-Me and $(TFA)_3Sn^{IV}$-Me functionalization barriers are larger than the TFAH protonolysis barriers. This is consistent with no hydrogen-deuterium exchange for alkane functionalization by Tl^{III} in TFAD,[Error! Bookmark not defined.7] but hydrogen-deuterium exchange of hydrocarbon C-H bonds catalyzed by $Sn^{IV}(TFA)_4$.[Error! Bookmark not defined.] Interestingly, while the functionalization barrier for $(TFA)_3Pb^{IV}$-Me is lower than $(TFA)_2Tl^{III}$-Me, $(TFA)_3Sn^{IV}$-Me and $(TFA)_2In^{III}$-Me have roughly similar barriers. The large functionalization barrier for Sn^{IV} is consistent with Grushin's report that suggests fast initial reaction with arene C-H bonds, but slow or no functionalization.[16]

For TFA complexes, Scheme 2-4 shows that the metal-dependent ordering of functionalization barriers follows $Pb^{IV} < Tl^{III} < Sn^{IV} = In^{III}$, and this ordering is the same as the thermodynamic stabilities of the metal-methyl intermediates, but the energy range is much larger, increasing from an ~25 kcal/mol range to an ~45 kcal/mol range. The metal-dependent functionalization trend for OAc complexes shown in Scheme 2-5 is very similar to the TFA complexes. Similar to the difference between TFA and OAc C-H activation barriers, OAc functionalization barriers have ~10 kcal/mol higher barriers. However, for functionalization, the effect of the carboxylate ligand, while similar in magnitude to the effect on C-H activation, is dwarfed by the impact of the main-group metal.

Because the functionalization barriers mirror the relative metal-methyl intermediate stabilities, this suggested to us that a likely correlation model for functionalization reactivity should be two-electron reduction energies. Indeed, there is a reasonable linear correlation between external functionalization barrier heights ($\Delta G^{\ddagger}$ values) and ΔG_{rxn} values $\Delta G^{\ddagger} = 0.4*\Delta G_{rxn} + 46.4$

kcal/mol; R^2 = 0.70, Figure 2-1). There is a similar linear correlation between internal functionalization barriers and ΔG_{rxn} values (see Appendix 1). This correlation is reasonable considering that the stabilities of $In^{I}(TFA)$, $Tl^{I}(TFA)$, $Sn^{II}(TFA)_2$, and $Pb^{II}(TFA)_2$ have the same ordering as the functionalization barriers, but an even larger range in their energies (~82.4 kcal/mol for TFA complexes and 64.5 kcal/mol for OAc complexes). Also, this correlation results from the relatively elongated metal-carbon partial bond lengths in the transition states where the methyl fragment develops some carbocation character and the metal is significantly reduced.

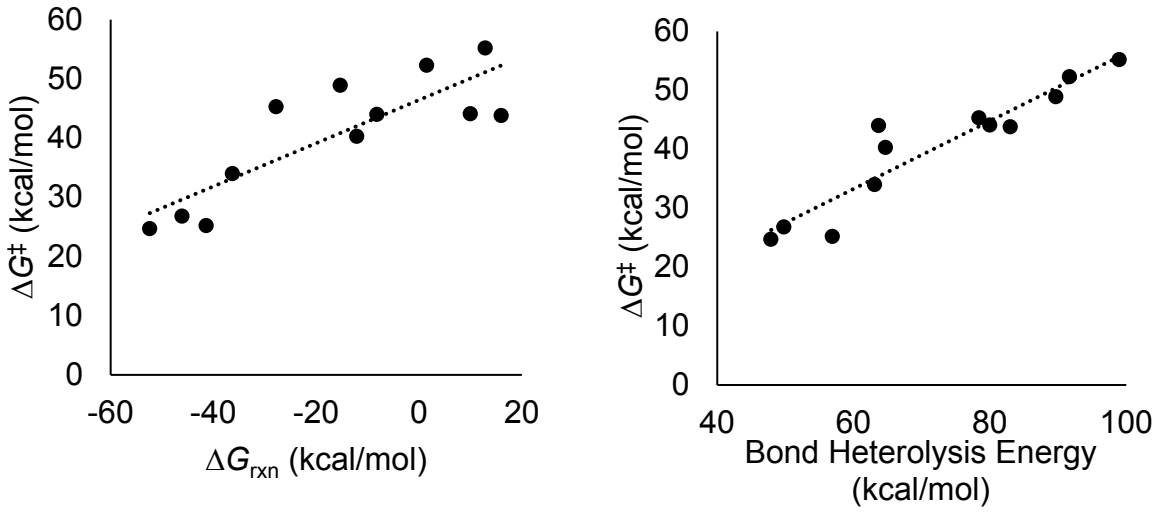

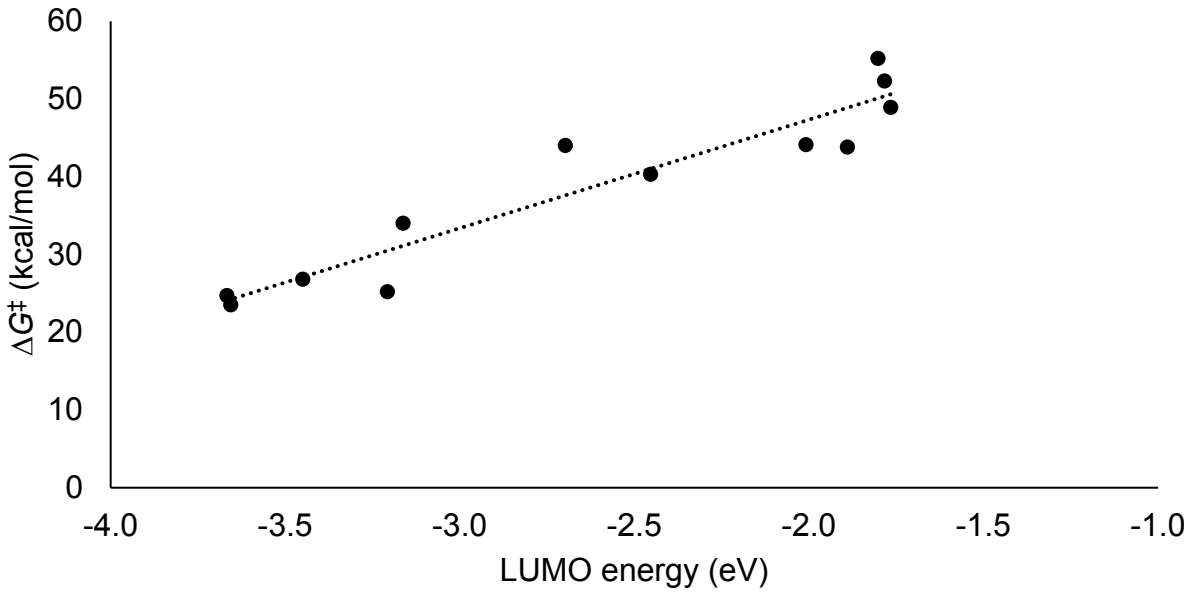

Figure 2-1. Correlation plots for $\Delta G^{\ddagger}$ (external functionalization) versus ΔG_{rxn}, metal-methyl bond heterolysis energy, and metal-methyl cation σ* orbital energies. These plots include the functionalization barriers of In^{III}-Me, Tl^{III}-Me, and Sn^{IV}-Me with OAc, monofluoroacetate, difluoroacetate, and TFA ligands. Linear correlations: $\Delta G^{\ddagger} = 0.4*\Delta G_{rxn} + 46.4$ kcal/mol; $R^2 = 0.70$. $\Delta G^{\ddagger} = 0.6*$BHE - 1.3 kcal/mol; $R^2 = 0.88$. $G^{\ddagger} = 14.0*$LUMO energy + 75.2 kcal/mol, $R^2 = 0.90$.

While experimental two-electron reduction potentials are known for these main-group metals, accurate estimates of potentials in carboxylic acid solvents could not be found. Therefore, for a direct comparison, we calculated the two electron reduction of the metal-methyl structures by heterolysis fragmentation to the corresponding methyl carbocation and reduced anionic metal structures. Plotting functionalization $\Delta G^{\ddagger}$ values versus metal-methyl bond heterolysis energies (BHE) shows a higher degree of linear correlation with $\Delta G^{\ddagger} = 0.6*$BHE - 1.3 kcal/mol and $R^2 =$ 0.88 (Figure 2-1). Because the functionalization transition states use the metal-methyl σ* for two-electron reduction and this orbital is highly skewed towards the metal being mainly composed of either metal 5*s* or 6*s* character, we also found that these orbital energies provide correlation with barriers, with $R^2 = 0.90$.

2.3 Conclusions

This work reported DFT calculations that compared the methane C-H activation and metal-methyl functionalization thermodynamics and barrier for high-oxidation state In^{III}, Tl^{III}, Sn^{IV}, and Pb^{IV} carboxylate complexes. We found that the main-group metal influences the C-H activation barrier height in a periodic manner, but the carboxylate ligand has a much larger quantitative impact on C-H activation and stable carboxylate anions have the lowest barriers. For metal-methyl reductive functionalization reactions, external functionalization is lowest in energy, carboxylate dissociation is relatively facile, and the main-group metal dramatically influences the barrier heights, which are correlated to reaction thermodynamics, bond heterolysis energies, and σ^* orbital energies as models two-electron reduction energies. Overall, this work begins to outline which main-group metals and carboxylate ligands could be useful for alkane functionalization systems that utilize C-H activation and metal-alkyl functionalization reactions. Because C-H activation reactions have a narrow range of barrier heights, and ligands can be used to decrease these barriers, significant attention should be paid to designing complexes where the kinetics and thermodynamics for two-electron reductive functionalization are feasible. While Tl^{III} and Pb^{IV} are viable, and have previously been demonstrated experimentally,[7] In^{III} and Sn^{IV} with simple carboxylate ligands are not viable, but could be significantly tuned by ligand effects.

2.4 References

1. a) Shilov, A. E.; Shulpin, G. B. “Activation and catalytic reactions of alkanes in solutions of metal complexes.” *Russ. Chem. Rev.* **1987**, *56*, 442-464. b) Shilov, A. E.; Shul'pin, G. B. “Activation of C− H bonds by metal complexes.” *Chem. Rev.* **1997**, *97*, 2879-2932. c) Stahl, S. S.; Labinger, J. A.; Bercaw, J. E. “Homogeneous oxidation of alkanes by electrophilic late transition metals.” *Angew. Chem. Int. Ed.* **1998**, *37*, 2180-2192. d) Sen, A. “Catalytic functionalization of carbon−hydrogen and carbon−carbon bonds in protic media.” *Acc. Chem. Res.* **1998**, *31*, 550-557. e) Crabtree, R. H. “Alkane C-H activation and functionalization with homogeneous transition metal catalysts; A century of progress - a new millennium in prospect [Erratum]” *J. Chem. Soc. Dalton* **2001**, 2951-2951. f) Labinger, J. A.; Bercaw, J. E. “Understanding and exploiting C–H bond activation.” *Nature* **2002**, *417*, 507-514. g) Crabtree, R. H. “Alkane C-H activation and functionalization with homogeneous transition metal catalysts; A century of progress - a new millennium in prospect.” *J. Chem. Soc., Dalton Trans.* 2001, 2437-2450. h) Webb, J. R.; Bolaño, Gunnoe, T. B. “Catalytic Oxy-Functionalization of Methane and Other Hydrocarbons: Fundamental Advancements and New Strategies.” *ChemSusChem* **2011**, *4*, 37-49. i) Gunnoe, T. B. In Alkane C-H Activation by Single-Site Metal Catalysts; Perez, P. J., Ed.; Springer: Dordrecht, **2012**; Vol. 38; pp 1-17. j) Shul’pin, G. B. “C–H functionalization: thoroughly tuning ligands at a metal ion, a chemist can greatly enhance catalyst's activity and selectivity.” *Dalton Trans.* **2013**, *42*, 12794-12818. k) Munz, D.; Strassner, T. “Alkane C–H functionalization and oxidation with molecular oxygen.” *Inorg. Chem.* **2015**, *54*, 5043-5052. l) Rudakov, E. S.; Shul’pin, G. B. “Stable organoplatinum complexes as intermediates and models in hydrocarbon functionalization.” *J. Organomet. Chem.* **2015**, *793*, 4-16. m) Shestakov, A. F.; Goldshleger, N. F. “Catalysts for C–H functionalization: Platinum, gold and even nanodiamonds.” *J. Organomet. Chem.* **2015**, *793*, 17-33. n) Kondratenko, E. V.; Peppel, T.; Seeburg, D.; Kondratenko, V. A.; Kalevaru, N.; Martin, A.; Wohlrab, S. “Methane conversion into different hydrocarbons or oxygenates: current status and future perspectives in catalyst development and reactor operation.” *Catal. Sci. Technol.* **2017**, *7*, 366-381. o) Tang, X.; Jia, X.; Huang, Z. “Challenges and opportunities for alkane functionalisation using molecular catalysts.” *Chem. Sci.* **2018**, *9*, 288-299. p) Shteinman, A. A. “Activation and selective oxy-functionalization of alkanes with metal complexes: Shilov reaction and some new aspects.” *J. Mol. Cat. A* **2017**, *426*, 305-315. q) Ravi, M.; Ranocchiari, M.; van Bokhoven, J. A. “A Critical Assessment of the Direct Catalytic Oxidation of Methane to Methanol.” *Angew. Chem. Int. Ed.* **2017**, *56*, 16464-16483.
2. a) Hashiguchi, B. G.; Bischof, S. M.; Konnick, M. M.; Periana, R. A. “Designing catalysts for functionalization of unactivated C–H bonds based on the CH activation reaction.” *Acc. Chem. Res.*

2012, *45*, 885-898. b) Gunsalus, N. J.; Konnick, M. M.; Hashiguchi, B. G.; Periana, R. A. "Discrete molecular catalysts for methane functionalization." *Isr. J. Chem.* **2014**, *54*, 1467-1480. c) Gunsalus, N. J.; Koppaka, A.; Park, S. H.; Bischof, S. M.; Hashiguchi, B. G.; Periana, R. A. "Homogeneous functionalization of methane." *Chem. Rev.* **2017**, *117*, 8521-8573.

3. For a Pt example see: a) Periana, R. A.; Taube, D. J.; Gamble, S.; Taube, H.; Satoh, T.; Fujii, H., "Platinum catalysts for the high-yield oxidation of methane to a methanol derivative." *Science* **1998**, *280*, 560-564. b) Konnick, M. M.; Bischof, S. M.; Yousufuddin, M.; Hashiguchi, B. G.; Ess, D. H.; Periana, R. A., "A mechanistic change results in 100 times faster CH functionalization for ethane versus methane by a homogeneous Pt catalyst." *J. Am. Chem. Soc.* **2014**, **136**, 10085-10094.
4. For Pd examples see: a) Kao, L.-C.; Hutson, A. C.; Sen, A. "Low-temperature, palladium (II)-catalyzed, solution-phase oxidation of methane to methanol derivative." *J. Am. Chem. Soc.* **1991**, *113*, 700-701. b) Periana, R. A.; Mironov, O.; Taube, D.; Bhalla, G.; Jones, C. J., "Catalytic, oxidative condensation of CH_4 to CH_3COOH in one step via CH activation." *Science* **2003**, 301, 814-818. c) Ahrens, S.; Zeller, A.; Taige, M.; Strassner, T., "Extension of the alkane bridge in BisNHC− palladium− chloride complexes. Synthesis, structure, and catalytic activity." *Organometallics* **2006**, *25*, 5409-5415.
5. Ouellette, R. J.; Shaw, D. L.; South, A., Jr. "The Cleavage of Cyclopropanes by Thallium Triacetate." *J. Am. Chem. Soc.* **1964**, *86*, 2744-2745. b) Ouellette, R. J.; South, A., Jr.; Shaw, D. L. "Oxidative Cleavage of Cyclopropanes. III.1,2 The Stereochemistry and Direction of Cleavage of Bicyclo[n.1.0]alkanes by Lead Tetraacetate and Thallium Triacetate." *J. Am. Chem. Soc.* **1965**, *87*, 2602-2607. c) Ouellette, R. J.; Kordosky, G.; Levin, C.; Williams, S. "Oxidation of substituted styrene by thallium triacetate." *J. Org. Chem.* **1969**, *34*, 4104-4108. d) Ouellette, R. J.; Williams, S. "Oxidative cleavage of cyclopropanes. VII. Kinetics of the cleavage of some bicyclo [n. 1.0] alkanes and spiro [n. 2] alkanes by thallium triacetate." *J. Org. Chem.* **1970**, *35*, 3210-3213. e) McKillop, A.; Fowler, J. S.; Zelesko, M. J.; Hunt, J. D.; Taylor, E. C.; McGillivray, G. "Thallium in organic synthesis. IX. Facile thallation of aromatic compounds with thallium (III) trifluoroacetate (1, 2)." *Tetrahedron Lett.* **1969**, *10*, 2423-2426. f) McKillop, A.; Fowler, J. S.; Zelesko, M. J.; Hunt, J. D.; Taylor, E. C.; McGillivray, G. "Thallium in organic synthesis. X. A one-step synthesis of aryl iodides." *Tetrahedron Lett.* **1969**, *10*, 2427-2430. g) McKillop, A.; Hunt, J. D.; Zelesko, M. J.; Fowler, J. S.; Taylor, E. C.; McGillivray, G.; Kienzle, F. "Thallium in organic synthesis. XXII. Electrophilic aromatic thallation using thallium (III) trifluoroacetate. Simple synthesis of aromatic iodides." *J. Am. Chem. Soc.* **1971**, *93*, 4841-4844. h) Taylor, E. C.; Kienzle, F.; Robey, R. L.; McKillop, A.; Hunt, J. D. "Thallium in organic synthesis. XXIII. Electrophilic

aromatic thallation. Kinetics and applications to orientation control in the synthesis of aromatic iodides." *J. Am. Chem. Soc.* **1971**, *93*, 4845-4850. i) Elson, I. H.; Kochi, J. K. "Thallium (III) in one-electron oxidation of arenes by electron spin resonance." *J. Am. Chem. Soc.* **1973**, *95*, 5060-5062. j) Lau, W.; Kochi, J. K. "Kinetics and mechanism of aromatic thallation. Identification and proof of competing electrophilic and electron-transfer pathways." *J. Am. Chem. Soc.* **1984**, *106*, 7100-7112. k) Lau, W.; Kochi, J. K. "Arene activation with mercury (II) and thallium (III) electrophiles. Mechanistic relevance of charge-transfer transitions in π-complexes as intermediates." *J. Am. Chem. Soc.* **1986**, *108*, 6720-6732.

6. Periana, R. A.; Taube, D. J.; Evitt, E. R.; Löffler, D. G.; Wentrcek, P. R.; Voss, G.; Masuda, T., "A mercury-catalyzed, high-yield system for the oxidation of methane to methanol." *Science* **1993**, *259*, 340-343.
7. Hashiguchi, B. G.; Konnick, M. M.; Bischof, S. M.; Gustafson, S. J.; Devarajan, D.; Gunsalus, N.; Ess, D. H.; Periana, R. A "Main-group compounds selectively oxidize mixtures of methane, ethane, and propane to alcohol esters." *Science* **2014**, *343*, 1232-1237.
8. a) Vargaftik, M. N.; Stolarov, I. P.; Moiseev, I. I., "Highly selective partial oxidation of methane to methyl trifluoroacetate." *J. Chem. Soc., Chem. Commun*. **1990**, 1049-1050. b) Stolarov, I. P.; Vargaftik, M. N.; Shishkin, D. I.; Moiseev, I. I., "Oxidation of ethane and propane with cobalt (II) catalyst: unexpected formation of 1, 2-diol esters and C–C bond cleavage." *J. Chem. Soc., Chem. Commun.* **1991**, 938-939. c) Strassner, T.; Ahrens, S.; Muehlhofer, M.; Munz, D.; Zeller, A., "Cobalt-Catalyzed Oxidation of Methane to Methyl Trifluoroacetate by Dioxygen" *Eur. J. Inorg. Chem.* **2013**, *2013*, 3659-3663. d) Sen, A., *Acc. Chem. Res.* **1998**, *31*, 550-557.
9. Elson, I. H.; Kochi, J. K., "Thallium (III) in one-electron oxidation of arenes by electron spin resonance." *J. Am. Chem. Soc.* **1973**, *95*, 5060-5062. b) Lau, W.; Kochi, J. K., "Kinetics and mechanism of aromatic thallation. Identification and proof of competing electrophilic and electron-transfer pathways." *J. Am. Chem. Soc.* **1984**, *106*, 7100-7112. c) Lau, W.; Kochi, J. K., "Arene activation with mercury (II) and thallium (III) electrophiles. Mechanistic relevance of charge-transfer transitions in. pi.-complexes as intermediates." *J. Am. Chem. Soc.* **1986**, *108*, 6720-6732.
10. Gustafson, S. J.; Fuller, J. T. III; Devarajan, D.; Snyder, J.; Periana, R. A.; Hashiguchi, B. G.; Konnick, M. M.; Ess, D. H. "Contrasting Mechanisms and Reactivity of Tl (III), Hg (II), and Co (III) for Alkane C–H Functionalization." *Organometallics* **2015**, *34*, 5485-5495.
11. Frisch, M. J.; Trucks, G. W.; Schlegel, H. B.; Scuseria, G. E.; Robb, M. A.; Cheeseman, J. R.; Scalmani, G.; Barone, V.; Mennucci, B.; Petersson, G. A.; Nakatsuji, H.; Caricato, M.; Li, X.; Hratchian, H. P.; Izmaylov, A. F.; Bloino, J.; Zheng, G.; Sonnenberg, J. L.; Hada, M.; Ehara, M.;

Toyota, K.; Fukuda, R.; Hasegawa, J.; Ishida, M.; Nakajima, T.; Honda, Y.; Kitao, O.; Nakai, H.; Vreven, T.; Montgomery, J. A., Jr.; Peralta, J. E.; Ogliaro, F.; Bearpark, M.; Heyd, J. J.; Brothers, E.; Kudin, K. N.; Staroverov, V. N.; Kobayashi, R.; Normand, J.; Raghavachari, K.; Rendell, A.; Burant, J. C.; Iyengar, S. S.; Tomasi, J.; Cossi, M.; Rega, N.; Millam, N. J.; Klene, M.; Knox, J. E.; Cross, J. B.; Bakken, V.; Adamo, C.; Jaramillo, J.; Gomperts, R.; Stratmann, R. E.; Yazyev, O.; Austin, A. J.; Cammi, R.; Pomelli, C.; Ochterski, J. W.; Martin, R. L.; Morokuma, K.; Zakrzewski, V. G.; Voth, G. A.; Salvador, P.; Dannenberg, J. J.; Dapprich, S.; Daniels, A. D.; Farkas, Ö.; Foresman, J. B.; Ortiz, J. V.; Cioslowski, J.; Fox, D. J. Gaussian 09, Revision B.01, Gaussian, Inc., Wallingford CT, **2009**.

12. a) Zhao, Y.; Truhlar, D., "The M06 suite of density functionals for main group thermochemistry, thermochemical kinetics, noncovalent interactions, excited states, and transition elements: two new functionals and systematic testing of four M06-class functionals and 12 other functionals." *Theor. Chem. Acc.* **2008**, *120*, 215-241. b) Zhao, Y.; Truhlar, D. G., "Density functionals with broad applicability in chemistry." *Acc. Chem. Res.* **2008**, *41*, 157-167.
13. a) Rappoport, D.; Furche, F. "Property-optimized Gaussian basis sets for molecular response calculations." *J. Chem. Phys.* **2010**, *133*, 134105-1-11. b) Metz, B.; Stoll, H.; Dolg, M. "Small-core multiconfiguration-Dirac–Hartree–Fock-adjusted pseudopotentials for post-d main group elements: Application to PbH and PbO." *J. Chem. Phys.* **2000**, *113*, 2563-2569.
14. Marenich, A. V.; Cramer, C. J.; Truhlar, D. G., "Universal Solvation Model Based on Solute Electron Density and on a Continuum Model of the Solvent Defined by the Bulk Dielectric Constant and Atomic Surface Tensions." *J. Phys. Chem. B.* **2009**, *113*, 6378-6396.
15. a) Munz, D.; Meyer, D.; Strassner, T., "Methane CH activation by palladium complexes with chelating bis (NHC) ligands: a DFT study." *Organometallics* **2013**, *32*, 3469-3480. b) Fu, R.; Nielsen, R. J.; Goddard III, W. A.; Fortman, G. C.; Gunnoe, T. B., "DFT Virtual Screening Identifies Rhodium–Amidinate Complexes As Potential Homogeneous Catalysts for Methane-to-Methanol Oxidation." *ACS Catal.* **2014**, *4*, 4455-4465. c) Konnick, M. M.; Hashiguchi, B. G.; Devarajan, D.; Boaz, N. C.; Gunnoe, T. B.; Groves, J. T.; Gunsalus, N.; Ess, D. H.; Periana, R. A., "Selective CH functionalization of methane, ethane, and propane by a perfluoroarene iodine (III) complex." *Angew. Chem., Int. Ed.* **2014**, *53*, 10490-10494.
16. a) Grushin, V. V.; Marshall, W. J.; Thorn, D. L. "Electrophilic Stannylation of Arenes: A New S_EAr Reaction." *Adv. Synth. Catal.* **2001**, *343*, 433-438. b) Sartori, P.; Weidenbruch, M. "On the representation and properties of perfluoracyloxy compounds of the fourth group of the periodic

table." *Chem. Ber.* **1967**, *100*, 2049-2063. c) Sara, A. N.; Augbøl, K. "Chlorotin carboxylates by direct substitution on tin tetrachloride." *J. Inorg. Nucl. Chem.* **1973**, *35*, 1827-1831.

17. a) Faggiani, R.; Brown, I. D. "Thallium triacetate monohydrate." *Acta Crystallographica Section B* **1982**, *38*, 2473-2475. b) Butler, R. N. "Comparative reactions of nitrogen compounds with the isoelectronic series mercury (II), thallium (III), and lead (IV) acetates. Principles of oxidation reactions." *Chem. Rev.* **1984**, *84*, 249-276.
18. Lau, W.; Huffman, J. C.; Kochi, J. K., "Molecular structure and charge transfer excitation of electron donor-acceptor complexes. Ion pairs from arenes and mercury (II)." *J. Am. Chem. Soc.* **1982**, *104*, 5515-5517.
19. a) Henry, P. M. "Thallation and coupling of aromatics." *J. Org. Chem.* **1970**, *35*, 3083-3086. b) Briody, J. M.; Moore, R. A. "Kinetics and mechanism of the thalliation of benzene and toluene by thallium(III) acetate catalyzed by perchloric and sulfuric acid in aqueous acetic acid." *J. Chem. Soc, Perkin Trans. 2* **1972**, 179-183. c) Kwok, P. Y.; Stock, L. M.; Wright, T. L. "Partial rate factors for the thallation of toluene." *J. Org. Chem.* **1979**, *44*, 2309-2311. d) Roberts, R. M. G., "Kinetics and mechanism of aromatic thalliation and mercuriation-an NMR study." *Tetrahedron* **1980**, *36*, 3281-3287.
20. a) Boutadla, Y.; Davies, D. L.; Macgregor, S. A.; Poblador-Bahamonde, A. I. "Mechanisms of C–H bond activation: rich synergy between computation and experiment." *Dalton Trans.* **2009**, 5820-5831. b) Davies, D. L.; Donald, S. M. A.; Macgregor, S. A. "Computational study of the mechanism of cyclometalation by palladium acetate." *J. Am. Chem. Soc.* **2005**, *127*, 13754-13755. c) Davies, D. L.; Donals, S. M. A.; Al-Duaij, O.; Macgregor, S. A.; Pölleth, M. "Electrophilic C− H Activation at {Cp* Ir}: Ancillary-Ligand Control of the Mechanism of C− H Activation." *J. Am. Chem. Soc.* **2006**, *128*, 4210-4211.
21. Ess, D. H.; Goddard, W. A. III; Periana, R. A. "Electrophilic, Ambiphilic, and Nucleophilic C−H Bond Activation: Understanding the Electronic Continuum of C−H Bond Activation Through Transition-State and Reaction Pathway Interaction Energy Decompositions." *Organometallics* **2010**, *29*, 6459-6472.
22. Balcells, D.; Clot, E.; Eisenstein, O. "C-H Bond Activation in Transition Metal Species from a Computational Perspective." *Chem. Rev.* **2010**, *110*, 749-823.
23. Ackermann, L. "Carboxylate-assisted transition-metal-catalyzed C−H bond functionalizations: mechanism and scope." *Chem. Rev.* **2011**, *111*, 1315-1345.

24. King, C. R.; Gustafson, S. J.; Ess, D. H. The Electronics of CH Activation by Energy Decomposition Analysis: From Transition Metals to Main-Group Metals in Structure and Bonding, Vol. 167, **2015**, 163-178.
25. a) Gonzales, J. M.; Distasio, R. Jr.; Periana, R. A.; Goddard, W. A. III; Oxgaard, J. "Methylrhenium Trioxide Revisited: Mechanisms for Nonredox Oxygen Insertion in an M−CH_3 Bond." *J. Am. Chem. Soc.* **2007**, *129*, 15794-15804. b) Conley, B. L.; Ganesh, S. K.; Gonzales, J. M.; Tenn, W. J. III; Young, K. J. H.; Oxgaard, J.; Goddard, W. A. III; Periana, R. A. "Facile functionalization of a metal carbon bond by O-atom transfer." *J. Am. Chem. Soc.* **2006**, *128*, 9018-9019. c) Pouy, M. J.; Milczek, E. M.; Figg, T. M.; Otten, B. M.; Prince, B. M.; Gunnoe, T. B.; Cundari, T. R.; Groves, T. J. "Flavin-catalyzed insertion of oxygen into rhenium–methyl bonds." *J. Am. Chem. Soc.* **2012**, *134*, 12920-12923. d) Tenn, W. J. III, Conley, B. L.; Hövelmann, Ahlquist, M.; Nielsen, R. J. Ess, D. H.; Oxgaard, J.; Bischof, S. M.; Goddard, W. A. III; Periana, R. A. "Oxy-functionalization of nucleophilic rhenium (I) metal carbon bonds catalyzed by selenium (IV)" *J. Am. Chem. Soc.* **2009**, *131*, 2466-2468. e) Mei, J.; Carsch, K. M.; Freitag, C. R.; Gunnoe, T. B.; Cundari, T. R. "Variable Pathways for Oxygen Atom Insertion into Metal–Carbon Bonds: The Case of Cp*$W(O)_2(CH_2SiMe_3)$" *J. Am. Chem. Soc.* **2013**, *135*, 424-435.
26. Prince, B. M.; Gunnoe, T. B.; Cundari, T. R. "Oxy-functionalization of Group 9 and 10 transition metal methyl ligands: use of pyridine-based hemi-labile ligands." *Dalton Trans.* **2014**, *43*, 7608-7614.
27. a) Figg, T. M.; Webb, J. R.; Cundari, T. R.; Gunnoe, T. B. "Carbon–oxygen bond formation via organometallic Baeyer–Villiger transformations: a computational study on the impact of metal identity" *J. Am. Chem. Soc.* **2012**, *134*, 2332-2339. b) Figg, T. M.; Cundari, T. R.; Gunnoe, T. B. "Non-redox Oxy-Insertion via Organometallic Baeyer–Villiger Transformations: A Computational Hammett Study of Platinum (II) Complexes" *Organometallics* **2011**, 30, 3779-3785. c) Figg, T. M.; Cundari, T. R. "Computational Hammett analysis of redox based oxy-insertion by Pt (II) complexes" *Dalton Trans.* **2013**, *42*, 4114-4121.
28. Garrett, E. C. III; Figg, T. M.; Cundari, T. R. "Impact of d-Orbital Occupation on Metal–Carbon Bond Functionalization." *Inorg. Chem.* **2014**, *53*, 7789-7798.
29. a) Zamashchikov, V. V.; Rudakov, E. S.; Mitchenko, S. A.; Pekhtereva, T. M. "Kinetics of decomposition of a methyl platinum(IV) complex in aqueous sodium chloride-sodium perchlorate solutions." *Koord. Khim.* **1985**, *11*, 69-72. b) Luinstra, G. A.; Labinger, J. A.; Bercaw, J. E. "Mechanism and stereochemistry for nucleophilic attack at carbon of platinum(IV) alkyls: model reactions for hydrocarbon oxidation with aqueous platinum chlorides." *J. Am. Chem. Soc.* **1993**,

115, 3004-3005. d) Williams, B. S.; Goldberg, K. I. "Studies of Reductive Elimination Reactions To Form Carbon−Oxygen Bonds from Pt (IV) Complexes." *J. Am. Chem. Soc.* **2001**, *123*, 2576-2587. e) Williams, B. S.; Holland, A. W.; Goldberg, K. I. "Direct Observation of C−O Reductive Elimination from Pt (IV)" *J. Am. Chem. Soc.* **1999**, *121*, 252-253.

30. Labinger, J. A. "Platinum-catalyzed C–H functionalization." *Chem. Rev.* **2017**, *117*, 8483-8496.
31. Gilbert, T. M.; Hristov, I.; Ziegler, T. "Comparison between Oxidative Addition and σ-Bond Metathesis as Possible Mechanisms for the Catalytica Methane Activation Process by Platinum(II) Complexes: A Density Functional Theory Study." *Organometallics* **2001**, *20*, 1183-1189. b) Hristove, I. H.; Ziegler, T. "The Possible Role of SO_3 as an Oxidizing Agent in Methane Functionalization by the Catalytica Process. A Density Functional Theory Study" *Organometallics* **2003**, *22*, 1668-1674.
32. Paul, Ankan, Musgrave, C. B. "A detailed theoretical study of the mechanism and energetics of methane to methanol conversion by cisplatin and catalytica." *Organometallics* **2007**, *26*, 793-809.
33. a) Kua, J.; Xu, X.; Periana, R. A.; Goddard, W. A. III "Stability and Thermodynamics of the $PtCl_2$ Type Catalyst for Activating Methane to Methanol: A Computational Study" *Organometallics* **2002**, *21*, 511-525. b) Ahlquist, M.; Nielsen, R. J.; Periana, R. A.; Goddard, W. A. III "Product protection, the key to developing high performance methane selective oxidation catalysts" *J. Am. Chem. Soc.* **2009**, *131*, 17110-17115. c) Mironov, O. A.; Bischof, S. M.; Konnick, M. M.; Hahiguchi, B. G.; Ziatdinov, V. R.; Goddard, W. A. III; Ahlquist, M.; Periana, R. A. "Using Reduced Catalysts for Oxidation Reactions: Mechanistic Studies of the "Periana-Catalytica" System for CH_4 Oxidation" *J. Am. Chem. Soc.* **2013**, *135*, 14644-14658.
34. Aseman, M. D.; Nabavizadeh, S. M.; Hosseini, F. N.; Wu, G.; Abu-Omar, M. "Carbon–Oxygen Bond Forming Reductive Elimination from Cycloplatinated (IV) Complexes" *Organometallics*, **2018**, *37*, 87-98.
35. a) Zerella, M.; Kahros, A.; Bell, A. T., "Methane oxidation to acetic acid catalyzed by Pd^{2+} cations in the presence of oxygen" *J. Catal.* **2006**, *237*, 111-117. b) Chempath, S.; Bell, A. T. "Density Functional Theory Analysis of the Reaction Pathway for Methane Oxidation to Acetic Acid Catalyzed by Pd^{2+} in Sulfuric Acid" *J. Am. Chem. Soc.* **2006**, *128*, 4650-4657.
36. a) Munz, D.; Meyer, D.; Strassner, T. "Methane CH activation by palladium complexes with chelating bis (NHC) ligands: a DFT study" *Organometallics* **2013**, *32*, 3469-3480. b) Munz, D.; Strassner, T. "On the Mechanism of the Palladium Bis (NHC) Complex Catalyzed CH Functionalization of Propane: Experiment and DFT Calculations" *Chem. Eur. J.* **2014**, *20*, 14872-14879.

37. a) Vedernikov, A. N.; Binfield, S. A.; Zavalij, P. Y.; Khusnutdinova, J. R. "Stoichiometric Aerobic Pt^{II}–Me Bond Cleavage in Aqueous Solutions to Produce Methanol and a Pt^{II}(OH) Complex" *J. Am. Chem. Soc.* **2006**, *128*, 82-83. b) Khusnutdinova, J. R. Zavalij, P. Y.; Vedernikov, A. N. "C−O Coupling of $LPt^{IV}Me(OH)X$ Complexes in Water (X = ^{18}OH, OH, OMe; L = di(2-pyridyl)methane sulfonate)" *Organometallics* **2007**, *26*, 3466-3483. c) Lotz, M. D.; Remy, M. S.; Lao, D. B.; Ariafard, A.; Yates, B. F.; Canty, A. J.; Mayer, J. M.; Sanford, M. S. "Formation of Ethane from Mono-Methyl Palladium (II) Complexes" *J. Am. Chem. Soc.* **2014**, *136*, 8237-8242.
38. Jones, C. J.; Taube, D.; Ziatdinov, V. R.; Periana, R. A.; Nielsen, R. J.; Oxgaard, J.; Goddard, W. A. "Selective Oxidation of Methane to Methanol Catalyzed, with C-H Activation, by Homogeneous, Cationic Gold." *Angew. Chem., Int. Ed.* **2004**, *43*, 4626-4629.
39. Scott, V. J.; Labinger, J. A.; Bercaw, J. E. "Mechanism of Reductive Elimination of Methyl Iodide from a Novel Gold (III)−Monomethyl Complex" *Organometallics*, **2010**, *29*, 4090-4096.
40. Fuller, J. T., III; Butler, S.; Devarajan, D.; Jacobs, A.; Hashiguchi, B. G.; Konnick, M. M.; Goddard, W. A., III; Gonzales, J.; Periana, R. A.; Ess, D. H. "Catalytic Mechanism and Efficiency of Methane Oxidation by Hg (II) in Sulfuric Acid and Comparison to Radical Initiated Conditions" *ACS Catal*. **2016**, *6*, 4312-4322.
41. Pahls, D. R.; Groves, J. T.; Gunnoe, T. B.; Cundari, T. R. "Theoretical Study of Reductive Functionalization of Methyl Ligands of Group 9 Complexes Supported by Two Bipyridyl Ligands: A Key Step in Catalytic Hydrocarbon Functionalization" *Organometallics* **2014**, *33*, 1936-1944.
42. a) O'Reilly, M. E.; Pahls, D. R.; Cundari, T. R.; Gunnoe, T. B. "Reductive Functionalization of a Rhodium (III)–Methyl Bond in Acidic Media: Key Step in the Electrophilic Functionalization of Methane" *Organometallics* **2014**, *33*, 6504-6510. b) O'Reilly, M. E.; Pahls, D. R.; Webb, J. R.; Boaz, N. C.; Majumdar, S.; Hoff, C. D.; Groves, J. T.; Cundari, T. R.; Gunnoe, T. B. "Reductive functionalization of a rhodium (III)–methyl bond by electronic modification of the supporting ligand" *Dalton Trans.* **2014**, *43*, 8273-8281.
43. Fu, R.; Nielsen, R. J.; Goddard, W. A. III; Fortman, G. C.; Gunnoe, T. B. "DFT Virtual Screening Identifies Rhodium–Amidinate Complexes As Potential Homogeneous Catalysts for Methane-to-Methanol Oxidation" *ACS Catal.* **2014**, *4*, 4455-4465.
44. Gallah, H.; Cundari, T. R. "Reductive functionalization of 3d metal–methyl complexes: The greater importance of ligand than metal" *Comput. Theor. Chem.* **2015**, *1069*, 86-95.
45. Konnick, M. M.; Hashiguchi, B. G.; Devarajan, D.; Boaz, N. C.; Gunnoe, T. B.; Groves, J. T.; Gunsalus, N.; Ess, D. H.; Periana, R. A. "Selective CH functionalization of methane, ethane, and propane by a perfluoroarene iodine (III) complex" *Angew. Chem. Int. Ed.* **2014**, *53*, 10490-10494.

46. a) Teaw, S. L.; Thornton, b. W.; Qian, J.; Jia, F.; Pahls, D.; Cundari, T. R. "DFT study of reductive functionalization in cis and trans cobalt–methyl–bipyridine complexes" *Comput. Theor. Chem.* **2015**, *1073*, 102-105. b) Fallah, H.; Horng, F.; Cundari, T. R. "Theoretical Study of Two Possible Side Reactions for Reductive Functionalization of 3d Metal–Methyl Complexes by Hydroxide Ion: Deprotonation and Metal–Methyl Bond Dissociation" *Organometallics* **2016**, *35*, 950-958.
47. Cheng, M-J.; Nielsen, R. J.; Goddard, W. A. III "A homolytic oxy-functionalization mechanism: intermolecular hydrocarbyl migration from M–R to vanadate oxo" *Chem. Commun.* **2014**, *50*, 10994-10996.
48. a) Fortman, G. C.; Boaz, N. C.; Munz, D.; Konnick, M. M.; Periana, R. A.; Groves, J. T.; Gunnoe, T. B. "Selective monooxidation of light alkanes using chloride and iodate" *J. Am. Chem. Soc.* **2014**, *136*, 8393-8401. b) Kalman, S. E.; Munz, D.; Fortman, G. C.; Boaz, N. C.; Groves, J. T.; Gunnoe, T. B. "Partial oxidation of light alkanes by periodate and chloride salts" *Dalton Trans.* **2015**, *44*, 5294-5298.
49. Schwartz, N. A.; Boaz, N. C.; Kalman, S. E.; Zhuang, T.; Goldberg, J. M.; Fu, R.; Nielsen, R. J.; Goddard, W. A. III; Groves, J. T.; Gunnoe, T. B. "Mechanism of Hydrocarbon Functionalization by an Iodate/Chloride System: The Role of Ester Protection" *ACS Catal.* **2018**, *8*, 3138-3149.
50. a) Boisvert, L.; Denney, M. C.; Hanson, S. K.; Goldberg, K. I "Insertion of molecular oxygen into a palladium (II) methyl bond: a radical chain mechanism involving palladium (III) intermediates" *J. Am. Chem. Soc.* **2009**, *131*, 15802-15814. b) Grice, K. A.; Goldberg, K. I. "Insertion of Dioxygen into a Platinum (II)−Methyl Bond To Form a Platinum (II) Methylperoxo Complex" *Organometallics* **2009**, 28, 953-955. c) Boisvert, L.; Goldberg, K. I. "Reactions of late transition metal complexes with molecular oxygen" *Acc. Chem. Res.* **2012**, 45, 899-910. d) Goldberg, K. I.; Goldman, A. S. "Large-scale selective functionalization of alkane" *Acc. Chem. Res.* **2017**, *50*, 620-626.
51. a) Taylor, R. A.; Law, D. J.; Sunley, G. J.; White, A. J. P.; Britovsek, G. J. P. "Towards photocatalytic alkane oxidation: The insertion of dioxygen into a platinum (II)–methyl bond" *Angew. Chem. Int. Ed.* **2009**, *48*, 5900-5903. b) Petersen, A. R.; Taylor, R. A.; Vincente-Hernández, I.; Mallender, P. R.; Olley, H.; White, A. J. P.; Britovsek, G. J. P. "Oxygen insertion into metal carbon bonds: formation of methylperoxo Pd (II) and Pt (II) complexes via photogenerated dinuclear intermediates" *J. Am. Chem. Soc.* **2014**, *136*, 14089-14099.
52. a) Lehman, M. C.; Boyle, P. D.; Sommer, R. D.; Ison, E. A. "Oxyfunctionalization with Cp*Ir^{III}(NHC)(Me)L Complexes" *Organometallics* **2014**, *33*, 5081-5084. b) Lehnman, M. C.; Pahls, D. R.; Meredith, J. M.; Sommer, R. D.; Heinekey, D. M.; Cundari, T. R.; Ison, E. A.

"Oxyfunctionalization with $Cp^*Ir^{III}(NHC)(Me)(Cl)$ with O_2: Identification of a Rare Bimetallic IrIV μ-Oxo Intermediate." *J. Am. Chem. Soc.* **2015**, *137*, 3574.

Chapter 3:

Arene C-H Functionalization by P-Block Metal Tl(III) Occurs at the Borderline of C-H Activation and Electron Transfer

3.1 Introduction

Modern arene C-H functionalization[1] reactions are dominated by 2nd-row and 3rd-row transition metals, such as Pd^{II},[2] Rh^{III},[3] and Ir^{III}.[4] Our computational group is interested in alternative p-block main-group elements and metals that mediate C-H activation reactions. Using density functional theory (DFT), we previously proposed that Tl^{III} and other main-group metals functionalize light alkane C-H bonds through a C-H activation mechanism that involves the formation of an organometallic metal-alkyl (MR) intermediate (Scheme 3-1a).[5] This discovery prompted us to examine the possibility that arene C-H functionalization by p-block main-group Tl^{III} that has traditionally been attributed to an electrophilic aromatic substitution (S_EAr) mechanism might also proceed by a C-H activation mechanism (Scheme 3-1b).

McKillop and co-workers[6] reported that thallation of benzene by $Tl^{III}(TFA)_3$ (TFA = trifluoroacetate), formed from Tl^{III} oxide in trifluoroacetic acid (TFAH), gives $(TFA)_2Tl^{III}(Ph)$ as an intermediate in route to iodobenzene (Scheme 1b). $(TFA)_2Tl^{III}(Ph)$ was directly observed using ^1H NMR. For alkyl substituted benzenes, such as toluene, para C-H substitution is highly favored, while for benzoic acid and methyl benzoate, ortho iodo functionalized arenes are the major product (Scheme 3-1c).[6c]

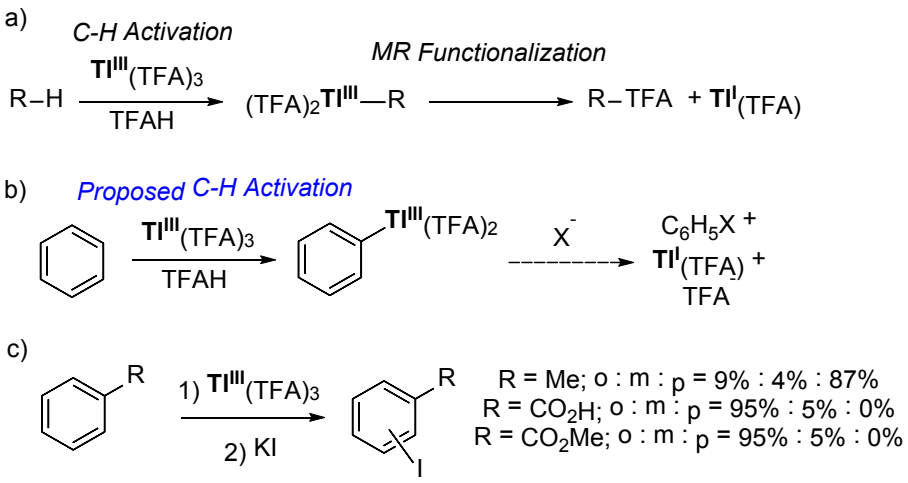

Scheme 3-1. a) Alkane C-H functionalization by Tl^{III}.[5] b) Arene C-H activation and functionalization.[6a] c) Arene thallation regioselectivity.[6b]

McKillop and co-workers suggested that $(TFA)_2Tl^{III}(Ph)$ is formed by an S_EAr mechanism with a Wheland-type (σ-complex) intermediate. However, Kochi[7] subsequently reported electron spin resonance (ESR) and spectroscopic studies that showed the presence of charge-transfer complexes and aryl radicals for arene functionalization reactions with $Tl^{III}(TFA)_3$. Biaryl products of up to ~10% yield were also reported for reactions with highly substituted arenes. Based on this evidence, and studies with added LiTFA, Kochi proposed that a reactive monocationic Tl^{III} species forms a charge-transfer complex that subsequently evolves to either a solvent-separated electron transfer (ET) pair or a Wheland intermediate leading to arene thallation (Scheme 3-2a).[7c]

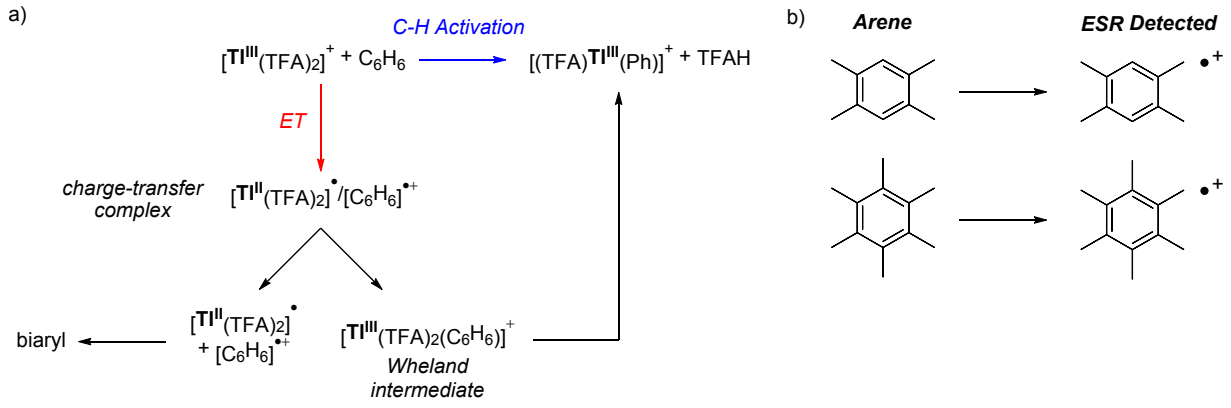

Scheme 3-2. a) Possible arene thallation mechanisms. b) Examples of ET intermediates observed.

Here we report density functional theory (DFT) calculations (M06/def2-TZVPPD//M06/6-31+G(d,p)[LANL2DZdp], SMD solvent)[8] that reveal benzene, mono-substituted arenes, and di-substituted arenes undergo a one-step C-H activation thallation mechanism that is akin to transition metal C-H bond activation. Calculations also show that similar to transition metal C-H activation, arene directing groups (e.g. carboxylate group) result in metal coordination and highly regioselective C-H activation. For highly substituted/electron-rich arenes, ET becomes competitive or even preferred over C-H activation, and outersphere ET energies correlate with the observed crossover from a C-H activation regime to an ET regime.

3.2 Results and Discussion

Based on our previous report of alkane C-H functionalization by $Tl^{III}(TFA)_3$, we adopted two Tl^{III} models. The first model is the neutral $Tl^{III}(TFA)_3$ without explicit solvent where each TFA coordinates with the Tl^{III} metal center through a κ^2 interaction (see Appendix 2 for low-energy $Tl^{III}(TFA)_3$ structures). A multinuclear Tl^{III} model (e.g. $Tl_2(TFA)_6$) was not used since kinetic studies of arene C-H bond oxidation by $Tl^{III}(TFA)_3$ show first-order rate dependence on Tl^{III}.[7b,9] While this is not definitive, it does suggest reactivity at a single metal site without pre-equilibrium dissociation of a multinuclear species. For a monocationic Tl^{III} model we used the explicit solvent stabilized complex $[Tl^{III}(TFA)_2(TFAH)]^+$, TFAH = trifluoroacetic acid. We previously estimated the energy to achieve $[Tl^{III}(TFA)_2(TFAH)]^+ + [(TFA)(TFAH)]^-$ as ΔH = ~25 kcal/mol (ΔG = ~30 kcal/mol). In general, this ΔH value suggests neutral Tl^{III} pathways may be lower in energy than monocationic pathways. Kochi's proposal of the reactive $[Tl^{III}(TFA)_2]^+$ species was based on rate studies in which added LiTFA resulted in a decrease of k_{obs} for arene C-H bond thallation. With a 1:1 ratio of $Tl(TFA)_3$: mesitylene in TFAH solvent, k_{obs} was found to be 0.36 s^{-1}.[7b] With two

equivalents of LiTFA k_{obs} decreases to 0.026 s^{-1}.[7b] While the rate suppression with added TFA could suggest a dissociative mechanism involving $[Tl^{III}(TFA)_2]^+$, it is also possible that added TFA results in formation of $[Tl^{III}(TFA)_4]^-$, which is less reactive than $Tl^{III}(TFA)_3$. This latter proposal is supported by our calculation where formation of $[Tl^{III}(TFA)_4]^-$ ΔH = -32 kcal/mol (ΔG = -19 kcal/mol) relative to the neutral species and TFA. This result is consistent with reports from Blixt and co-workers suggesting that $[Tl^{III}(X)_4]^-$ complexes (X = Cl, Br, CN) are dominant in solutions containing excess anions.[10]

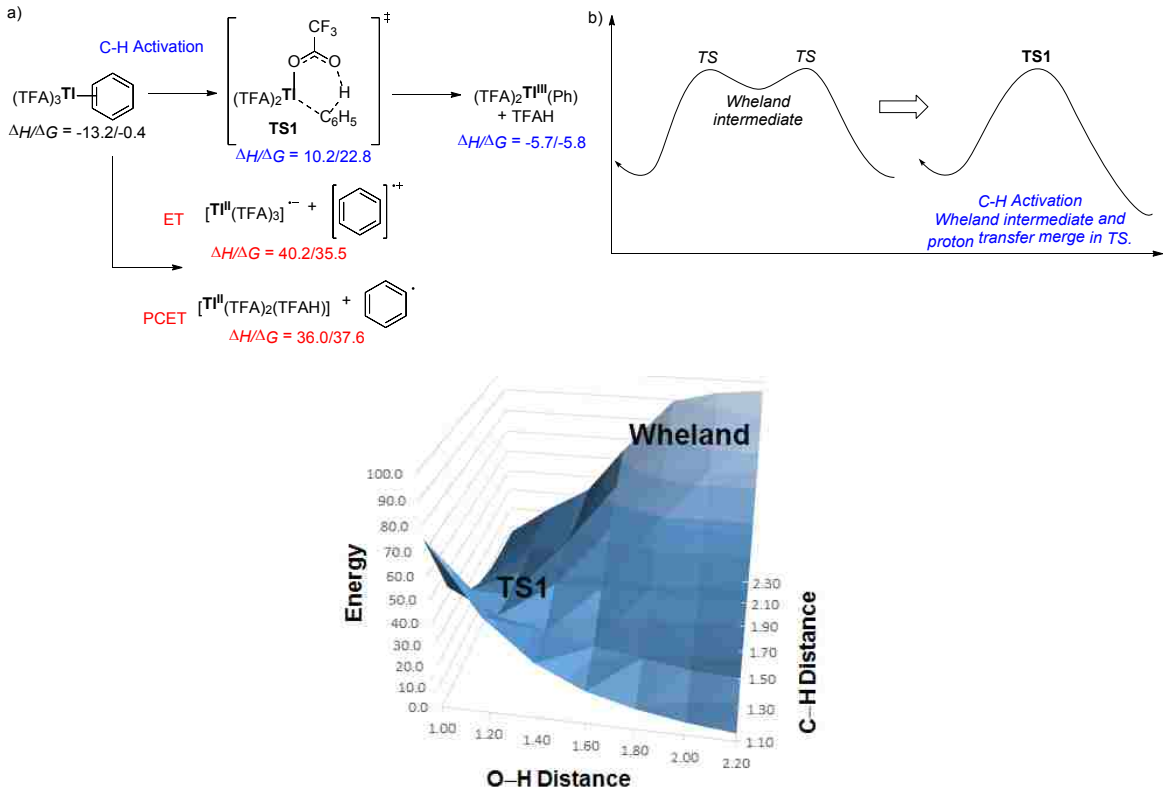

Scheme 3-3. Top: a) Mechanisms branching from the Tl-benzene charge-transfer complex. Energies relative to $Tl^{III}(TFA)_3$ + benzene. (kcal/mol) b) Diagram showing the merging of a Wheland intermediate and proton transfer into a one-step C-H activation process. Bottom: Potential energy surface with fixed Tl-C bond length of 2.43 Å. (kcal/mol, Å)

To begin, we examined π-coordination complexes between benzene and $Tl^{III}(TFA)_3$. Because the LUMO orbital of $Tl^{III}(TFA)_3$ is mainly 6s in character with little sp hybridization,

there is significant flexibility in benzene coordination ranging from η^1 to η^6 that are close in energy (see SI). While there is an enthalpic stabilization for forming $(TFA)_3Tl^{III}(\eta^2\text{-}C_6H_6)$ (ΔH = –13.3 kcal/mol, Scheme 3-3), ΔG is only exergonic by 1.2 kcal/mol relative to separated $Tl^{III}(TFA)_3$ and benzene. CHelpG and ESP atomic charges indicate that there is ~0.35 e of charge transfer from benzene to Tl^{III} in $(TFA)_3Tl^{III}(\eta^1\text{-}C_6H_6)$, see SI. This relatively large amount of charge transfer is consistent with UV excitations observed by Kochi,[7] and our TD-DFT calculations that show excitation from the benzene HOMO to the Tl^{III} LUMO (see Appendix 2).

There are multiple reaction pathways stemming from $(TFA)_3Tl^{III}(\eta^1\text{-}C_6H_6)$. The first pathway involves electrophilic C-H activation via **TS1** that forms $(TFA)_2Tl^{III}(Ph)$ by proton transfer to a TFA ligand with simultaneous formation of a Tl-Ph bond (Scheme 3a, Figure 3). Structurally, **TS1** is very similar to our previously reported Tl^{III}-alkane C-H activation transition state[5] and transition metal C-H activation transition states.[1d,11] With $\Delta H^{\ddagger}$ = 10.2 kcal/mol ($\Delta G^{\ddagger}$ = 22.8 kcal/mol) for **TS1** this C-H activation pathway is more viable than alternative ET or proton-coupled ET (PCET) pathways.[12] The short Tl-Ph bond length in **TS1** has structural similarities to a Wheland-type intermediate. However, the potential energy surface showed no definitive energy minimum for a Wheland intermediate (see Appendix 2). Extensive structure searching for Wheland-type intermediates with a fully formed Tl-Ph bond and dearomatized benzene either converged to π-complexes or **TS1**. This indicates that Tl-Ph bond formation merges with proton transfer to become a one-step C-H activation transition state (Scheme 3-3b). A similar concerted mechanism was proposed by Galabov and Schleyer for sulfonation of benzene in nonpolar solvent.[13] This proposal is consistent with the potential energy landscape at the bottom of Scheme 3-3 where proton transfer (O-H C-H distances) is plotted with a constant Tl-C bond length and TS1 is clearly a saddle point whereas Wheland-type structures are significantly higher in energy.

Alternative to C-H activation, we also considered the ET and PCET pathways shown in Scheme 3-3. Separation of the charge-transfer complex into $[Tl^{II}(TFA)_3]^{\bullet-}/[C_6H_6]^{\bullet+}$ results in formal outersphere ET and requires $\Delta H = 39.6$ kcal/mol ($\Delta G = 35.5$ kcal/mol). We considered that outersphere ET would be more viable from the monocationic Tl^{III}. Indeed, formation of $[Tl^{II}(TFA)_2]^{\bullet}/[C_6H_6]^{\bullet+}$ is more favorable with ΔH = 7.7 kcal/mol (ΔG = 3.4 kcal/mol), but combined with the ~25 kcal/mol energy for complete TFA dissociation this pathway is higher in energy than C-H activation for benzene. To avoid charge separated species, PCET could occur by ET from benzene to the Tl^{III} metal center with simultaneous proton transfer to a TFA ligand to give $[Tl^{II}(TFA)_2(TFAH)]^{\bullet}$ and $[C_6H_6]^{\bullet}$. The PCET pathway for benzene is only slightly lower in enthalpy than ET (~4 kcal/mol lower). Our proposal of C-H activation rather than ET and PCET for benzene is consistent with Kochi's report[7a] that only highly substituted arenes react with $Tl^{III}(TFA)_3$ to form biphenyls and show ESR active species. Also, the calculated C-H/C-D kinetic isotope effect (KIE) of ~5 for the C-H activation transition state between $Tl^{III}(TFA)_3$ and benzene based on zero-point energies is qualitatively consistent with the experimental value of 7.4 reported for the mesitylene arene C-H bond.[7,14]

We further examined the C-H activation free energy barriers for methyl-substituted benzenes. The barriers are plotted in Figure 3-1 and show that $\Delta G^{\ddagger}$ decreases from ~20 kcal/mol for benzene to ~10 kcal/mol for pentamethylbenzene. The nearly monotonic decrease in C-H activation $\Delta G^{\ddagger}$ suggests that the electron-donating capacity of the methyl groups outweighs destabilizing steric interactions. The thermodynamic ΔG for ET between $Tl^{III}(TFA)_3$ and methyl-substituted benzenes is also plotted in Figure 3-1. Outersphere ET becomes significantly more favorable with increasing methyl group substitution of benzene and ET becomes competitive with C-H activation at 3-4 methyl groups. This calculated crossover region from C-H activation to

competitive ET is consistent with radical cation ESR signals and arene dimer products observed by Kochi for tri- and tetra-substituted benzenes.[7b] The correct prediction of the crossover region using ET thermodynamics suggests that the kinetic ET barriers are similar to the ΔG values. Indeed, Marus theory estimates of $\Delta G^{\ddagger}$ for ET between $Tl^{III}(TFA)_3$ and benzene to be ~37 kcal/mol, which is ~14 kcal/mol higher in free energy than **TS1** (see Appendix 2). For ET between $Tl^{III}(TFA)_3$ and pentamethylbenzene the $\Delta G^{\ddagger}$ is ~13 kcal/mol, which shows competitive C-H activation and ET.

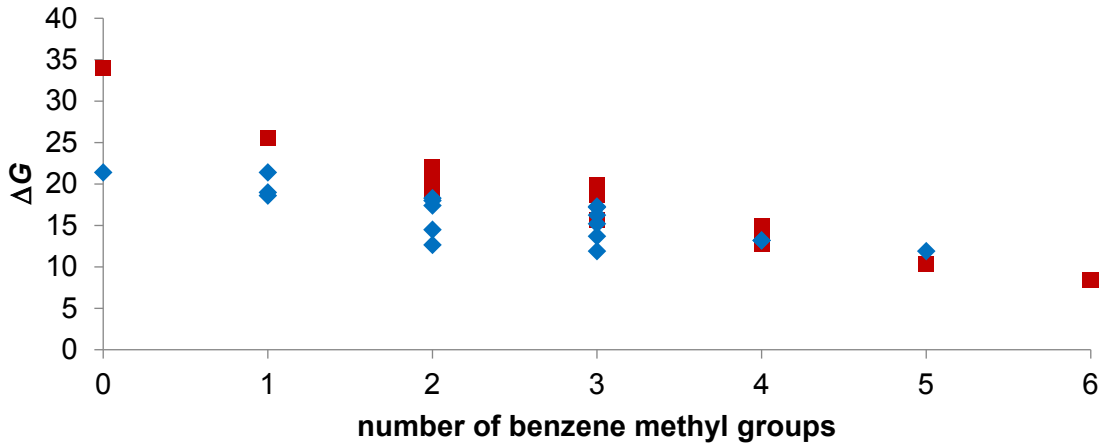

Figure 3-1. Plot of C-H activation free energy barriers (◆) and outersphere ET free energy (■) versus the number of benzene methyl group. (kcal/mol)

The Kochi and Olah[15] groups independently measured relative thallation reaction rates for methyl-substituted arenes with $Tl^{III}(TFA)_3$. The top of Figure 3-2 plots the calculated C-H activation $\Delta\Delta G^{\ddagger}$ values versus the experimental $\Delta\Delta G^{\ddagger}$ values derived from reaction rates (see Appendix 2). For nearly all arenes the relative C-H activation barriers display the correct qualitative reactivity. The bottom of Figure 3-2 shows a moderate R^2 of 0.76 for linear correlation between calculated and experimental $\Delta\Delta G^{\ddagger}$ values. This qualitative agreement of relative arene thallation reactivity supports the proposed C-H activation mechanism.

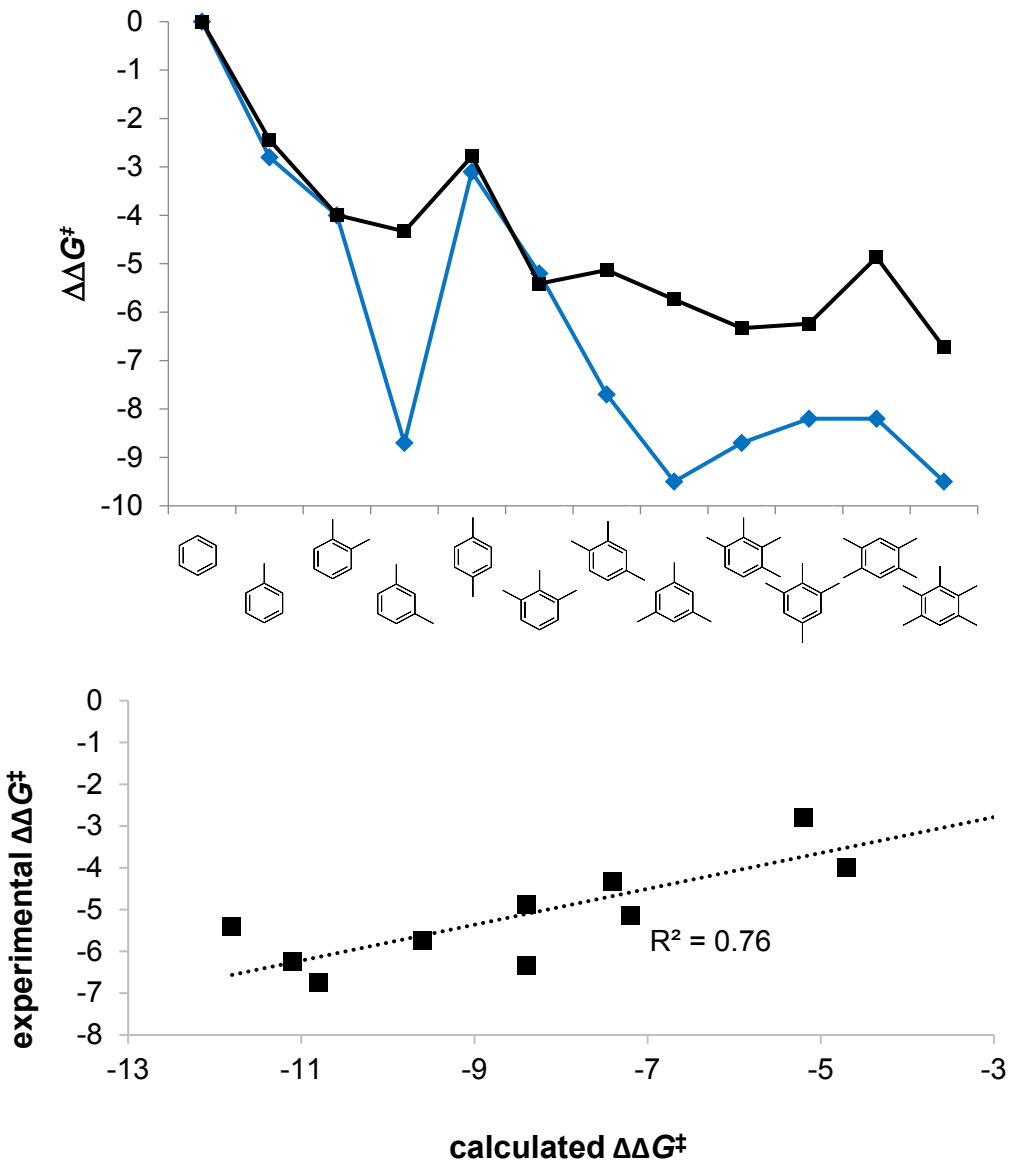

Figure 3-2. Top: Plot of calculated (◆) and experimental (■) $\Delta\Delta G^{\ddagger}$ values for C-H activation of methyl-substituted benzenes. Bottom: Linear correlation plot of calculated and experimental $\Delta\Delta G^{\ddagger}$ values. (kcal/mol) Experimental values used from reference 7b.

Thallation regioselectivity of arenes provides another means to test the proposed C-H activation mechanism. For toluene there is a significant preference for para thallation while for methyl benzoate there is a significant preference for ortho thallation. Figure 3-3 shows the

similarity between **TS1** and the para C-H activation transition state for toluene. For toluene the $\Delta\Delta G^{\ddagger}$ values for ortho, meta, and para C-H activation provide qualitative and semiquantitative correlation with the experimentally observed regioselectivity. For example, the transition state for para thallation of toluene is 1.6 kcal/mol lower in enthalpy than the transition state for ortho thallation, and 3.6 kcal/mol lower in enthalpy than the meta thallation transition state. This is consistent with the 9:6:85 ortho:meta:para ratio reported by Olah.[15] For methylbenzoate, the ortho C-H activation is 7.2 and 8.8 kcal/mol lower in enthalpy than para and meta C-H activation transition states, respectively, and thus overestimates the 95:5:0 ortho:meta:para ratio reported by McKillop.[6b] The preference for the ortho transition state is due to the CO_2Me group-Tl metal center interaction that directs C-H activation akin to ortho directing group interactions in transition metal C-H activation.[2c]

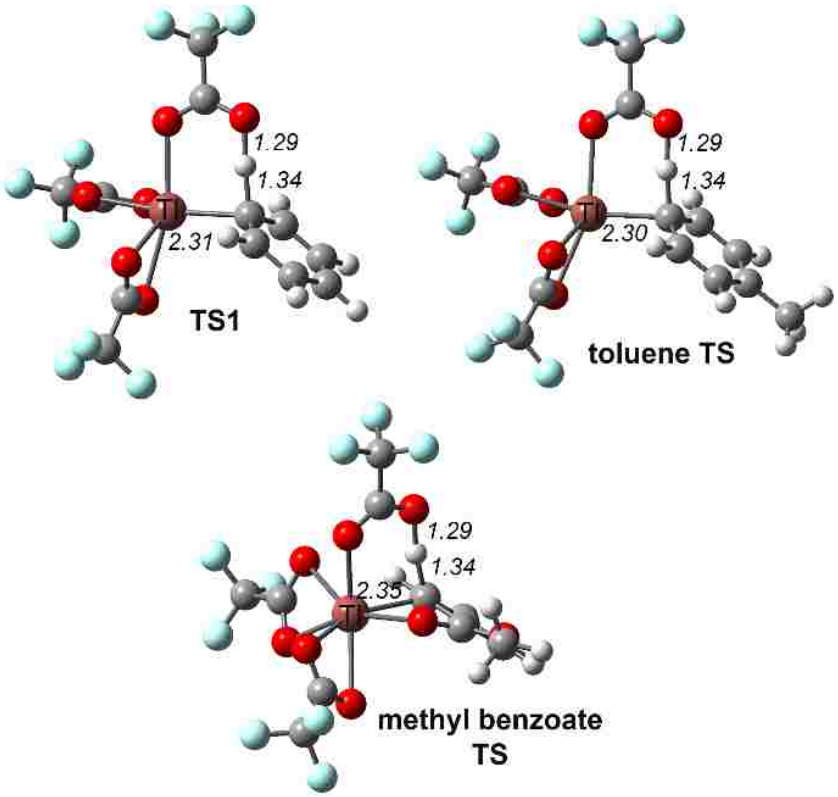

Figure 3-3. C-H activation transition-state structures. (Å)

3.3 Conclusions

M06 DFT calculations were used to compare C-H activation, ET, and PCET mechanisms for reaction of benzene with $Tl^{III}(TFA)_3$. An electrophilic C-H activation transition state by a neutral Tl^{III} is lowest energy and the calculated primary C-H/C-D KIE is consistent with experiment. The C-H activation transition state is similar to transition metal-mediated C-H activation transition states. The proposed C-H activation mechanism also provides an explanation for regioselective arene thallation with chelating and non-chelating arene functional groups. C-H activation is the lowest energy pathway for $Tl^{III}(TFA)_3$ reaction with benzene, toluene, and xylenes. However, for trimethyl and tetramethyl substituted benzenes, ET becomes the preferred pathway and calculations correctly predict the experimentally reported ET crossover region. Overall, these calculations provide evidence for arene C-H activation promoted by p-block main-group metal complexes. These calculations also provide details showing that changes in the functional groups of arenes can cause a shift from C-H activation to ET.

3.4 Computational Details

Calculations were performed with Gaussian 09.[16] Enthalpies and free energies refer to M06/def2-TZVPPD//M06/6-31+G(d,p)[LANL2DZdp].[8] We previously showed that this level of theory reproduces electron affinities for Tl cations.[5b] Minima and transition-state structures were verified by normal mode analysis and intrinsic reaction coordinate (IRC) calculations. A modified SMD solvent model for water,[8i] which accurately reproduces monocation Tl solvation, was used for TFAH solvent with radius = 2.479 Å and $\varepsilon = 8.42$. This strategy has been used in previous reports.[17] For CHelpG and ESP atomic charges the thallium Van der Waals radius was 1.96 Å.[18]

All enthalpies and free energies reported include ΔG_{solv}. Details of deriving $\Delta\Delta G^{\ddagger}$ values derived from reaction rates are given in Appendix 2.

3.5 References

1. For very recent reviews see: (a) Gensch, T.; Hopkinson, M. N.; Glorius, F.; Wencel-Delord, J., *Chem. Soc. Rev.* **2016**, *45*, 2900-2936. (b) Kapdi, A. R., *Dalt. Trans.* **2014**, *43*, 3021-3034. (c) Li, B.-J.; Shi, Z.-J., Homogeneous transition-metal-catalyzed C-H bond functionalization. In Homogeneous Catalysis for Unreactive Bond Activation, John Wiley & Sons, Inc.: Hoboken, NJ, **2015**; 441-573. For a review of computational aspects of C-H functionalization see: (d) Balcells, D.; Clot, E.; Eisenstein, O., *Chem. Rev.* **2010**, *110,* 749-823.
2. (a) Engle, K. M.; Mei, T.-S.; Wasa, M.; Yu, J.-Q., *Acc. Chem. Res.* **2012**, *45*, 788-802. (b) Topczewski, J. J.; Sanford, M. S., *Chem. Sci.* **2015**, *6*, 70-76. (c) Cook, A. K.; Sanford, M. S.*, J. Am. Chem. Soc.* **2015**, *137*, 3109-31018.
3. (a) Kuhl, N.; Hopkinson, M. N.; Wencel-Delord, J.; Glorius, F., *Angew. Chem. Int. Ed.* **2012**, *51*, 10236-10254. (b) Kuhl, N.; Schröder, N.; Glorius, F., *Adv. Synth. Catal.* **2014**, *356*, 1443-1460.
4. (a) Owens, C. P.; Varela-Alvarez, A.; Boyarskikh, V.; Mu-saev, D. G.; Davies, H. M. L.; Blakey, S. B., *Chem. Sci.* **2013**, *4*, 2590-2596. (b) Kim, J.; Chang, S., *Angew. Chem. Int. Ed.* **2014**, *53*, 2203-2207. (c) Schafer, A. G.; Blakey, S. B., *Chem. Soc. Rev.* **2015**, *44*, 5969-5980.
5. (a) Hashiguchi, B. G.; Konnick, M. M.; Bischof, S. M.; Gus-tafson, S. J.; Devarajan, D.; Gunsalus, N.; Ess, D. H.; Periana, R. A., *Science (Washington, DC, U. S.)* **2014**, *343*, 1232-1237. (b) Gus-tafson, S. J.; Fuller, J. T.; Devarajan, D.; Snyder, J.; Periana, R. A.; Hashiguchi, B. G.; Konnick, M. M.; Ess, D. H., *Organometallics* **2015**, *34*, 5485-5495.

6. (a) McKillop, A.; Fowler, J. S.; Zelesko, M. J.; Hunt, J. D.; Taylor, E. C.; McGillivray, G., *Tetrahedron Lett.* **1969**, *10*, 2423-2426. (b) McKillop, A.; Hunt, J. D.; Zelesko, M. J.; Fowler, J. S.; Taylor, E. C.; McGillivray, G.; Kienzle, F., *J. Am. Chem. Soc.* **1971**, *93*, 4841-4844. (c) Taylor, E. C.; Kienzle, F.; Robey, R. L.; McKil-lop, A.; Hunt, J. D., *J. Am. Chem. Soc.* **1971**, *93*, 4845-4850.
7. (a) Elson, I. H.; Kochi, J. K., *J. Am. Chem. Soc.* **1973**, *95*, 5060-5062. (b) Lau, W.; Kochi, J. K., *J. Am. Chem. Soc.* **1984**, *106*, 7100-7112. (c) Lau, W.; Kochi, J. K., *J. Am. Chem. Soc.* **1986**, *108*, 6720-6732.
8. (a) Zhao, Y.; Truhlar, D. G., *Theor. Chem. Acc.* **2007**, *120*, 215-241. (b) Rappoport, D.; Furche, F., *J. Chem. Phys.* **2010**, *133*, 134105. (c) Metz, B.; Stoll, H.; Dolg, M., *J. Chem. Phys.* **2000**, *113*, 2563-2569. (d) Krishnan, R.; Binkley, J. S.; Seeger, R.; Pople, J. A., *J. Chem. Phys.* **1980**, *72*, 650-654. (e) Frisch, M. J.; Pople, J. A.; Binkley, J. S., *J. Chem. Phys.* **1984**, *80*, 3265-3269. (f) Clark, T.; Chandrasekhar, J.; Spitznagel, G. W.; Schleyer, P. V. R., *J. Comput. Chem.* **1983**, *4*, 294-301. (g) Wadt, W. R.; Hay, P. J., *J. Chem. Phys.* **1985**, *82*, 284-298. (h) Feller, D., *J. Comput. Chem.* **1996**, *17*, 1571-1586. (i) Schuchardt, K. L.; Didier, B. T.; Elsethagen, T.; Sun, L.; Gurumoorthi, V.; Chase, J.; Li, J.; Windus, T. L., *J. Chem. Inf. Model.* **2007**, *47*, 1045-1052. (j) Marenich, A. V.; Cramer, C. J.; Truhlar, D. G., *J. Phys. Chem. B* **2009**, *113*, 6378-6396.
9. Roberts, R. M. G., *Tetrahedron* **1980**, *36*, 3281-3287.
10. (a) Blixt, J.; Gyori, B.; Glaser, J., *J. Am. Chem. Soc.* **1989**, *111*, 7784-7791. (b) Banyai, I.; Glaser, J., *J. Am. Chem. Soc.* **1989**, *111*, 3186-3194. (c) Banyai, I.; Glaser, J., *J. Am. Chem. Soc.* **1990**, *112*, 4703-4710. (d) Blixt, J.; Glaser, J.; Mink, J.; Persson, I.; Persson, P.; Sandstroem, M., *J. Am. Chem. Soc.* **1995**, *117*, 5089-5104. (e) Bányai, I.; Glaser, J.; Losonczi, J., *Inorg. Chem.* **1997**, *36*, 5900-5908.
11. (a) Boutadla, Y.; Davies, D. L.; Macgregor, S. A.; Poblador-Bahamonde, A. I., *Dalton Trans.* **2009**, 5820-5831. (b) Balcells, D.; Eisenstein, O. In Theoretical studies on the reaction mechanism of metal-assisted C-H activation, Elsevier B.V.: **2013**; pp 695-726. (c) Di Giuseppe, A.; Castarlenas, R.; Oro, L. A., *C. R. Chim.* **2015**, *18*, 713-741.
12. (a) Weinberg, D. R.; Gagliardi, C. J.; Hull, J. F.; Murphy, C. F.; Kent, C. A.; Westlake, B. C.; Paul, A.; Ess, D. H.; McCafferty, D. G.; Meyer, T. J., *Chem. Rev.* **2012**, *112*, 4016-4093. (b) Shaik, S.; Shurki, A., *Angew. Chem. Inter. Ed.* **1999**, *38*, 586-625.
13. Koleva, G.; Galabov, B.; Kong, J.; Schaefer, H. F.; Schleyer, P. V. R., *J. Am. Chem. Soc.* **2011**, *133*, 19094-19101.
14. Briody, J. M.; Moore, R. A., *J. Chem. Soc., Perkin Trans. 2* **1972**, 179-83.

15. Olah, G. A.; Hashimoto, I.; Lin, H. C., *Proc. Natl. Acad. Sci. U.S.A.* **1977**, *74*, 4121-4125.
16. Frisch, M. J.; Trucks, G. W.; Schlegel, H. B.; Scuseria, G. E.; Robb, M. A.; Cheeseman, J. R.; Scalmani, G.; Barone, V.; Mennucci, B.; Petersson, G. A.; Nakatsuji, H.; Caricato, M.; Li, X.; Hratchian, H. P.; Izmaylov, A. F.; Bloino, J.; Zheng, G.; Sonnenberg, J. L.; Hada, M.; Ehara, M.; Toyota, K.; Fukuda, R.; Hasegawa, J.; Ishida, M.; Nakajima, T.; Honda, Y.; Kitao, O.; Nakai, H.; Vreven, T.; Montgomery Jr., J. A.; Peralta, J. E.; Ogliaro, F.; Bearpark, M. J.; Heyd, J.; Brothers, E. N.; Kudin, K. N.; Staroverov, V. N.; Koba-yashi, R.; Normand, J.; Raghavachari, K.; Rendell, A. P.; Burant, J. C.; Iyengar, S. S.; Tomasi, J.; Cossi, M.; Rega, N.; Millam, N. J.; Klene, M.; Knox, J. E.; Cross, J. B.; Bakken, V.; Adamo, C.; Jaramil-lo, J.; Gomperts, R.; Stratmann, R. E.; Yazyev, O.; Austin, A. J.; Cammi, R.; Pomelli, C.; Ochterski, J. W.; Martin, R. L.; Morokuma, K.; Zakrzewski, V. G.; Voth, G. A.; Salvador, P.; Dannenberg, J. J.; Dapprich, S.; Daniels, A. D.; Farkas, Ö.; Foresman, J. B.; Ortiz, J. V.; Cioslowski, J.; Fox, D. J. Gaussian 09, Gaussian, Inc.: Walling-ford, CT, USA, **2009**.
17. (a) Munz, D.; Meyer, D.; Strassner, T., *Organometallics* **2013**, *32*, 3469-3480. (b) Fu, R.; Nielsen, R. J.; Goddard, W. A.; Fortman, G. C.; Gunnoe, T. B., *ACS Catal.* **2014**, *4*, 4455-4465. (c) Konnick, M. M.; Hashiguchi, B. G.; Devarajan, D.; Boaz, N. C.; Gunnoe, T. B.; Groves, J. T.; Gunsalus, N.; Ess, D. H.; Periana, R. A., *Angew. Chem. Int. Ed.* **2014**, *53*, 10490-10494.
18. Atomic Radii of the Elements, CRC handbook of chemistry and physics (Online) **1999**, Electronic ed.

Chapter 4:

Computational Comparison of C-H Activation, Hydride Transfer, and Protonation Pathways for Methane and Isobutane by SbF_5

4.1 Introduction

Reaction of methane with Sb^VF_5, especially in the presence of a Brønsted acid (e.g HF or HSO_3F), is assumed to induce reversible formation of methanium ($[CH_5]^+$) that fragments to H_2 and methyl cation (Scheme 4-1a), which can further react leading to alkane oligomerization.[1] For methane, the first step of this superacid-induced reaction pathway is supported by the experimental observation of methane hydrogen-to-deuterium (H/D) exchange.[2-4] However, density functional theory (DFT) studies reported competitive low energy transition-state structures for alkane protonation and concerted hydrogen exchange, and both pathways can account for H/D exchange in methane.[5-8] The second step in the methanium to methyl cation pathway is tenuous because H_2 is generally not observed.[1,9] Alternatively, H_2 *is* observed for larger alkanes, such as isobutane, although typically in less than stoichiometric amount.[10-13]

There are several reasons to explore possible alternative mechanisms for reaction of methane with Sb^VF_5, in particular for conditions without excess Brønsted acid. Hogeveen[14] and de Rege[15] reported that the reaction of methane with neat Sb^VF_5 in the presence of CO at 60 and 80 ^oC led to formation of $[CH_3CO]^+$ and reduced Sb^{III} with no observation of H_2 (Scheme 4-1b). Experiments also showed that while H_2 is capable of reducing Sb^V to Sb^{III}, under these conditions the rate of reduction is inconsistent with its formation and rapid reaction without observation.[15] This suggests that the methanium to methyl cation pathway outlined in Scheme 4-1a is an unlikely

route to $[CH_3CO]^+$. Additionally, the relatively mild conditions of this reaction are inconsistent with the ~40 kcal/mol energy required to dissociate H_2 from methanium.[16,17]

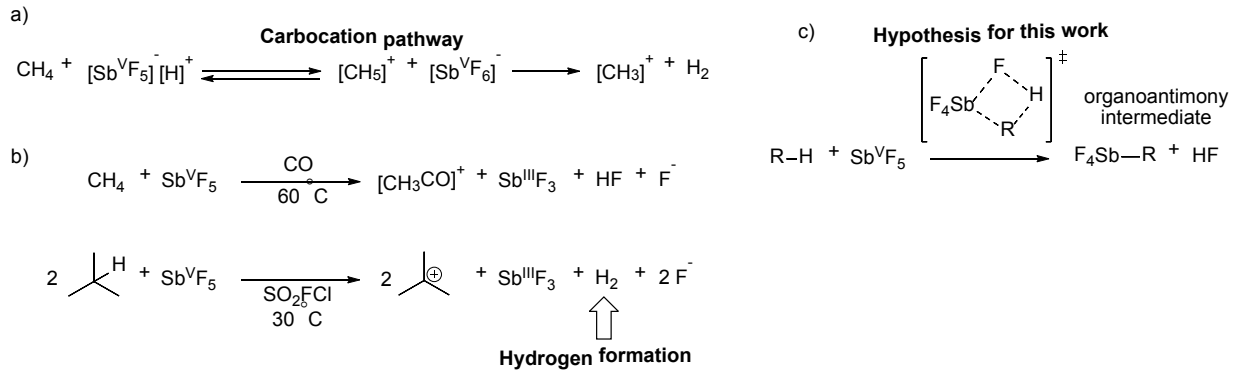

Scheme 4-1. a) Outline of methyl cation pathway for reaction of me-thane with $[Sb^VF_6]^-[H]^+$. b) Overview of methane and isobutane oxidation reactions with Sb^VF_5. c) Possible C-H activation transition state and organoantimony intermediate as the first mechanistic step for the oxidation of alkanes by Sb^VF_5.

In contrast to the methane reaction, Sommer and coworkers reported that the reaction of isobutane with neat Sb^VF_5 results in $Sb^{III}F_3$ with observation of both H_2 and *tert*-butyl cation.[11,12] While this result would seemingly fit with a protonation-induced carbocation pathway, Sommer used acetone as a Brønsted base to demonstrate that the small quantity of protons in Sb^VF_5 are unlikely to be involved with the Sb^V to Sb^{III} reduction. Alternative to a carbocation pathway is a pathway that involves direct hydride transfer from isobutane to Sb. However, Olah and others dismissed this pathway with citation of the formation of a very weak Sb-H bond, and unfavorable thermodynamics.[4]

While previous DFT studies examined reaction pathways for H/D exchange by Sb^VF_5 superacids, there has been no computational consideration of mechanisms involving C-H activation/metalation (Scheme 4-1c) or hydride transfer that provide a route for Sb^V to Sb^{III} reduction. The possibility of C-H activation with an alkylantimony (Sb-R) intermediate is

intriguing because the most prominent examples of C-H activation involve transition-metal complexes, and only recently has the possibility of p-block, main-group metals facilitating C-H activation been suggested.[18]

Here we report DFT calculations that compare C-H activation, hydride transfer, and protonation pathways for oxidation of methane and isobutane with $Sb^{V}F_5$. We found that the $Sb^{V}F_5$-mediated C-H activation pathway is viable and results in an Sb^{V}-Me intermediate, which can be functionalized by CO resulting in $[CH_3CO]^+$ and Sb^{III}. Because methyl cation is very unstable, this C-H activation pathway is lower in energy than hydride transfer and protonation pathways. In contrast, for isobutane, the hydride transfer transition pathway is a significantly lower energy route than C-H activation, which leads to *tert*-butyl cation and an Sb^{V}-H intermediate that provides a pathway to H_2 formation.

4.2 Results and Discussion

4.2.1 Models and Methods

$Sb^{V}F5$ contains small quantities of HF, and protons are produced in the reaction with methane. Therefore, reaction pathways were referenced to the ground state of $[Sb^{V}F_6]^-[H]^+$ (and $[Sb^{V}_2F_{11}]^-[H]^+$ for a dinuclear model). Dinér[8] used a similar ground state, and this is consistent with Estevez et al's[5-7] previous DFT reports examining plausible structures for the combination of $Sb^{V}F_5$ and HF. Because of the limited quantity of HF in $Sb^{V}F_5$ we did not use the $[Sb^{V}F_6]^-[H_2F]^+$ model, which was identified by Kim and Klein's Car-Parrinello molecular dynamics simulations.[19-22] Importantly, this ground state allowed direct comparison of protonation and Sb-mediated reaction pathways.

We used M06/Def2-TZVPDD[23-25]//M06/6-31+G**[LANL2DZdp[26,27] for Sb][28] in Gaussian 09[29] to optimize all minima and transition-state structures, and energies correspond to 298 K. Free energies are the sum of $E_{(SCF,Def2\text{-}TZVPDD)} + E_{ZPE(6\text{-}31G^{**}[LANL2DZdp])} + U_{(6\text{-}31G^{**}[LANL2DZdp])} + nRT - TS_{(6\text{-}31G^{**}[LANL2DZdp])} + \Delta G_{solv(Def2\text{-}TZVPDD)}$. Because the isobutane reaction was carried out in SO_2FCl, as an approximation for bulk solvent effects, particularly dielectric stabilization, we used the SMD continuum solvent model for dimethylsulfoxide. While this approach is crude, inclusion of solvent-induced electrostatic stabilization is important because hydride transfer and protonation pathways transition states develop significant charge. We also used this continuum solvent model for the methane oxidation reaction, however, because this reaction was reported in neat Sb^VF_5, we also report relevant gas phase values, which is similar to nearly all previous DFT studies that examined Sb^VF_5.

4.2.2 Methane Oxidation

We began by examining the methanium pathway outlined in Scheme 4-1a. With $[Sb^VF_6]^-[H]^+$ as the ground state, we located the methane protonation transition state, **TS1** (Scheme 2-2a,d). This transition state was previously reported by Dinér, and our intrinsic reaction coordinate (IRC) calculation shows it connects to the $[Sb^VF_6]^-[CH_5]^+$ ion pair. Our M06 $\Delta G^{\ddagger}$ value is 15.3 kcal/mol ($\Delta H^{\ddagger}$ = 5.7 kcal/mol). This relatively low barrier for protonation is consistent with Raugei and Klein's molecular dynamics study of reaction of light alkanes with Sb^VF_5 in HF that identified highly reactive protons and low barriers for alkane protonation resulting from coordination of HF to Sb^VF_5.[21,22] While there is a low barrier for methane protonation, even with the continuum solvent stabilization, H_2 dissociation is unlikely. The ΔG to achieve separated $[Sb^VF_6]^-$, $[CH_3]^+$, and H_2 is 53.3 kcal/mol, and our estimate for achieving $[Sb^VF_6]^-[CH_3]^+$ and H_2 is ~42 kcal/mol. This

relatively large value for H_2 separation from $[CH_5]^+$ is consistent with Dinér's[8] previously calculated value and the experimentally measured gas phase value of ~40 kcal/mol.[30]

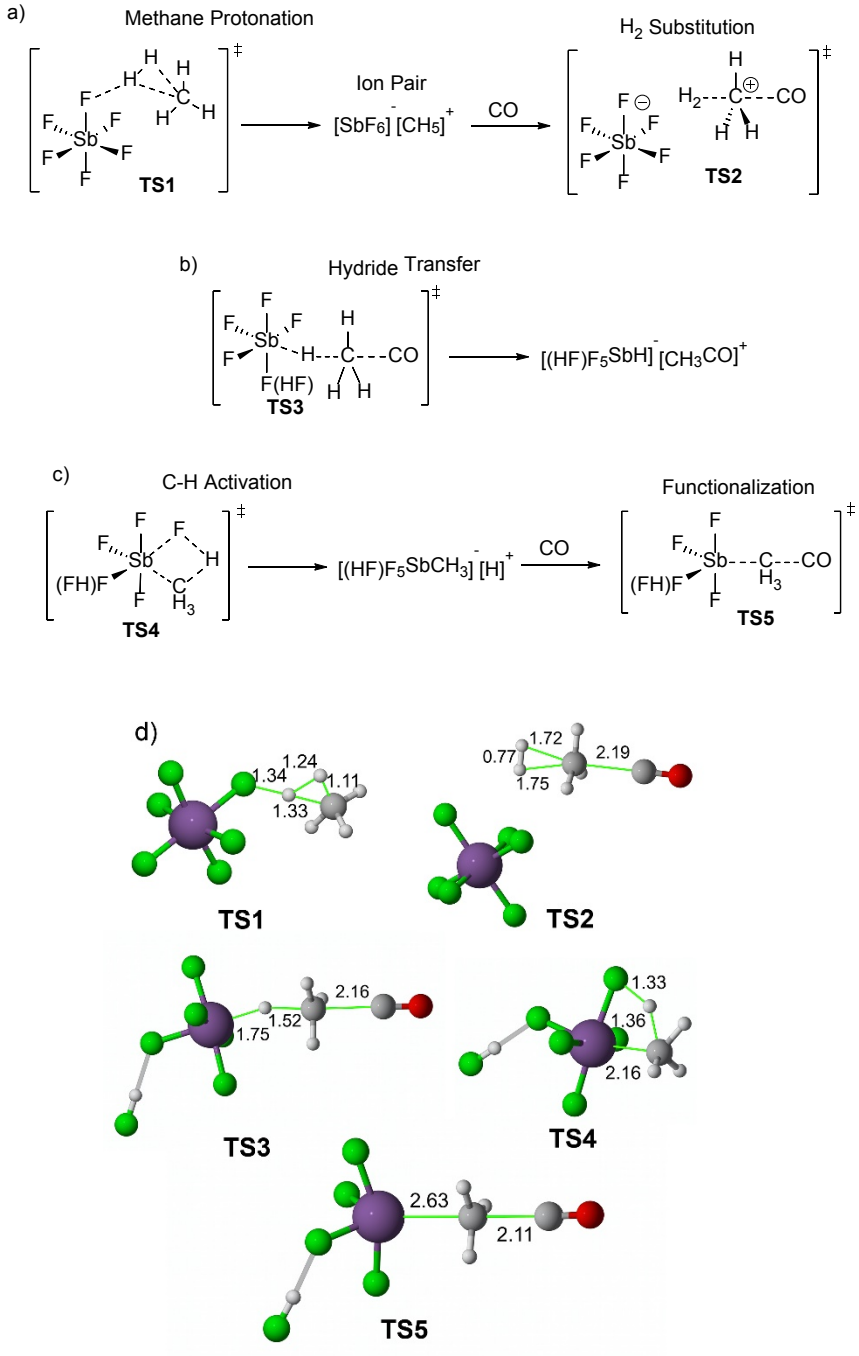

Scheme 4-2. a) Calculated methyl cation pathway that begins with the methane protonation transition state **TS1**. b) Calculated hydride transfer with simultaneous CO capture of methyl cation. c) C-H activation and CO functionalization transition states. d) 3D depictions of **TS1-TS5**, rendered using CYLView.[31]

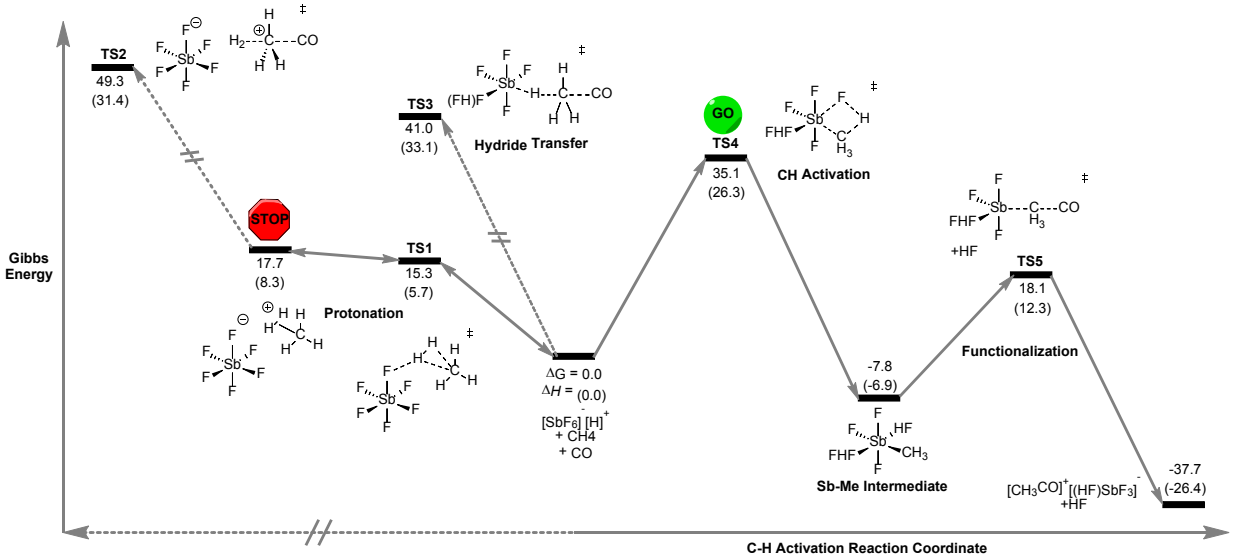

Scheme 4-3. Energy landscape comparing methane protonation, hydride transfer, and C-H activation reaction pathways for the mononuclear Sb model. Gibbs free energies (enthalpies) in kcal/mol.

With our best estimates indicating the formation of methyl cation to be unlikely, we considered pathways that circumvent this high-energy intermediate. Therefore, we examined CO induced H_2 displacement from $[Sb^VF_6]^-[CH_5]^+$ through transition state **TS2** (Scheme 4-2a). This transition state provides H_2 and the $[CH_3CO]^+[Sb^VF_6]^-$ ion pair. This pathway is only slightly lower in energy than H_2 dissociation from $[Sb^VF_6]^-[CH_5]^+$ with a $\Delta G^{\ddagger}$ of 49.3 kcal/mol, which suggests that H_2 dissociation is not feasible. We also located a transition state similar to **TS2**, but with $[Sb^VF_6]^-$ displacing H_2, which was higher in energy than **TS2**. This suggests that methane protonation occurs to achieve $[Sb^VF_6]^-[CH_5]^+$, but that this ion pair is impeded from losing H_2 and this is unlikely to be a productive avenue for formation of $[CH_3CO]^+$ (Scheme 3-3 pathway), which

is consistent with both the experimentally observed H/D exchange in methane and lack of observed H_2.

With the protonation pathway unlikely to account for formation of $[CH_3CO]^+$, we then explored Sb-mediated hydride transfer, which could then undergo reductive elimination to give $Sb^{III}F_3$ and HF. While Hogeveen suggested the possibility of a hydride transfer mechanism between alkanes and $Sb^{V}F_5$,[14] this mechanism was dismissed by Olah.[4] However, this type of mechanism is generally proposed for carbocation formation for reaction between $Sb^{V}F_5$ and alkyl fluorides.[32] For methane, hydride abstraction of methane by $Sb^{V}F_5$ requires $\Delta G^{\ddagger}$ = 56.9 kcal/mol ($\Delta H^{\ddagger}$= 45.3 kcal/mol) and gives the $[(HF)F_5SbH]^-[CH_3]^+$ ion pair. While this relatively large barrier for hydride abstraction is perhaps not unexpected, based on the hydride affinity of methyl cation (312 kcal/mol),[33] we examined if hydride transfer would be more feasible if facilitated by CO leading to overall hydride substitution. **TS3** (Scheme 4-2b,d) with a relatively bent Sb-H-C angle and highly stretched C-H partial bond length provides a one-step route to $[(HF)F_5Sb^{V}H]$-$[CH_3CO]^+$. Indeed, the presence of CO does lower the hydride transfer barrier to $\Delta G^{\ddagger}$ = 41.0 kcal/mol and $\Delta H^{\ddagger}$ = 33.1 kcal/mol. However, the >40 kcal/mol $\Delta G^{\ddagger}$ value is unlikely to account for reactivity at 60 or 80 °C. Also, if $[(HF)F_5Sb^{V}H]^-$ were to be formed it would likely generate H_2 or transfer the hydride to $[CH_3CO]^+$ to give acetaldehyde. Consistent with this argument, the calculated barrier for protonation of [(HF)F5SbH]- with HF is 50.7 kcal/mol, indicating that an Sb^{V}-H bond is highly acidic.

With protonation and hydride transfer pathways being inconsistent with the relatively mild conditions for conversion of methane to $[CH_3CO]^+$, we then considered the possibility of C-H activation involving an Sb^{V}-Me intermediate, which could undergo Sb^{V} to Sb^{III} reduction. The C-

H activation transition state involves coordination of the methane C-H bond to the Sb metal center followed by a σ-bond metathesis type transition state **TS4** (Scheme 4-2c,d) that leads to $[(HF)F_5Sb^V\text{-}Me]^-[H]^+$. Relative to $[Sb^VF_6]^-[H]^+$, the $\Delta G^‡$ for **TS4** is 35.1 kcal/mol and $\Delta H^‡$ is 26.3 kcal/mol. The ΔH for forming $[(HF)F_5Sb^V\text{-}Me]^-[H]^+$ is slightly exergonic with ΔG = -7.8 kcal/mol. Perhaps surprisingly, **TS4** is 5.9 kcal/mol lower in Gibbs energy and 6.8 kcal/mol lower in enthalpy compared with **TS3**. In the gas phase the ΔΔG‡ value between **TS4** and **TS3** increases to 18.3 kcal/mol. Also, comparison of **TS4** and **TS3** at 80 °C and at 34 atm of methane and 19 atm of CO (de Rege conditions) did not significantly change this energy difference. All other functionals and basis sets examined also show that **TS4** is lower in energy than **TS3**. For example, ωB97X-D/Def2-TZVPDD gave ΔΔG‡(**TS3**-**TS4**) values of 15.0. With the viability of **TS4**, we examined several variations. For example, we explored the possibility of a C-H activation transition state from the more reactive $[F_4Sb^V]^+$. However, fluoride dissociation is very unfavorable (ΔG = 86.3 kcal/mol) and while intramolecular fluoride transfer can occur for $Sb^V{}_2F_{10}$, the fluoride bridges and provides a vacancy around Sb for methane coordination and activation.

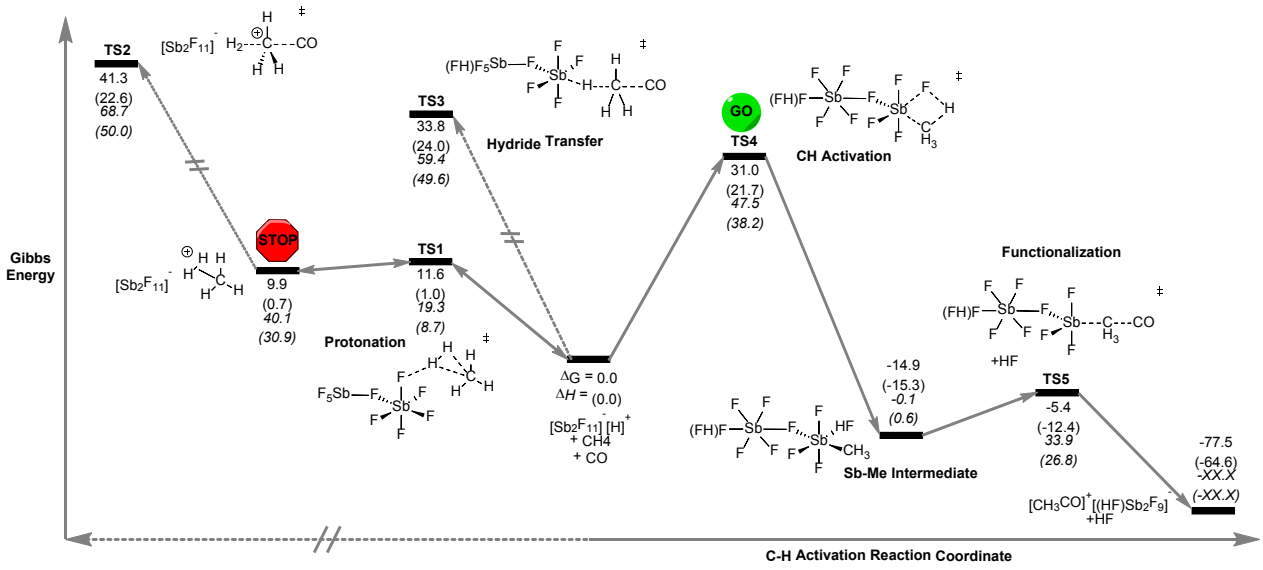

Scheme 4-4. Energy landscape comparing methane protonation, hydride transfer, and C-H activation reaction pathways for the dinuclear Sb mod-el. Gibbs free energies (enthalpies) in kcal/mol. Italicized values are in the gas phase.

Upon C-H activation, a plausible route to $[CH_3CO]^+$ involves Sb^V-Me bond functionalization with CO. We located **TS5** (Scheme 4-2c,d) where there is displacement of reduced Sb with simultaneous C-C bond formation. The overall reaction thermodynamics leading to $[CH_3CO]^+$ and Sb^{III} is ΔG = -37.7 kcal/mol. While the Sb^V-Me intermediate is slightly exergonic relative to the starting ground state, which indicates it is potentially observable, the barrier for functionalization is relatively low. The $\Delta G^{\ddagger}$ for **TS5** is 25.9 kcal/mol ($\Delta H^{\ddagger}$ = 19.2) relative to the Sb^V-Me intermediate. This suggest that at the temperature and pressure conditions required to undergo C-H activation that the Sb^V-Me intermediate should rapidly undergo CO functionalization. We also explored alternative Sb^V-Me bond functionalization pathways that were found to be higher in energy. For example, Sb^V-Me bond heterolysis without CO is 24.3 kcal/mol higher in energy than **TS5** and Sb^V-Me bond ho-molysis requires >60 kcal/mol.

With C-H activation and CO functionalization identified as a plausible pathway to explain the observation of $[CH_3CO]^+$ without forming H_2, we continued to examine several other less plausible pathways. For example, we examined the possibility of Sb^VF_5 undergoing reductive elimination to give $Sb^{III}F_3$ and F_2, which could oxidize methane. While the ΔG for this reaction is exergonic, one-step and two-step reductive elimination mechanisms require transition states with very large barriers ($\Delta G^{\ddagger}$ >80 kcal/mol). We also ruled out fluorine and Sb centered radical pathways resulting from Sb-F bond homolysis, which has a bond strength of >80 kcal/mol.

While the mononuclear Sb model suggests that C-H activation is a lower energy route to methane oxidation than either protonation or hydride transfer pathways, we wondered if a dinuclear Sb model would alter this conclusion. Therefore, we examined these pathways beginning with the ground state model $[Sb^V_2F_{11}]^-[H]^+$. Scheme 4-4 presents the solvent stabilized and gas phase dinuclear pathway energies. The qualitative shape of this dinuclear surface is similar to the mononuclear surface. Again, methane protonation $[Sb^V_2F_{11}]^-[H]^+$ leading to the $[Sb^V_2F_{11}]^-[CH_5]^+$ ion pair is low in energy, but H^2 dissociation via **TS2** is relatively high in energy at 41.3 kcal/mol. While this relatively large free energy fits with the experimental lack of H_2 formation, and is close to the experimental barrier for H_2 dissociation from $[CH_5]^+$, the entropy penalty is likely overestimated. Importantly, even though TS2 is an ion pair, in the gas phase this transition state is significantly higher in energy, with $\Delta G^{\ddagger}$ = 68.7 kcal/mol and $\Delta H^{\ddagger}$ = 50.0 kcal/mol.

Similar to the mononuclear energy surface, the dinuclear hydride and C-H activation transition states are lower in energy than **TS2**. The C-H activation transition state is lower in Gibbs free energy and enthalpy, but only by 2.8 and 2.3 kcal/mol, respectively. While there remains a clear preference for the C-H activation pathway, the smaller energy difference with the dinuclear

model could mean that the hydride pathway may occur as a competitive pathway. In the gas phase, however, as expected due to the lack of stabilization for the charge build up in **TS3**, the C-H activation transition state is lower in Gibbs free energy and enthalpy by more than 10 kcal/mol. We also examined the relative energies of **TS3** and **TS4** using M06-2X and ωB97X-D functionals. For M06-2X/Def2-TZVPPD and M06-2X/aug-cc-PVTZ the C-H activation transition state **TS4** is lower in Gibbs free energy by 5.3 and 5.7 kcal/mol, respectively. For ωB97X-D/Def2-TZVPPD and ωB97X-D /aug-cc-PVTZ the C-H activation transition state **TS4** is lower in Gibbs free energy by 5.2 and 5.7 kcal/mol, respectively. All of these calculations suggest that while hydride transfer could be competitive it would likely contribute in a minor amount to forming $[CH_3CO]^+$. Again, similar to the mononuclear energy surface, while the Sb^V-Me intermediate is slightly exergonic the barrier for functionalization is <10 kcal/mol on the Gibbs surface and <5 kcal/mol on the enthalpy surface. However, these very low barriers are due to solvent stabilization of the polarized transition state **TS5**.

4.2.3 Isobutane Oxidation

As outlined in Scheme 4-1b, reaction of isobutane with Sb^VF_5 was reported without CO, and results in $Sb^{III}F_3$ with observation of both H_2 and tert-butyl cation. While the C-H activation pathway provides an explanation for the methane oxidation, it is unlikely that C-H activation would result in isobutane oxidation and generate H_2. Therefore, for isobutane, using mononuclear and dinuclear Sb models, we examined protonation and hydride transfer, and compared these pathways to the C-H activation (Scheme 4-5).

To us, it was surprising that the barrier for protonation of isobutane through **TS6** ($\Delta G^‡$ = 15.2 kcal/mol and $\Delta H^‡$ = 2.2 kcal/mol for the dinuclear case, Scheme 4-5a) is similar to the barrier

for methane protonation. However, this is consistent with previous computational results.[3] In contrast to the more than 50 kcal/mol endergonic value to forming methyl cation and H_2 from $[CH_5]^+$, it is exergonic to form *tert*-butyl cation and H_2 from $[C_4H_{11}]^+$. With $[Sb^V_2F_{11}]^-$ as a weak assisting nucleophile, there is a low barrier for H_2 dissociation by **TS7** (Scheme 4-5a).

While there are relatively low barriers for isobutane protonation and H_2 dissociation, there is a lower barrier for hydride transfer. PCET, ET, and HAT have significantly larger barriers or unfavorable thermodynamics compared to hydride transfer. Relative to $[Sb^V_2F_{11}]^-[H]^+$ and isobutane, **TS8** (Scheme 4-5b) has a $\Delta G^{\ddagger}$ value of 7.8 kcal/mol, which is ~26 kcal/mol lower in energy than **TS3** for methane, and is consistent with the significantly lower hydride affinity of *tert*-butyl cation compared to methyl cation. The ΔG of the anionic Sb^V-H and tert-butyl cation ion pair is -20.2 kcal/mol, which is consistent with its experimental observation.

To confirm that C-H activation is a higher energy pathway than hydride transfer and protonation for isobutane, we calculated **TS9** (Scheme 4-5c). Although the tertiary C-H bond of isobutane is homolytically weaker than the methane C-H bonds, the C-H activation $\Delta G^{\ddagger}$ of 47.4 kcal/mol (Scheme 4-5, **TS9**) for isobutane is somewhat larger than the barrier for methane, likely because of steric repulsion. The slightly larger isobutane C-H activation barrier compared to methane is consistent with previous computational studies with a similar conclusion.[34,35] More importantly, because the barrier for C-H activation is relatively insensitive to the alkane structure this allows non-C-H activation pathways to become favored where they are more dramatically influenced by the alkane structure, as is demonstrated here for hydride transfer.

We examined several possible pathways for formation of H_2 after generation of the anionic Sb^V-H, and several plausible pathways emerged. The most viable is by Sb^V-H protonation of

isobutane through **TS10** (Scheme 4-5d). Importantly, the anionic Sb^V-H hydrogen is highly acidic, and we found an extremely low barrier for protonation of isobutane. **TS10** has a $\Delta G^{\ddagger}$ value of <5 kcal/mol relative the Sb^V-H intermediate. This protonation also results in Sb^V to Sb^{III} reduction. Generation of H_2 follows by dissociation by **TS7**. This proposed pathway for H_2 formation is consistent with experiments that show that the ratio of H_2 to isobutane is < 1.[3,4,11,12]

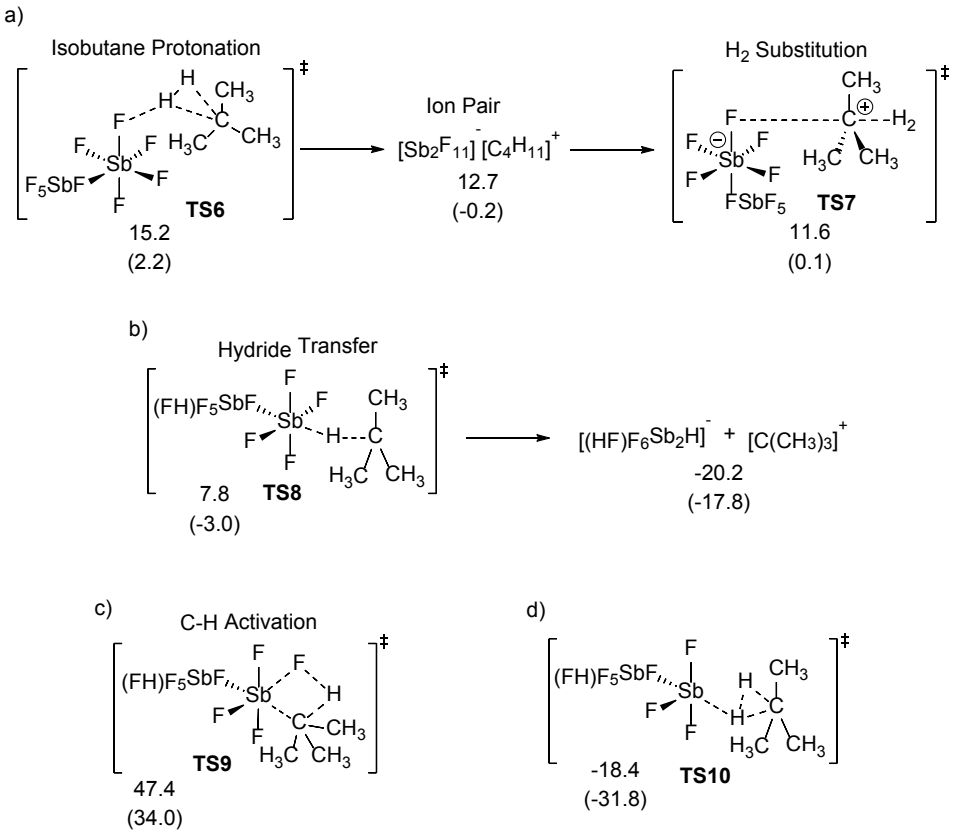

Scheme 4-5. a) Calculated *tert*-butyl cation pathway that begins with protonation of isobutane. b) Isobutane hydride transfer transition state. c) Isobutane C-H activation transition state. d) Protonation of isobutane by Sb^V-H formed from hydride transfer.

4.3 Conclusions

DFT calculations were presented that support a new mechanism for oxidation of methane with Sb^VF_5. A low barrier for methane protonation by $[Sb^VF_6]^-[H]^+$ was found, but this pathway is

a dead end and reversible because the barrier for H_2 dissociation is very large due to the instability of methyl cation. Reversible methane protonation is consistent with the experimentally observed hydrogen-to-deuterium exchange. As a viable alternative to the methyl cation pathway, the C-H activation/σ-bond metathesis mechanism results in an Sb^V-Me intermediate, which can be functionalized by CO resulting in $[CH_3CO]^+$. In contrast to methane, due to the significantly lower carbocation hydride affinity, hydride transfer is a much lower pathway for isobutane and results in *tert*-butyl carbocation and H_2 is formed by the resulting Sb^V-H protonation of isobutane.

4.4 References

1. Olah, G. A., "Electrophilic methane conversion." *Acc. Chem. Res.* **1987**, *20*, 422-428.
2. Olah, G. A.; Klopman, G.; Schlosberg, R. H., "Super acids. III. Protonation of alkanes and intermediacy of alkanonium ions, penta-coordinated carbon cations of CH_5^+ type. Hydro-gen exchange, protolytic cleavage, hydrogen abstraction; polycondensation of methane, ethane, 2,2-dimethylpropane and 2,2,3,3-tetramethylbutane in FSO_3H-SbF_5." *J. Amer. Chem. Soc.* **1969**, *91*, 3261-3268.
3. Olah, G. A.; Halpern, Y.; Shen, J.; Mo, Y. K., "Electrophilic reactions at single bonds. III. H-D exchange and protolysis (deuterolysis) of alkanes with superacids. The mechanism of acid-catalyzed hydrocarbon transformation reactions involving the σ electron pair donor ability of single bonds via three-center bond formation." *J. Amer. Chem. Soc.* **1971**, *93*, 1251-1256.
4. Olah, G. A.; Halpern, Y.; Shen, J.; Mo, Y. K., "Electrophilic reactions at single bonds. XII. Hydrogen-deuterium ex-change, protolysis (deuterolysis), and oligocondensation of alkanes with superacids." *J. Amer. Chem. Soc.* **1973**, *95*, 4960-4970.
5. Esteves, P. M.; Alberto, G. G. P.; Ramirez-Solis, A.; Mota, C. J. A., "The alkane σ-bond basicity scale revisited." *J. Am. Chem. Soc.* **1999**, *121*, 7345-7348.
6. Esteves, P. M.; Ramírez-Solís, A.; Mota, C. J. A.; "A Theoretical Study of Alkane Protonation in HF/SbF_5 Superacid System." *J. Braz. Chem. Soc.* **2000**,*11*, 345-348.
7. Esteves, P. M.; Ramirez-Solis, A.; Mota, C. J. A., "DFT Calculations on the Protonation of Alkanes on HF/SbF_5 Super-acids Using Cluster Models." *J. Phys. Chem. B* **2001**, *105*, 4331-4336.

8. Dinér, P., "Superacid-Promoted Ionization of Alkanes without Carbonium Ion Formation: A Density Functional Theory Study." *J. Phys. Chem. A* **2012**, *116*, 9979-9984.
9. Hogeveen, H.; Gaasbeek, C. J., "Chemistry and spectroscopy in strongly acidic solutions. XV. Electrophilic substitution at methane." *Recl. Trav. Chim. Pays-Bas* **1968**, *87*, 319-320.
10. Hogeveen, H.; Bickel, A. F., "Formation of trimethylcarbon-ium ions from isobutane and protons. Basicity of isobutene." *Recl. Trav. Chim. Pays-Bas* **1967**, *86*, 1313-1315.
11. Culmann, J. C.; Sommer, J., "Hydrocarbon oxidation by an-timony pentafluoride." *J. Am. Chem. Soc.* **1990**, *112*, 4057-4058.
12. Sommer, J.; Bukala, J., "Selective electrophilic activation of alkanes." *Acc. Chem. Res.* **1993**, *26*, 370-376.
13. Olah, G. A.; Prakash, G. K. S.; Molnár, Á.; Sommer, J. Superacid Chemistry, Second Edition, John Wiley & Sons, Inc., Hoboken, New Jersey, 2009, 511-517.
14. Hogeveen, H.; Lukas, J.; Roobeek, C. F., "Trapping of the methyl cation by carbon monoxide; formation of acetic acid from methane." *J. Chem. Soc. D* **1969**, 920-921.
15. De Rege, P. J. F.; Gladysz, J. A.; Horvath, I. T., "Facile and selective carbonylation of methane in superacids." *Adv. Synth. Catal.* **2002**, *344*, 1059-1062.
16. Hiraoka, K.; Kebarle, P., "Stabilities and energetics of penta-coordinated carbonium ions. The isomeric protonated ethane ions and some higher analogs: protonated propane and pro-tonated butane." *J. Amer. Chem. Soc.* **1976**, *98*, 6119-6125.
17. Raghavachari, K.; Whiteside, R. A.; Pople, J. A.; Schleyer, P. V. R., "Molecular orbital theory of the electronic structure of organic molecules. 40. Structures and energies of C1-C3 carbocations including effects of electron correlation." *J. Amer. Chem. Soc.* **1981**, *103*, 5649-5657.
18. Hashiguchi, B. G.; Konnick, M. M.; Bischof, S. M.; Gustafson, S. J.; Devarajan, D.; Gunsalus, N.; Ess, D. H.; Periana, R. A., "Main-Group Compounds Selectively Oxidize Mixtures of Methane, Ethane, and Propane to Alcohol Esters." *Science* **2014**, *343*, 1232.
19. Kim, D.; Klein, M. L., "Liquid Hydrogen Fluoride with an Excess Proton: Ab Initio Molecular Dynamics Study of a Superacid." *J. Amer. Chem. Soc.* **1999**, *121*, 11251-11252.
20. Kim, D.; Klein, M. L., "Ab Initio Molecular Dynamics Study of the Superacid System SbF_5/HF Solution." *J. Phys. Chem. B* **2000**, *104*, 10074-10079.
21. Raugei, S.; Klein, M. L., "Structure of the strongly associated liquid antimony pentafluoride: An ab initio molecular dy-namics study." *J. Chem. Phys.* **2002**, *116*, 7087-7093.

22. Raugei, S.; Klein, M. L., "Hydrocarbon Reactivity in the Superacid SbF_5/HF: an ab Initio Molecular Dynamics Study." *J. Phys. Chem. B* **2002**, *106*, 11596-11605.

23. Metz, B.; Stoll, H.; Dolg, M., "Small-core multiconfiguration-Dirac–Hartree–Fock-adjusted pseudopotentials for post-d main group elements: Application to PbH and PbO." *J. Chem. Phys.* **2000**, *113*, 2563-2569.

24. Rappoport, D.; Furche, F., "Property-optimized Gaussian basis sets for molecular response calculations." *J. Chem. Phys.* **2010**, *133*, 134105.

25. Weigend, F.; Ahlrichs, R., "Balanced basis sets of split va-lence, triple zeta valence and quadruple zeta valence quality for H to Rn: Design and assessment of accuracy." *Phys. Chem. Chem. Phys.* **2005**, *7*, 3297-3305.

26. Check, C. E.; Faust, T. O.; Bailey, J. M.; Wright, B. J.; Gil-bert, T. M.; Sunderlin, L. S., "Addition of Polarization and Diffuse Functions to the LANL2DZ Basis Set for P-Block Elements." *J. Phys. Chem. A* **2001**, *105*, 8111-8116.

27. Wadt, W. R.; Hay, P. J., "Ab initio effective core potentials for molecular calculations. Potentials for main group ele-ments Na to Bi." *J. Chem. Phys.* **1985**, *82*, 284-298.

28. Schuchardt, K. L.; Didier, B. T.; Elsethagen, T.; Sun, L.; Gurumoorthi, V.; Chase, J.; Li, J.; Windus, T. L., "Basis Set Exchange: A Community Database for Computational Sciences." *J. Chem. Inf. Mod.* **2007**, *47*, 1045-1052. Basis sets were obtained from the basis set exchange: https://www.basissetexchange.org/

29. Frisch, M. J.; Trucks, G. W.; Schlegel, H. B.; Scuseria, G. E.; Robb, M. A.; Cheeseman, J. R.; Scalmani, G.; Barone, V.; Mennucci, B.; Petersson, G. A.; Nakatsuji, H.; Caricato, M.; Li, X.; Hratchian, H. P.; Izmaylov, A. F.; Bloino, J.; Zheng, G.; Sonnenberg, J. L.; Hada, M.; Ehara, M.; Toyota, K.; Fu-kuda, R.; Hasegawa, J.; Ishida, M.; Nakajima, T.; Honda, Y.; Kitao, O.; Nakai, H.; Vreven, T.; Montgomery Jr., J. A.; Peralta, J. E.; Ogliaro, F.; Bearpark, M. J.; Heyd, J.; Brothers, E. N.; Kudin, K. N.; Staroverov, V. N.; Kobayashi, R.; Nor-mand, J.; Raghavachari, K.; Rendell, A. P.; Burant, J. C.; Iyengar, S. S.; Tomasi, J.; Cossi, M.; Rega, N.; Millam, N. J.; Klene, M.; Knox, J. E.; Cross, J. B.; Bakken, V.; Adamo, C.; Jaramillo, J.; Gomperts, R.; Stratmann, R. E.; Yazyev, O.; Austin, A. J.; Cammi, R.; Pomelli, C.; Ochterski, J. W.; Martin, R. L.; Morokuma, K.; Zakrzewski, V. G.; Voth, G. A.; Salvador, P.; Dannenberg, J. J.; Dapprich, S.; Daniels, A. D.; Farkas, Ö.; Foresman, J. B.; Ortiz, J. V.; Cioslowski, J.; Fox, D. J. Gaussian 09, Gaussian, Inc.: Wallingford, CT, USA, **2009**.

30. Hiraoka, K.; Kebarle, P., "An application of ion equilibria measurements: Protonated alkanes, protolysis of alkanes and hydride transfer reactions between alkyl cations and alkanes." *Rad. Phys. Chem. (1977)* **1982**, *20*, 41-49.

31. CYLview, 1.0b; Legault, C. Y., Université de Sherbrooke, **2009** (http://www.cylview.org)

32. Olah, G. A.; DeMember, J. R.; Schlosberg, R. H., "Friedel-Crafts chemistry. III. Methyl fluoride-antimony pentafluoride, a powerful new methylating agent. Methylation reactions and the polycondensation of methyl fluoride." *J. Am. Chem. Soc.* **1969**, *91*, 2112-2113.

33. Anslyn, E. V. D., Dennis A., page 89 in Modern Physical Organic Chemistry. University Science Books: Sausalito, California, **2006**; pp 1099.

34. Bakhoda, A.; Jiang, Q.; Badiei, Y. M.; Bertke, J. A.; Cundari, T. R.; Warren, T. H., "Copper-Catalyzed C(sp^3)−H Amidation: Sterically Driven Primary and Secondary C−H Site-Selectivity." *Angew. Chem. Inter. Ed.* **2019**, *58*, 3421-3425.

35. Bellows, S. M.; Cundari, T. R.; Jones, W. D., "Methane Is the Best Substrate for C(sp^3)–H Activation with Cp*(PMe_3)Co(Me)(OTf): A Density Functional Theory Study." *Organometallics* **2015**, *34*, 4032-4038.

Appendix 1: Supporting Information for Chapter 2

A1.1 Comparison of Experimental and Computational Atomic Redox Energies

In order to assess the accuracy in computing electronic energies of several different functional/basis set combinations, we computed the absolute gas phase atomic oxidation potentials for the relevant oxidation states of the several metals by three different DFT functionals (M06,[1] M06-L,[2] ωB97X-D[3]) and two different basis sets (Def2-TZVPPD[4] (Table A1-2) and aug-cc-PVTZ[5] (Table A1-3)) and then compared these simulated values to those calculated from experimental gas phase ionization energies (Table A1-1).[6] For each combination of basis set and functional, we performed a linear regression of the computational energies against the experimental energies. The accuracy of the M06 functional for these systems is reflected in this functional showing the smallest MUE's. We have previously[7] used M06/Def2-TZVPPD, and since use of the aug-cc-pVTZ offered only slight improvement, we continued to use M06/Def2-TZVPPD for this study. Def2-TZVPPD and aug-cc-pVTZ basis sets were obtained from the Basis Set Exchange[8] (https://bse.pnl.gov/bse/portal).

Table A1-1. Gas-phase atomic oxidation potentials from experiment, and from computations using the Def2-TZVPPD basis set. All energies are in eV.

	Exptl	**M06**	**M06-L**	**ωB97X-D**
$\mathbf{In^{+} \rightarrow In^{3+} + 2e^{-}}$	46.9	46.3	46.2	46.8
$\mathbf{Tl^{+} \rightarrow Tl^{3+} + 2e^{-}}$	50.3	49.8	49.3	49.8
$\mathbf{Sn^{2+} \rightarrow Sn^{4+} + 2e^{-}}$	71.3	70.6	70.6	74.0
$\mathbf{Pb^{2+} \rightarrow Pb^{4+} + 2e^{-}}$	74.3	73.6	73.3	73.9
MUE	-	0.2	0.8	0.9

Table A1-2. Gas-phase atomic oxidation potentials from experiment, and from computations using the aug-cc-pVTZ basis set. All energies are in eV.

	Exptl	**M06**	**M06-L**	**ωB97X-D**
$In^+ \rightarrow In^{3+} + 2e^-$	46.9	47.1	49.2	46.8
$Tl^+ \rightarrow Tl^{3+} + 2e^-$	50.3	50.1	49.3	49.8
$Sn^{2+} \rightarrow Sn^{4+} + 2e^-$	71.3	71.6	70.6	71.2
$Pb^{2+} \rightarrow Pb^{4+} + 2e^-$	74.3	74.2	73.6	74.8
MUE	-	0.2	1.2	0.3

Table A1-3. Experimental gas-phase atomic ionization energies[6] for In, Tl, Sn, and Pb used to calculate absolute gas phase atomic oxidation potentials in Tables S1 and S2. Energies given in eV.

element	**1st**	**2nd**	**3rd**	**4th**
In	5.79	18.87	28.03	54.0
Tl	6.11	20.43	29.83	[a]
Sn	7.34	14.63	30.50	40.74
Pb	7.42	15.03	31.94	42.32

[a]Not available.

A1.2 Solvent Model Parameters

In order to simulate a solution environment, we used the SMD solvation model developed by Truhlar and co-workers, as implemented in Gaussian 09. This model includes the bulk dielectric constant (ε) and solvent radius as parameters. Since, of these two, variations in the dielectric constant have a greater effect on the computed energies,[9] we assessed the effect of varying the dielectric constant on the CH activation and internal functionalization transition states (see Scheme

2-3 in Chapter 2) of our $Tl(TFA)_3$ model system. The structures of the transition states did not change appreciably with changes in the dielectric constant. The CH activation energy and the activation energy for internal functionalization are plotted in Figure A1-1 as a function of dielectric constant.

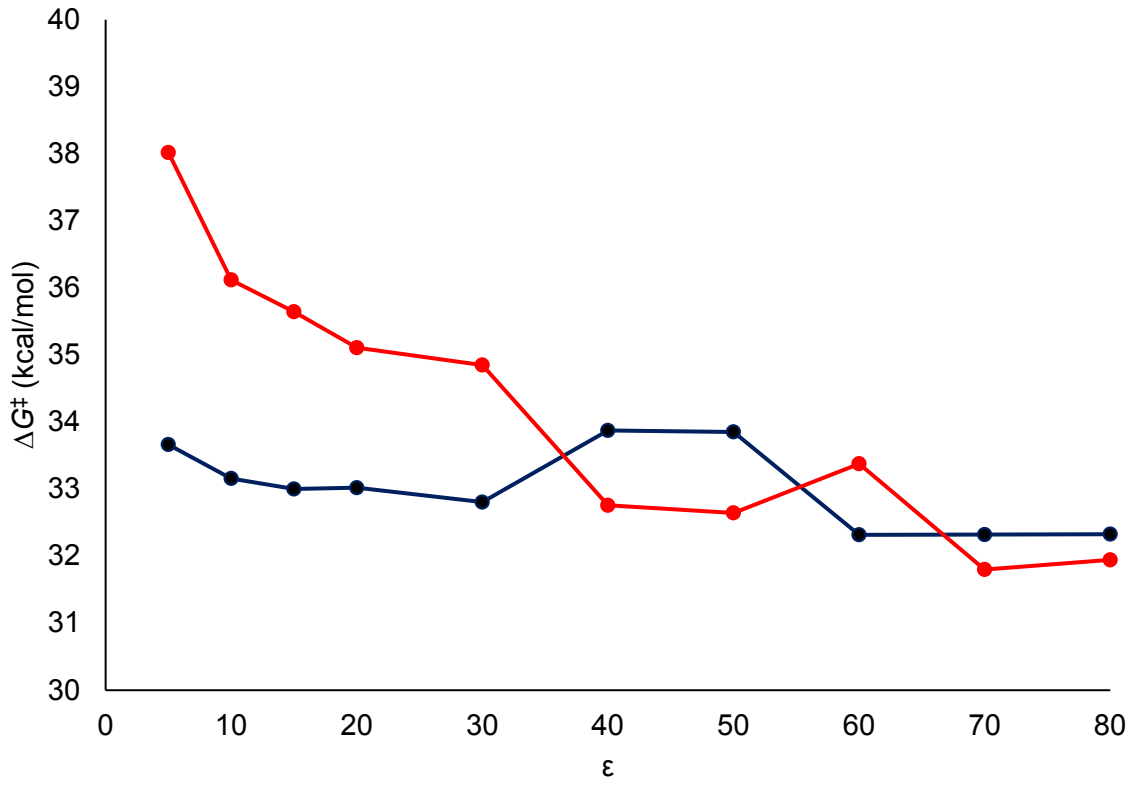

Figure A1-1. The free energy of CH activation (black, Scheme S1a) and the free energy of internal functionalization (red, Scheme S1b) versus ε.

Our results show that the relatively non-polar CH activation transition state has minor variations (<2 kcal/mol) with dielectric constant while the relatively more polar internal functionalization transition state (vide infra) is about 8 kcal/mol more stable at a dielectric constant of 80 than at a dielectric constant of 5.

A1.3 Modeling Ionization and Dissociation

In order to assess the likelihood that cationic metal trifluoroacetate might form in trifluoroacetic solution, we computed the following ionization reaction energies using explicit solvent molecules to stabilize the ions, in which M = In (n = 3), Tl (n = 3), Sn (n = 4), Pb (n = 4); TFA = trifluoroacetate:

Reaction A1-1: $M(TFA)_n + (TFAH)_5 \rightarrow [M(TFA)_{n-1}(TFAH)]^+ + [(TFAH)_4(TFA)]^-$

Reaction A1-2: $M(CH_3)(TFA)_{n-1} + (TFAH)_5 \rightarrow [M(CH_3)(TFA)_{n-2}(TFAH)]^+ + [(TFAH)_4(TFA)]^-$

Table A1-4. Energies for ionization reactions of metal trifluoroacetate complexes including explicit solvent molecules. All energies in kcal/mol.

	Reaction A1-1		**Reaction A1-2**	
M	**Δ*H***	**Δ*G***	**Δ*H***	**Δ*G***
In	19.6	21.9	10.3	14.7
Sn	24.3	27.6	16.4	20.3
Tl	16.1	21.4	4.0	7.3
Pb	19.5	23.3	10.2	12.8

Strassner and co-workers have previously[10] shown that computationally, trifluoroacetate ions are stabilized by the addition of explicit solvent molecules with no additional stabilization being seen after the addition of four explicit solvent molecules, therefore we used a four-molecule solvent cluster to stabilize the trifluoroacetate ion, while stabilizing the metallic cation with an additional solvent molecule. On the other hand, the addition of a methyl ligand decreases the thermodynamic barrier to forming a cationic species between 7 and 14 kcal/mol. The barriers for

external functionalization of the methyl cation complexes are significantly lower than the external functionalization barrier for neutral complexes.

A1.4 Dinuclear Model for $Tl(TFA)_3$

To examine our assumptions that reaction pathways would not be fundamentally altered by the presence of di- and polynuclear species, we optimized the a structure for a dinuclear $Tl_2(TFA)_6$ complex in which four of the TFA ligands bridge the two Tl centers (Scheme S2a). We found that the free energy of formation of this complex from individual $Tl(TFA)_3$ units is favorable, with ΔG = -7.0 (ΔH = -26.9). However, the CH activation transition state (Scheme S2b) has $\Delta G^{\ddagger}$ = 35.2 ($\Delta H^{\ddagger}$ = 23.8), which is ~4 kcal/mol higher than the energy of the CH activation transition state for the mononuclear model.

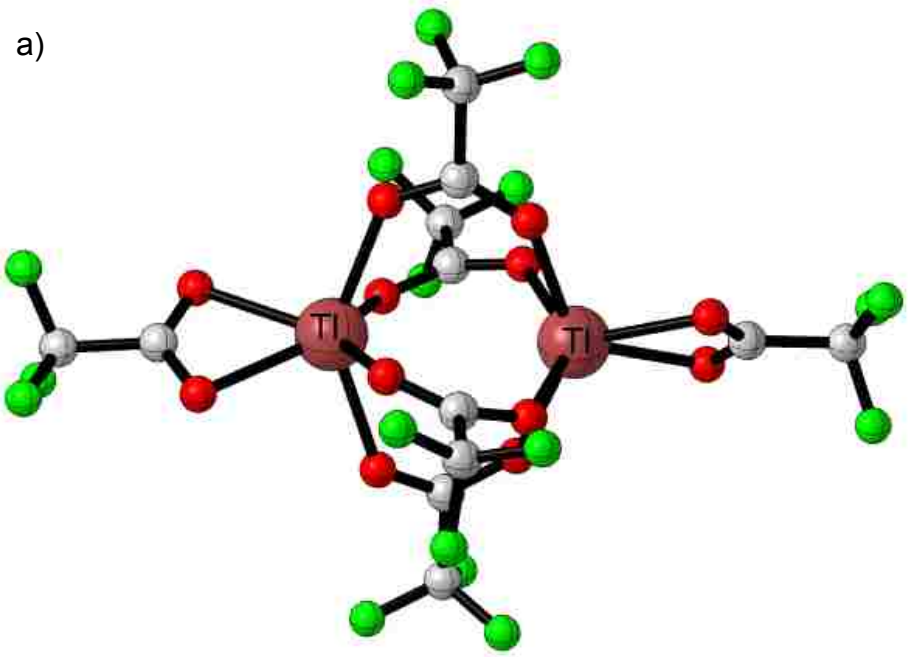

b)

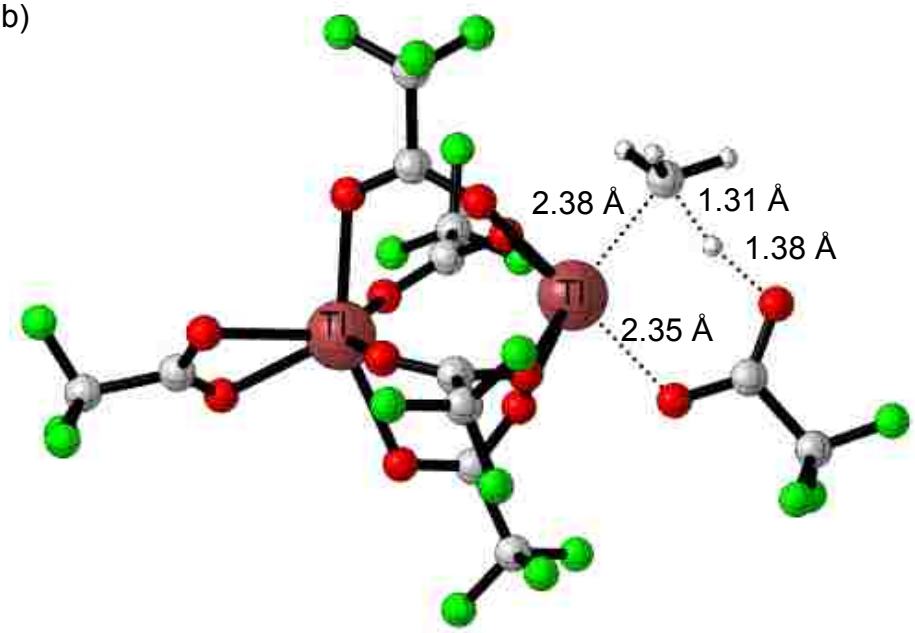

Scheme A1-1. a) Structure of dinuclear thallium trifluoroacetate complex. b) Structure of CH activation transition state for dinuclear thallium complex.

A1.5 CH Activation with Mixed Ligand Sets of Trifluoroacetate and Acetate

Figure A1-2 shows the energy of the CH activation transition state for various combinations of trifluoroacetate and acetate ligands. The energy of the transition state is qualitatively more dependent on the ratio of trifluoroacetate ligands to acetate ligands present in the complex than on the type of ligand acting as a proton acceptor.

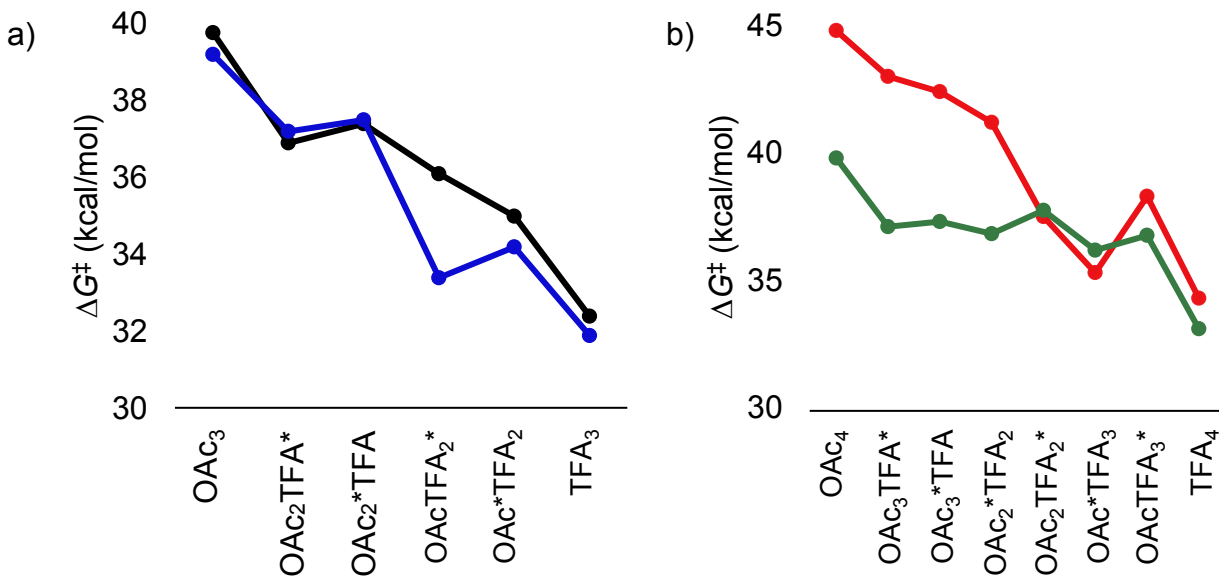

Figure A1-2. a) Plot of CH activation energies with methane for TlX_3 (blue) and InX_3 (black), where X = trifluoroacetate (TFA) or acetate (Ac) as indicated and b) plot of CH activation energies with methane for PbX_4 (green) and SnX_4 (black), where X = trifluoroacetate (TFA) or acetate (OAc) as indicated. When both TFA and OAc are present, the * indicates the ligand acting as a proton acceptor in the transition state structure.

A1.6 Correlation of CH Activation and LUMO Energies

To test our hypothesis that the electrophilicity of the metal complexes is the principle factor in determining the energy of the CH activation transition state, we plotted the CH activation energies for several complexes of Tl with their LUMO energies (a measure of electrophilicity) (Figure A1-3a). We found that a strong correlation exists between these LUMO energies and the CH activation energy. However, when we extended this plot to include complexes of other metals (Figure A1-3b), we found that this correlation was lost.

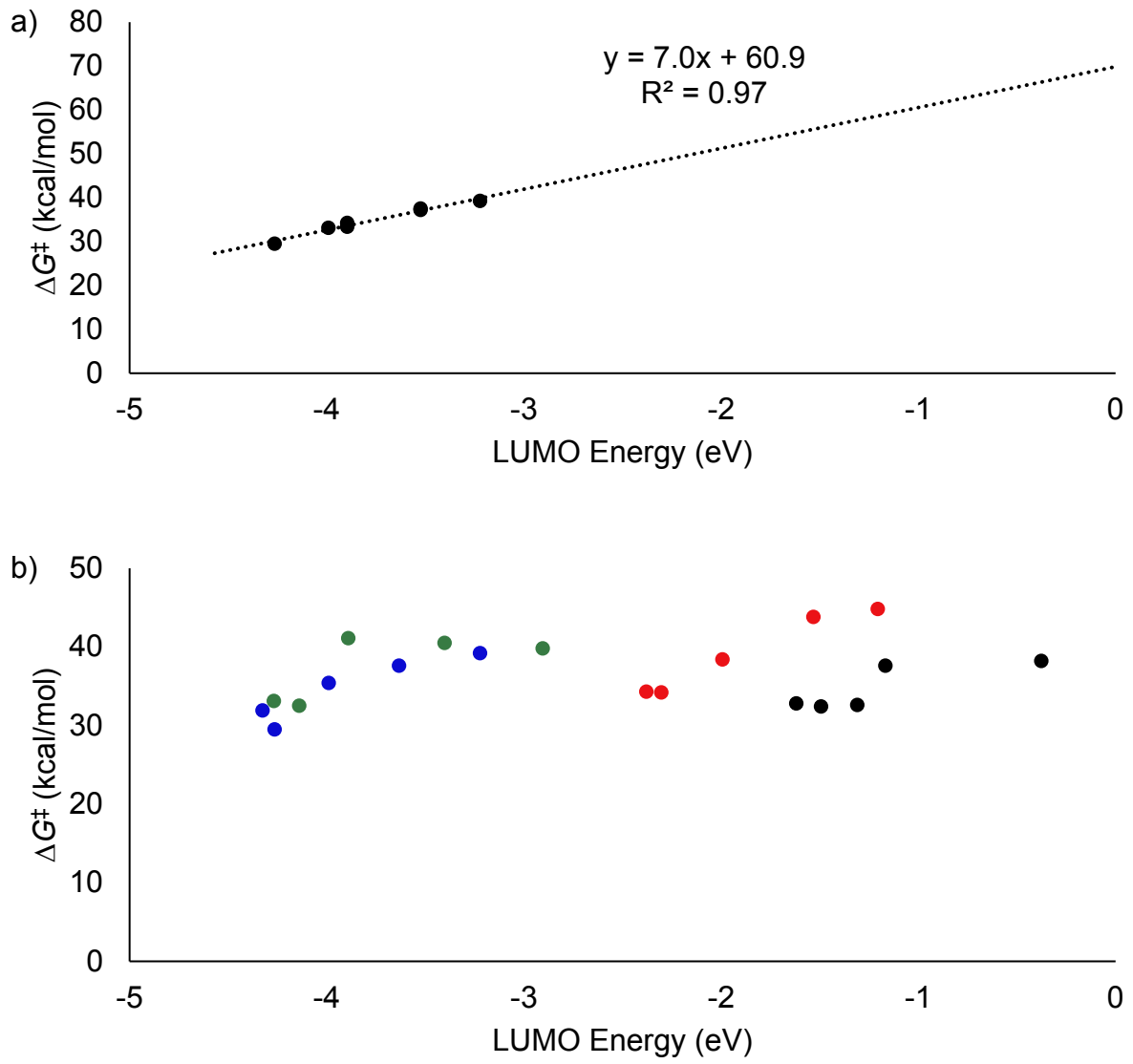

Figure A1-3. a) CH activation transition state energies for $Tl(X)_3$ with methane for X = nitrate, trifluoroacetate, difluoroacetate, monofluoroacetate, trichloroacetate, acetate, and methyl, plotted against LUMO energies. b) CH activation transition state energies for $M(X)_n$, M = In (n = 3), Sn (n = 4), Tl (n = 3), Pb (n = 4); X = trifluoroacetate, difluoroacetate, monofluoroacetate, trichloroacetate; plotted against LUMO energies.

A1.7 Structure and Charge Comparison for Internal and External Functionalization Pathways for $Tl(TFA)_3$

We found that of two possible functionalization pathways, external or internal, that external was favorable with the possible exception of the $Pb(TFA)_4$ system, for which an external transition state could not be found. Through an analysis of the structure and charges for the $Tl(TFA)_3$ system, we found that the higher energy of the internal functionalization transition states is explained, at least in part, by the greater degree to which the internal functionalization transition state structure contains a methyl cationic fragment. Figure A1-4a and b show structures for external and internal functionalization transition states. Figure A1-4c and d show how the electrostatic charge on the methyl group (as assigned by several schemes available in Gaussian 09) changes over the course of the intrinsic reaction coordinate. The plots show that in the transition state structure, the internal functionalization transition state carries is about 0.4 atomic charge units more positive than in the external functionalization transition state.

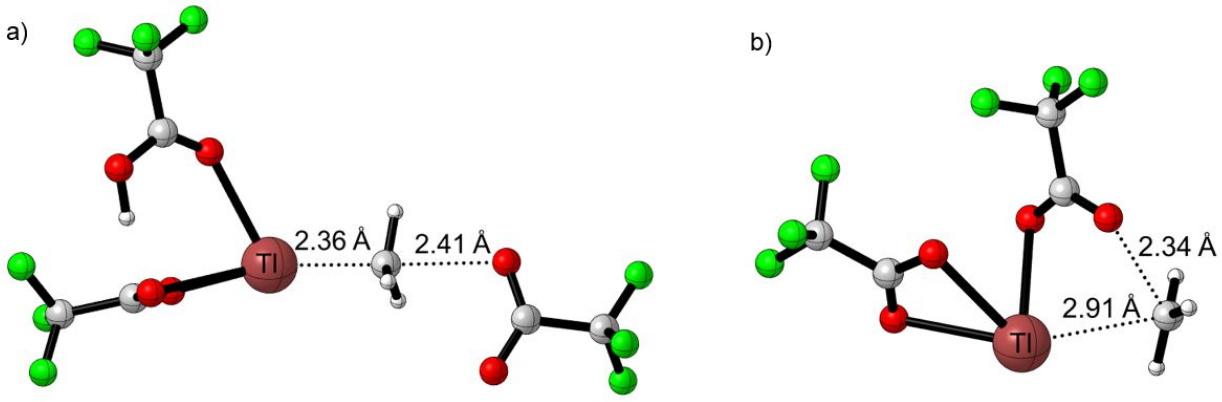

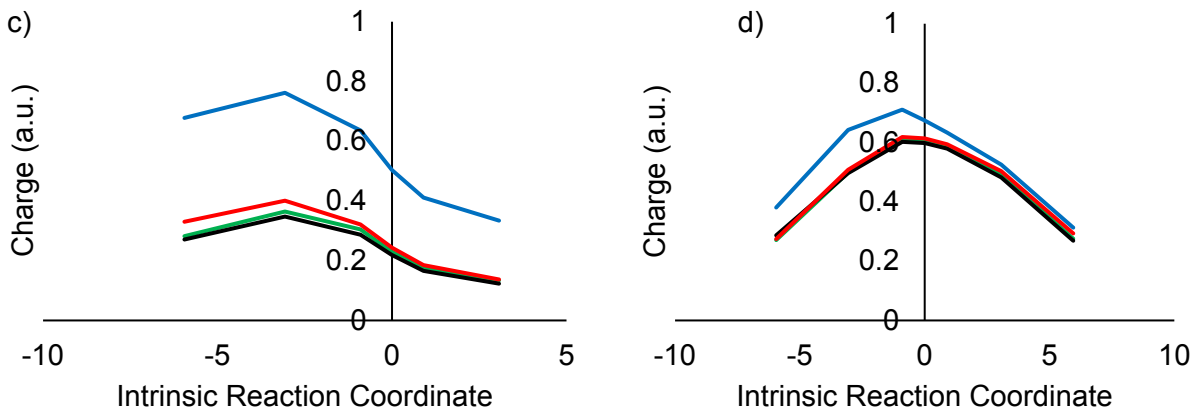

Figure A1-4. a) External functionalization transition state structure for Tl(TFA)3 system. b) Internal functionalization transition state structure for $Tl(TFA)_3$ system. c) charge assigned to the methyl group in the external functionalization transition state by the Mulliken (blue), HLYGAt (red), CHELPG (black), MKUFF (green) schemes as implemented in Gaussian 09. d) charge assigned to the methyl group in the internal functionalization transition state by the Mulliken (blue), HLYGAt (red), CHELPG (black), MKUFF (green) schemes as implemented in Gaussian 09. Note that for the plots in c) and d) the charge is given in units of elementary charge and the intrinsic reaction coordinate, which follows the gradient of the potential energy surface, is generally not assigned units.

A1.8 Potential Energy Surface for External Functionalization of $Pb(CH_3)(TFA)_2(TFAH)^+$

As part of our efforts to locate a transition state structure for the external functionalization of Pb-methyl intermediate, we performed a 2-dimensional relaxed potential energy surface scan by systematically varying the C-Pb and C-O distances in the structure shown in Scheme A1-3. The potential energy surface generated is shown in Figure A1-6. An examination of this surface shows that while it flattens out in the region of the expected transition state, there is no local maximum in either of the two critical internal coordinates. In Schemes A1-4 and A1-5, the energy required to form the methylcation (see Table A1-5 *vide supra*) was used as an estimate for the functionalization transition state energy, since it likely provides an upper bound.

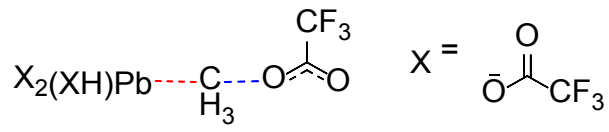

Scheme A1-2. Structure used to generate the potential surface shown in Figure A1-1. The lengths shown in red (Pb-C) and blue (C-O) were varied between 2.1 and 3.1 Å (Pb-C), and 1.5 and 2.5 Å (C-O).

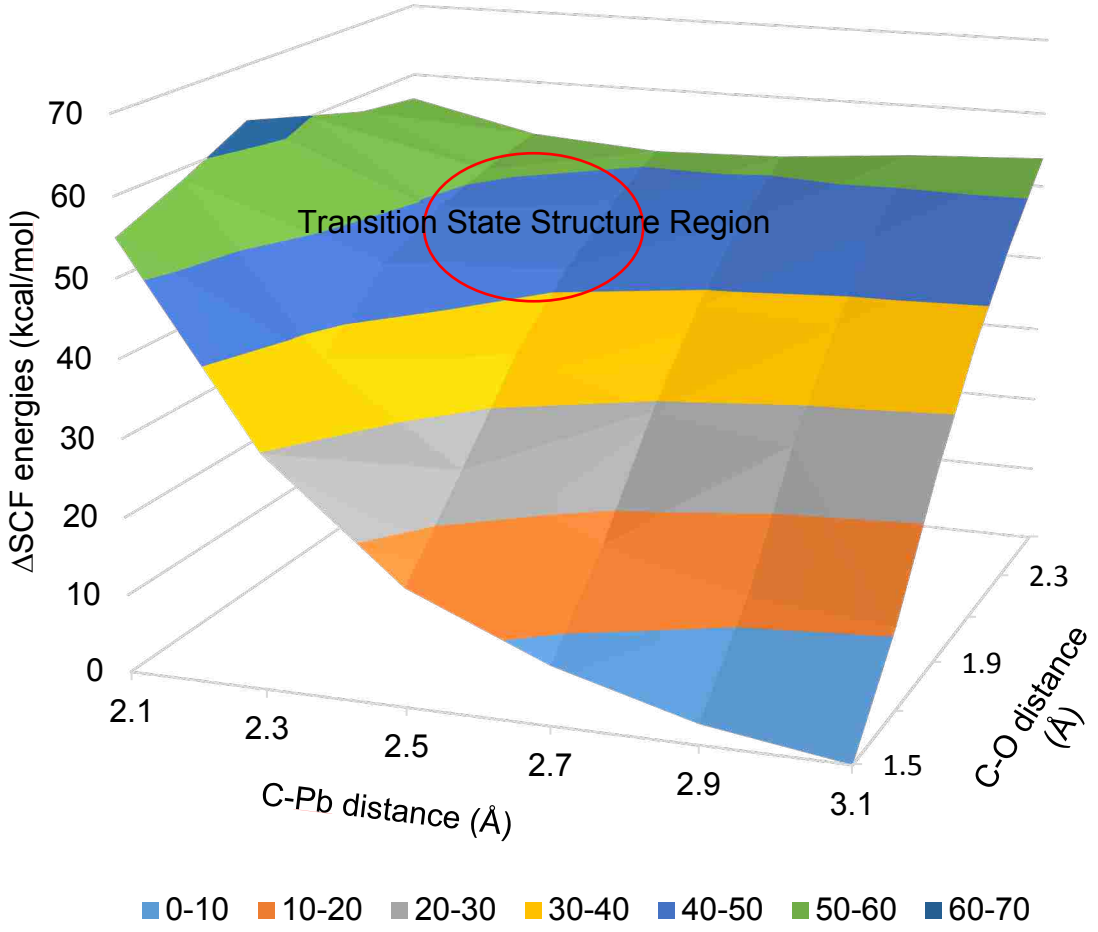

Figure A1-5. Potential surface generated by systematically varying the indicated C-Pb and C-O distances in the structure shown in Scheme A1-1. All other internal coordinates were allowed to relax freely. Energies were generated by DFT using M06//6-311G+(d,p)/LANL2DZDP.

A1.9 Further Analysis of Internal Functionalization Transition States

The internal functionalization transition state structures were more variable than the CH activation transition states for the various metals. We were able to find internal functionalization transition states for all systems studied. We further found that the energy of these structures correlates well with both the overall reaction energy and the bond heterolysis energy, defined here as the energy required to break the methylmetal complexes into methyl cation and metal anion fragments.

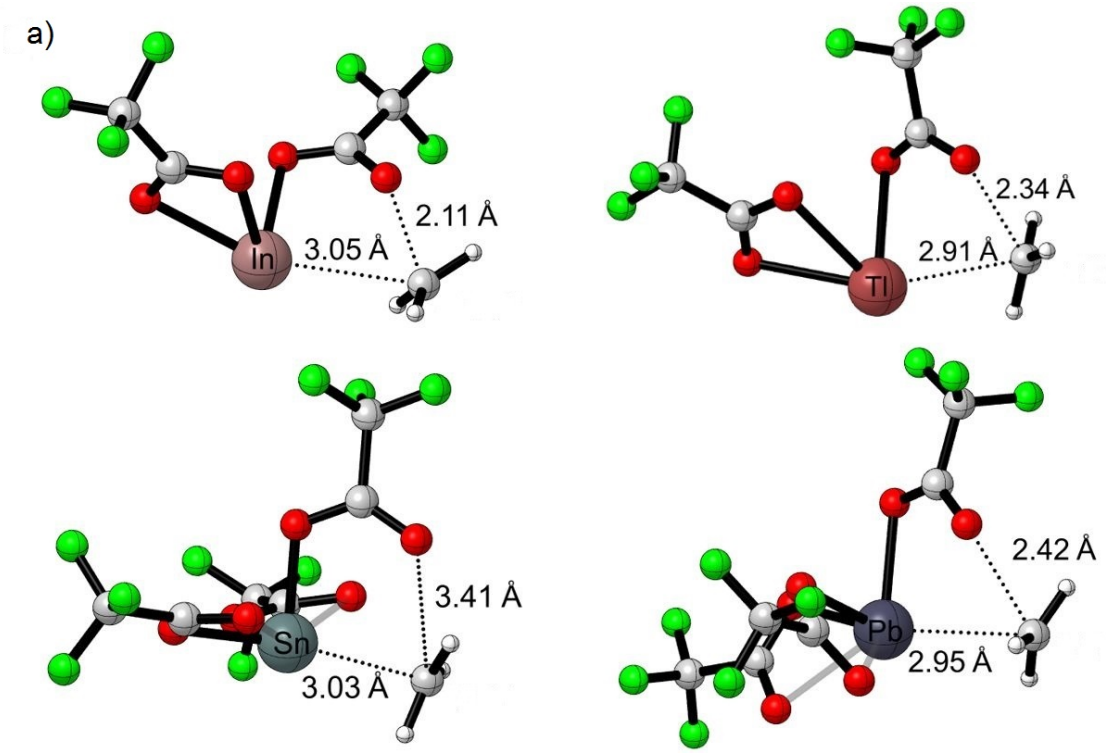

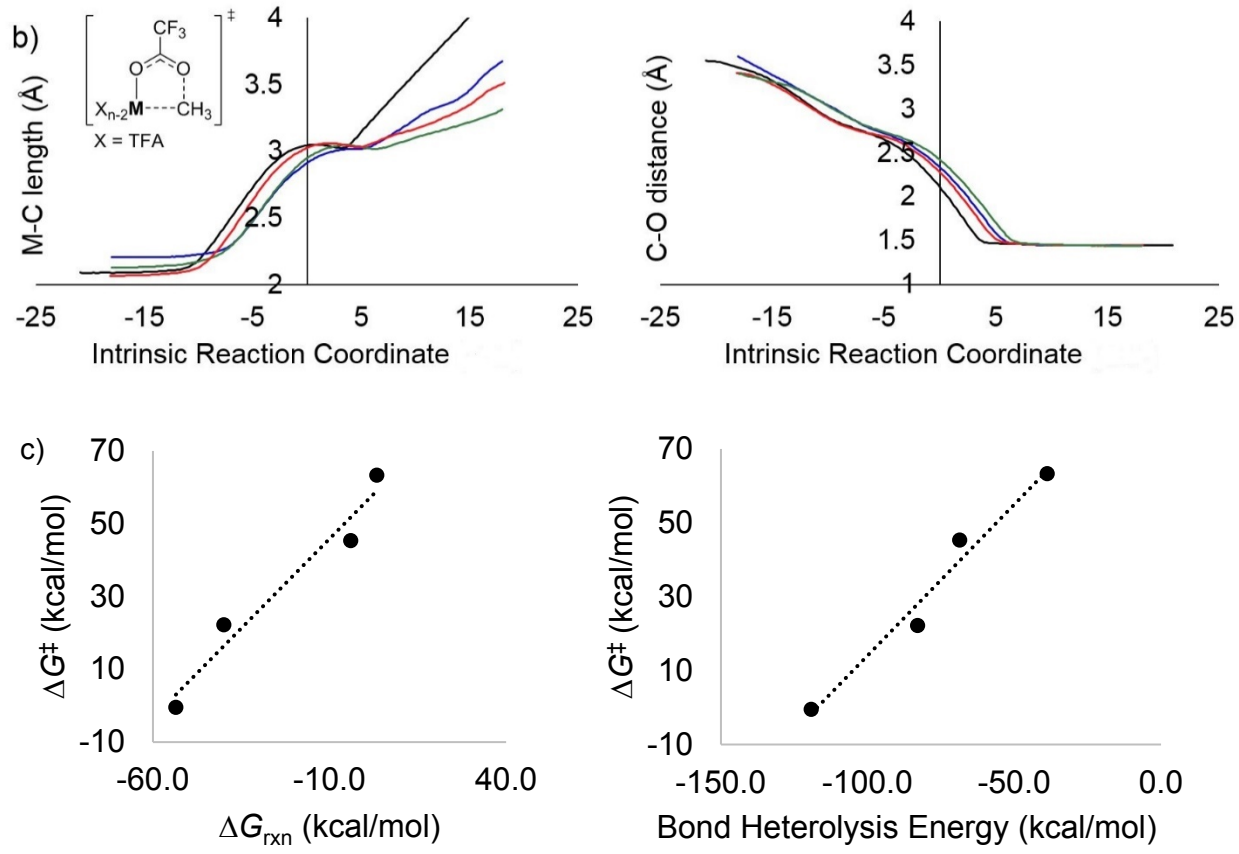

Figure A1-6. a) Internal functionalization transition-state geometries for metal-methyl structures. b) Bond length changes as a function of IRC. M = In (black), Tl (blue), Sn (red), Pb (green) c) Correlation plots for $\Delta G^{\ddagger}$ (internal functionalization) versus ΔG_{rxn} and $\Delta G^{\ddagger}$ versus metal-methyl bond heterolysis energy for the metal systems with trifluoroacetate ligands.

A1.10 Further Analysis of External Functionalization Transition States

On the other hand, the external functionalization transition states, whose structures with TFA ligands are shown in Scheme 2-4a, do not exhibit a fully broken methyl-metal bond in the transition state, and are less strongly correlated to the bond heterolysis energy (as shown in Figure 2-1 of Chapter 2). Not unexpectedly, the LUMO orbitals (Scheme 2-4b shows an example for the thallium trifluoroacetate system) of the metal cation fragment show that, in addition to containing

σ* character, they contain a significant amount of 5*s* or 6*s* character (depending on the metal involved).

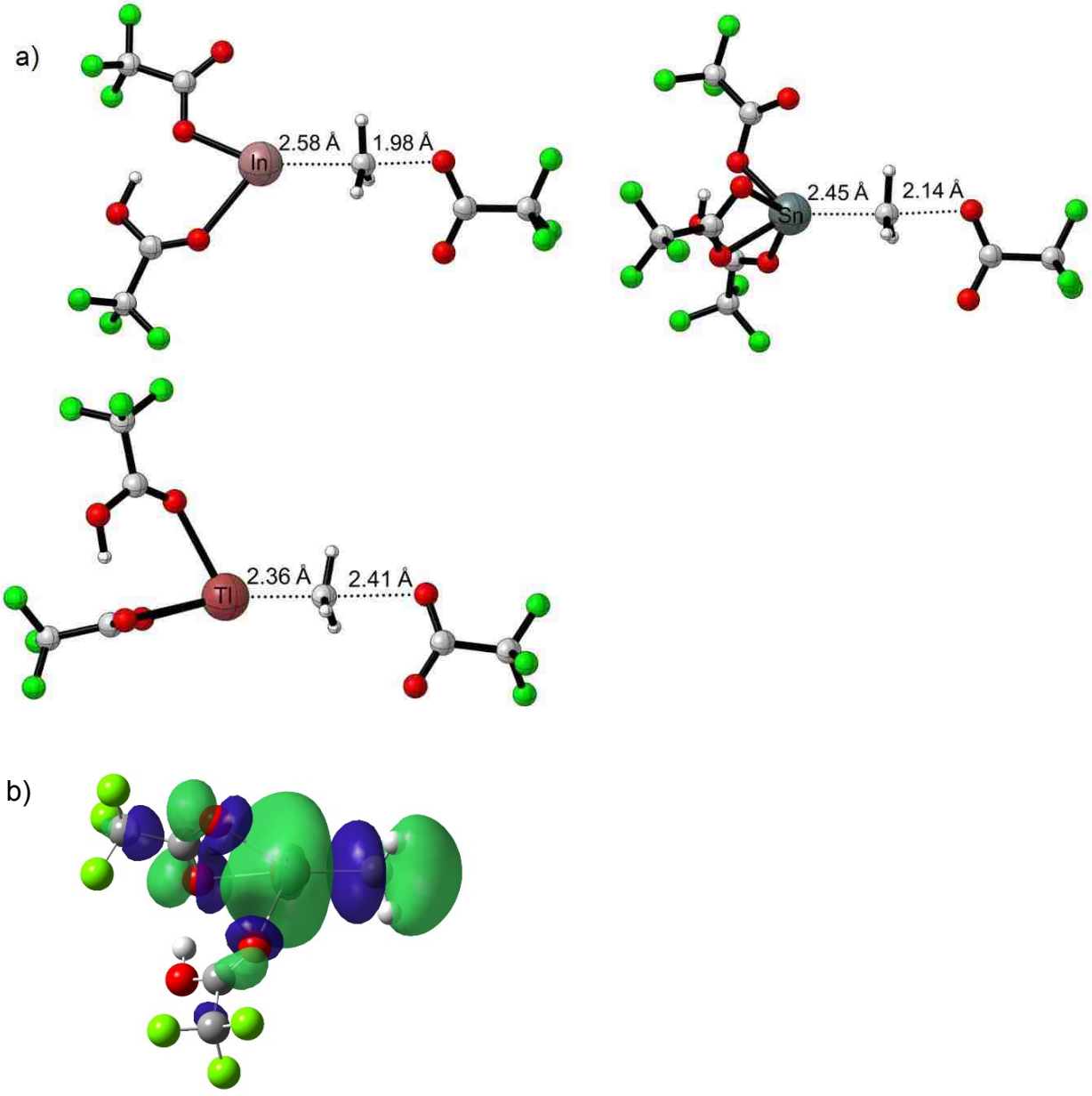

Scheme A1-3. a) Structures for In^{III}-Me, Sn^{IV}-Me, and Tl^{III}-Me external functionalization transition states with trifluoroacetate ligands; b) Visualization of the Kohn-Sham LUMO orbital for Tl^{III}-Me trifluoroacetate cation fragment.

A1.11 Data for Figure 2-1

The following reactions were used to compute the data in Table A1-6, which was used to generate Figure 2-1. Reaction A1-3 gives the bond heterolysis energy, Reaction A1-4 is the formation of products from the metal-methyl intermediate, and Reaction A1-5 is the formation of the external functionalization transition state. In these reactions, X = acetate (Ac), monofluoroacetate (MFA), difluoroacetate (DFA), trifluoroacetate (TFA); M = In (n = 3), Sn (n = 4), Tl (n = 3), Pb (n = 4).

Reaction A1-3: $M(X)_{n-1}(CH_3) \rightarrow [M(X)_{n-1}]^- + [CH_3]^+$

Reaction A1-4: $M(X)_{n-1}(CH_3) \rightarrow M(X)_{n-2} + CH_3X$

Reaction A1-5: $M(X)_{n-1}(CH_3) + XH \rightarrow [M(X)_{n-2}(XH)—CH_3—X]^‡$

Table A1-5. data used to generate Figure 2-1. All energies, except LUMO energies, are given in kcal/mol. The LUMO is for the species $[M(X)_{n-2}(XH)CH_3]^+$

		Reaction A1-3		**Reaction A1-4**		**Reaction A1-5**		**LUMO**
X	**M**	**Δ*H***	**Δ*G***	**Δ*H***	**Δ*G***	**Δ*H***	**Δ*G***	**(eV)**
Ac	**In**	110.1	99.0	27.9	12.9	43.9	55.2	-1.80
Ac	**Sn**	104.1	91.7	17.9	1.5	41.2	52.3	-1.78
Ac	**Tl**	75.0	63.1	-23.5	-36.3	20.9	34.0	-3.16
Ac	**Pb**	56.6	44.0	-34.8	-47.0	[a]	[a]	[a]
MFA	**In**	101.8	89.7	25.0	-15.3	38.0	48.9	-1.77
MFA	**Sn**	90.9	78.4	14.6	-27.8	35.9	45.3	[a]
MFA	**Tl**	71.6	56.9	-27.8	-41.4	14.9	25.2	-3.21
MFA	**Pb**	46.6	33.9	-37.0	-76.9	[a]	[a]	[a]

DFA	**In**	95.0	83.0	31.5	16.0	33.1	43.8	-1.89
DFA	**Sn**	77.1	64.7	3.0	-12.1	30.7	40.3	-2.45
DFA	**Tl**	62.2	49.8	-31.5	-46.1	16.3	26.8	-3.45
DFA	**Pb**	39.2	26.4	-34.5	-69.5	[a]	[a]	[a]
TFA	**In**	92.1	80.0	25.5	10.0	33.1	44.1	-2.01
TFA	**Sn**	73.5	63.7	10.5	-8.2	32.2	44.0	-2.70
TFA	**Tl**	62.0	47.9	-37.3	-52.4	13.1	24.7	-3.67
TFA	**Pb**	34.5	20.9	-41.8	-53.6	[a]	[a]	-3.94

[a]Value not computed.

A1.12 Effect of Adding Explicit Solvent Molecules in Functionalization Reaction

Since the external functionalization structures that we analyzed require that an acetate anion must be transferred to at least the second solvation shell, we endeavored to find external functionalization transition states that include solvent molecules interacting with the anion. For the external functionalization of thallium, the addition of one explicit solvent molecule solvating the incoming nucleophile changed the transition state energy from $\Delta G^{\ddagger}$ = 12.1 ($\Delta H^{\ddagger}$ = 2.7) to $\Delta G^{\ddagger}$ = 13.4 ($\Delta H^{\ddagger}$ = -6.9).

A1.13 References

1. Zhao Y.; D. G. Truhlar, D. G. *Theor. Chem. Acc.*, **2008,** *120,* 215-41.
2. Zhao, Y.; Truhlar, D. G. *J. Chem. Phys.*, **2006**, *125*, 194101: 1-18.
3. Chai, J.-D.; Head-Gordon, M. *Phys. Chem. Chem. Phys.*, **2008**, *10,* 6615-20.
4. a) (basis functions) Rappoport, D.; Furche, F. *J. Chem. Phys.* **2010**, *133*, 134105. b) (ECP for In, Sn, Tl, Pb) Metz, B.; Stoll, H.; Dolg, M. *J. Chem. Phys.*, **2000**, *113*, 2563-2569.

5. a) (basis functions for In,Sn,Tl,Pb) Peterson, K. A. *J. Chem. Phys.* **2003,** *119*, 11099. b) (basis functions for H,C,O,F) Dunning, Jr., T. H. *J. Chem. Phys.* **1989** *90*, 1007. c) (ECP for Tl) Metz, B., Schweizer, M.; Stoll, H.; Dolg, M.; Liu, W. *Theor. Chem. Acc.* **2000**, *104*, 22. d) (ECP for In, Sn, Pb) Metz, B.; Stoll, H.; Dolg, M. *J. Chem. Phys.* **2000**, *113*, 2563-2569.

6. *CRC handbook of chemistry and physics* (Online) **1999**, Electronic ed.

7. King, C. R.; Gustafson, S. J.; Black, B. R.; Butler, S. K.; Konnick, M. M.; Periana, R. A.; Hashiguchi, B. M.; Ess, D. H., *Organometallics* **2017**, *36* (1), 109-113.

8. a) Feller, D., *J. Comp. Chem.*, **1996**, *17*, 1571-1586. b) Schuchardt, K. L.; Didier, B. T.; Elsethagen, T.; Sun, L.; Gurumoorthi, V.; Chase, J.; Li, J.; Windus, T. L. *J. Chem. Inf. Model.*, **2007**, 47, 1045-1052.

9. Marenich, A. V.; Cramer, C. J.; Truhlar, D. G. *J. Phys. Chem. B*, **2009**, *113*, 6378-96.

10. Munz,D.; Meyer,D.; Strassner T. *Organometallics* **2013** *32*, 3469-3480.

Appendix 2: Supporting Information for Chapter 3

A2.1 $Tl(TFA)_3$ Structures

Structure 1A shown in figure A2-1 below is the $Tl(OAc)_3$ x-ray structure.[1] Change of acetate ligands to TFA ligands and optimization resulted in structure 1B. We also located low-energy structures 1C and 1D. The lowest energy structures are 1C and 1D that both have Cs symmetry. The enthalpies of these structures are within about 1.1 kcal/mol of each other. The energy of 1D was adopted as the ground state energy.

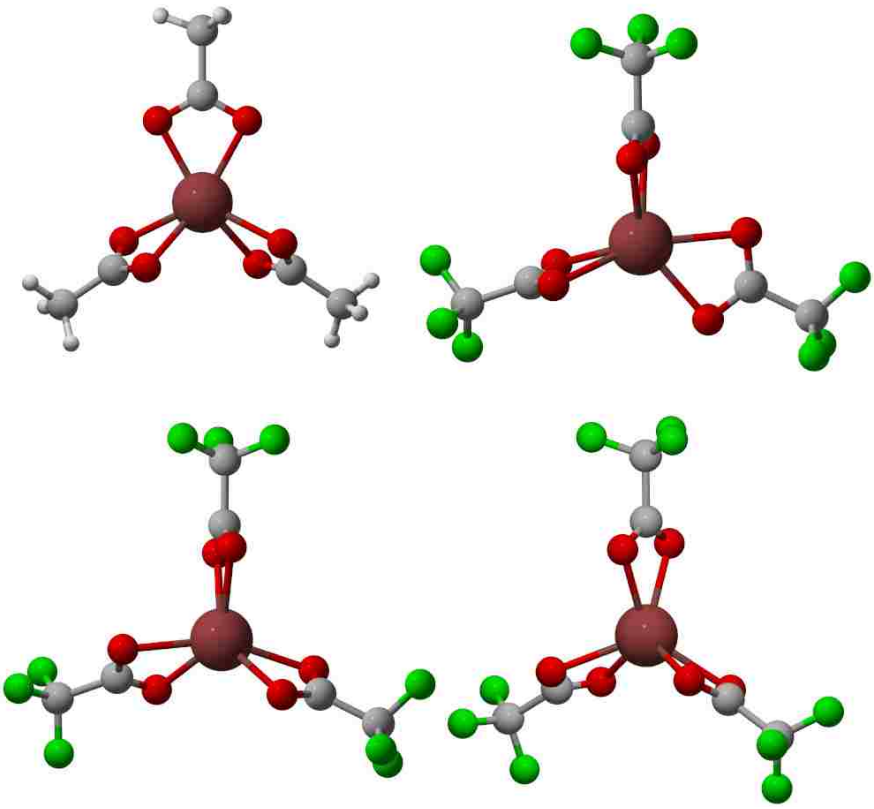

Figure A2-1. Top: $Tl(OAc)_3$ x-ray structure and the corresponding $Tl(TFA)_3$ structure optimized in implicit trifluoroacetic acid solvent. Bottom: Low-energy $Tl(TFA)_3$ structures.

A2.2 TD-DFT Results

The table below (table A2-1) lists the major M06 TDDFT excitations for π-complexes between benzene with $Tl(TFA)_3$, $[Tl(TFA)_2]^+$, and $[Tl(TFA)_2(TFAH)]^+$ (Figure A2-2). All excitations are qualitatively consistent with the spectra reported by Kochi, and therefore, this does not provide a way to distinguish between neutral and cationic species.[2]

Table A2-1. TDDFT results.

Structure	Excitation Wavelength	Oscillator Strength
$[Tl(TFA)_3(C_6H_6)]$	329	0.24
$[Tl(TFA)_2(C_6H_6)]^+$	345	0.30
$[Tl(TFA)_2(TFAH)(C_6H_6)]^+$	336	0.32

Figure A2-2 shows the Kohn-Sham orbitals that give rise to the TDDFT excitation at 329 nm for the $Tl(TFA)_3$-benzene π complex. These orbitals show the charge-transfer character from the arene to the Tl metal center. This wavelength is close to the wavelength reported by Kochi and Lau for charge transfer between benzene and Tl(III) in trifluoroacetic acid solvent.

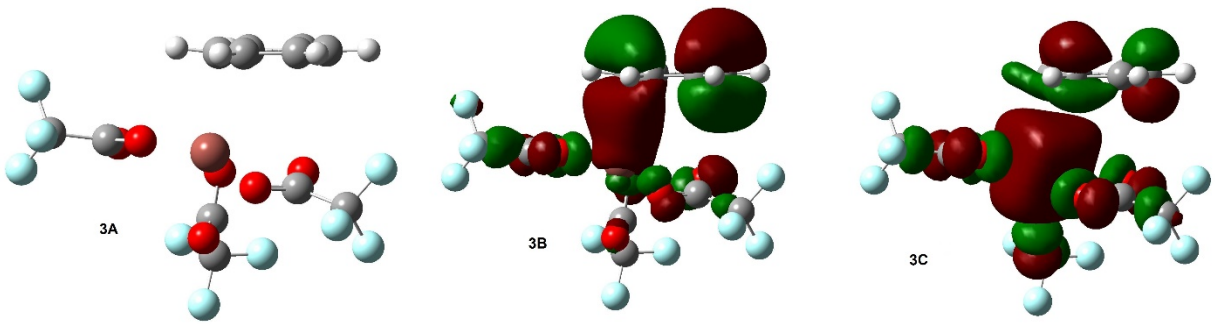

Figure A2-2. Relevant Kohn-Sham M06 orbitals for the 329 nm excitation.

A2.3 Benzene-Thallium Complexes

We examined the coordination modes of benzene to $Tl(TFA)_3$ by starting with structures in which benzene was constrained in various coordination modes. All of the internal coordinates of these structures were allowed to relax except for C-Tl distances, which were fixed to maintain the proper coordination mode. When all modes were allowed to relax, the preferred binding modes were found to be η^1 or η^2 (see Table A2-2 and Figure A2-3).

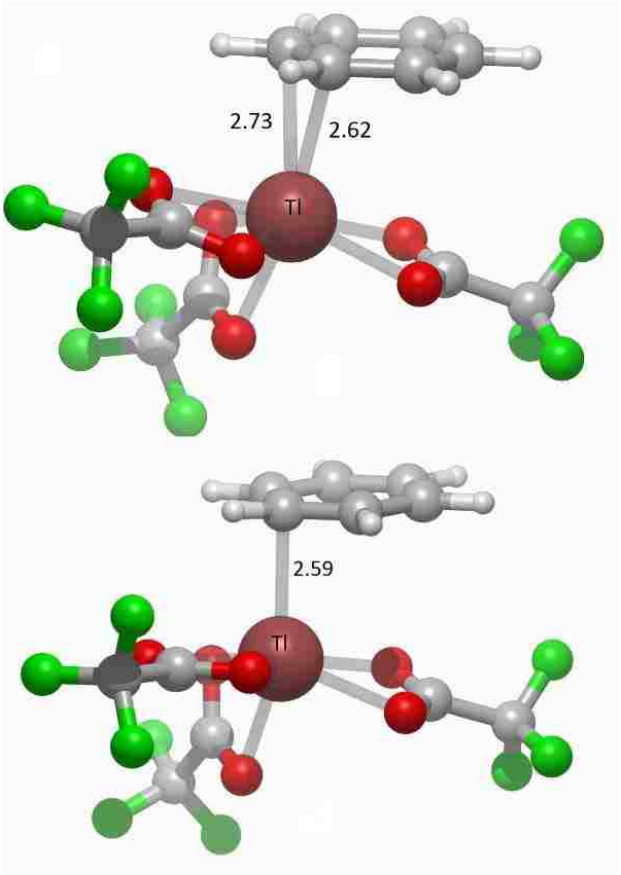

Figure A2-3. Representative π-complex structures of benzene and $Tl(TFA)_3$.

Table A2-2. Relative energies of various π-complexes of benzene and $Tl(TFA)_3$.

Constrained coordination mode	**constrained C-Tl distance (Å)**	**Relative[a] electronic energy[b] of constrained structure (kcal/mol)**	**Relative[a] electronic energy[b] of relaxed[c] structure (kcal/mol)**	**ΔH (ΔG)[a,d] of relaxed structure (kcal/mol)**
η^1	2.4	-14.2	-15.5	-12.6 (0.2)

η^2	2.5	-13.5	-15.4	-12.7 (0.2)
η^3	2.6	-1.9	-15.5	-12.5 (2.1)
η^4	2.7	0.5	-15.7	-12.9 (1.4)
η^5	2.8	-2.4	-15.6	-12.3 (2.5)
η^6	2.9	-4.8	-15.8	-13.2 (-0.4)

[a] Relative to separated benzene and $Tl(TFA)_3$.
[b] Electronic energy from M06/6-31+G(d,p)[LANL2DZdp] SMD solvent calculation.
[c] All structures relaxed to η^1 or η^2 complexes.
[d] Free energies and enthalpies from M06/def2-TZVPPD//M06/6-31+G(d,p)[LANL2DZdp] with SMD solvent.

A2.4 Note on CHelpG and ESP Charges

A value of ~0.35 e of charge transfer from benzene to Tl^{III} in $(TFA)_3Tl^{III}(\eta^1\text{-}C_6H_6)$ was based on CHelpG and ESP atomic charges. This value is the result of summing atomic charges on all atoms in the $Tl(TFA)_3$ fragment of the complex and summing the atomic charges on the benzene fragment in the complex. The atomic charges used are determined by fitting partial atomic charges to a molecular electrostatic potential. The CHelpG and ESP algorithms select points in a grid surrounding the Van der Waals surface.[3]

A2.5 Marcus Estimates

Marcus theory estimates the kinetic barrier for outer-sphere electron transfer (ET) by using reorganization energy, λ, and free energy change:

$$\Delta G^{\ddagger} = \frac{(\lambda + \Delta G^0)^2}{4\lambda}$$

The internal structural reorganization energy (λ_i) is given by[4,5]:

$$\lambda_i = E_R(R_P) - E_R(R_R) + E_P(R_R) - E_P(R_P)$$

The solvent/outersphere reorganization energy (λ_o) is given by:

$$\lambda_0 = (\Delta e)^2 \left(\frac{1}{2r_A} + \frac{1}{2r_b} + \frac{1}{r_{AB}}\right)\left(\frac{1}{\varepsilon_\infty} - \frac{1}{\varepsilon_0}\right)$$

For trifluoroacetic acid, $\varepsilon_\infty = 1.285$ and $\varepsilon_o = 8.42$.

For ET between $Tl(TFA)_3$ and arenes, the Marcus estimates reported in the main text ignore solvent reorganization energy. For benzene this estimate is $\Delta G^{\ddagger}$ = 36.8 kcal/mol. For pentamethylbenzene, $\Delta G^{\ddagger}$ = 13.5 kcal/mol. Estimate of the solvent reorganization energy is dependent on the radii. For intermolecular distances of less than 10 Å, including the solvent reorganization energy increases the overall $\Delta G^{\ddagger}$ by less than 5 kcal/mol.

A2.6 Explanation of Activation Energies

Relative arene thallation rates (Figure 3-2 in Chapter 3) were converted into free energy differences ($\Delta\Delta G^{\ddagger}$) using standard transition state theory with cancellation of pre-exponential factors, i.e.: $k_r = k_1/k_2 = e^{-(\Delta G_1^{\ddagger} - \Delta G_2^{\ddagger})/RT}$. For regioselectivity data reported by McKillop[6] and Olah[7], free energy differences were derived from product ratios by assuming that the reported product ratio is equal to a ratio of rate constants.

A2.7 Potential Energy Landscapes

Figure A2-4 shows the energy landscape where the Tl-C bond has been scanned from the distance in the π complex (~2.6 Å) to the distance in the thallation product (~2.2 Å), and the Tl-C-H angle has been scanned from that in the π complex (~90°) to an approximately tetrahedral angle (~110°) that might be expected in a Wheland intermediate. Importantly, all Wheland-type structures are much higher in energy than the η^1 π-complex structure. Additionally, scans of the same coordinates as shown in Scheme 3-3 were performed using energies from the ωB97xd, M06L, and B3LYP functionals, and the M06 functional with an IEF-PCM solvent model. PES's from these scans are qualitatively identical to the one shown in Scheme 3-3.

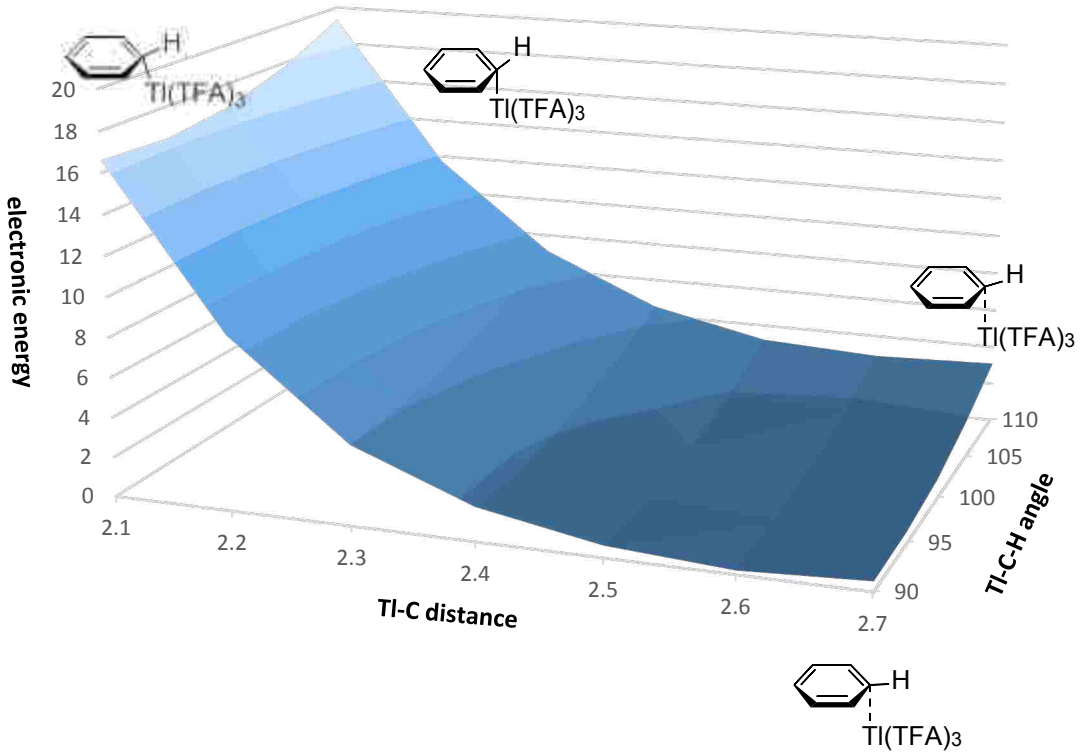

Figure A2-4. PES generated by scanning the Tl-C distance in increments of 0.1 Å and scanning the Tl-C-H (θ) angle in increments of 5°. All other coordinates were unconstrained. (kcal/mol)

The following plots (Chart A2-1) of different combinations of bond lengths and angles also indicate that a Wheland-type structure is not an energy minimum.

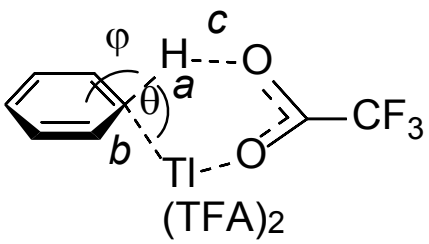

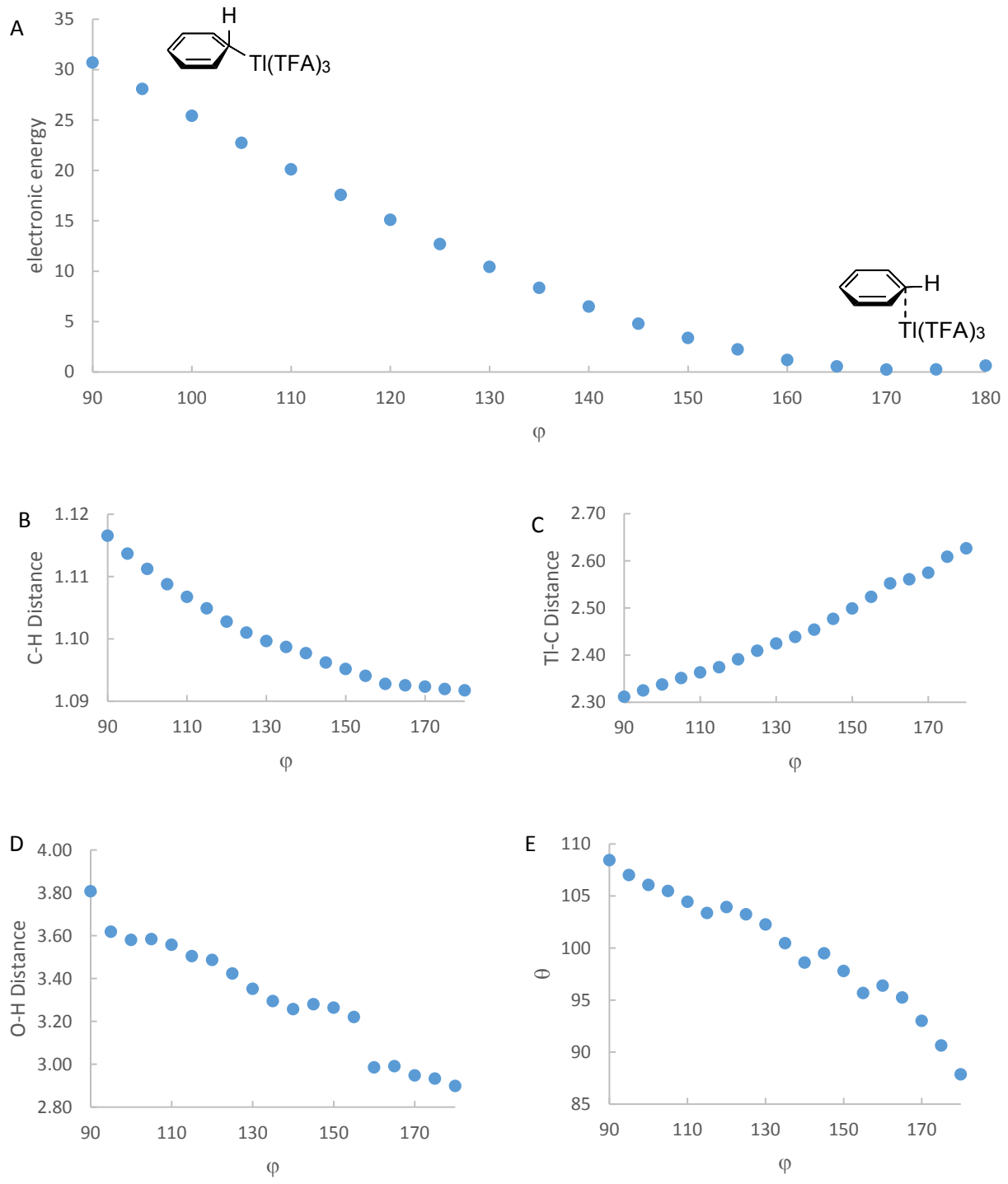

Figure A2-5. A) Potential energy scan generated by varying the angle between the reactive hydrogen atom and the arene plane (φ) in increments of 5°, while all other internal coordinates were allowed to relax. The same angle is ~173°in the π complex structure, and ~128° in the C-H activation transition state structure.

B) Plot showing the effect of φ on C-H distance (*a*). C) Plot showing the effect of φ on Tl-C distance (*b*). D) Plot showing the effect of φ on O-H distance (*c*). E) Plot showing the effect of φ on Tl-C-H angle (θ).

A2.8 Arene Coordination versus Activation Barriers

Plot A in Figure A2-5 shows the free energies for π-complex formation between methyl-substituted arenes and $Tl(TFA)_3$. Plot B shows the trend in $\Delta G^{\ddagger}$ for **TS1** of chapter 3 plotted against the π-complex, which is relatively constant.

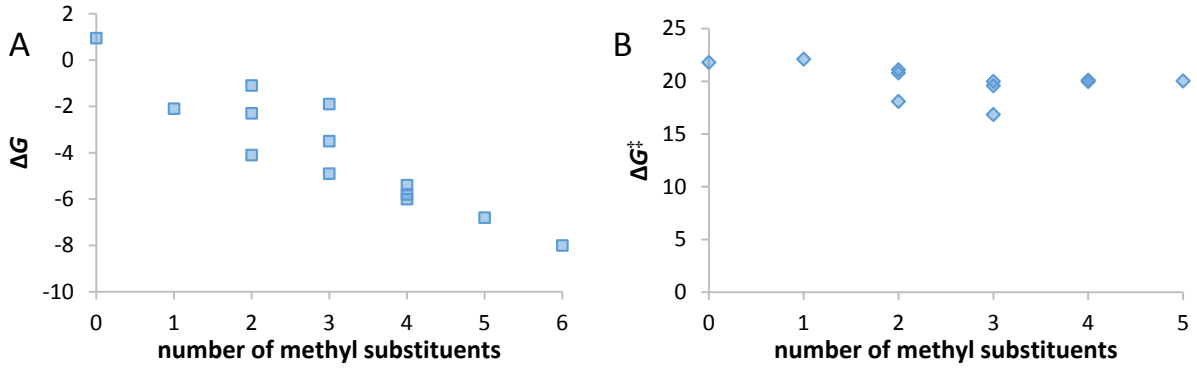

Figure A2-6. (kcal/mol)

A2.9 References

1. Faggiani, R.; Brown, I. D. *Acta Crystallogr., Sect. B* **1978**, *B34*, 2845-2846.
2. W. Lau, J. K. Kochi, *J. Am. Chem. Soc.* **1986**, *108*, 6720-6732.
3. Cramer, C. J., "Charge Distribution and Spectroscopic Properties" in Essentials of computational chemistry: Theories and models. 2nd ed.; J. Wiley: Hoboken, NJ, **2004**.
4. Anderson, G. M.; Cameron, I.; Murphy, J. A.; Tuttle, T., *RSC Adv.* **2016**, *6*, 11335-11343.
5. Guo, Y.; Wang, W.; Shao, R.; Yin, S., *Comp. Theor. Chem.* **2015**, *1057*, 67-73.
6. E. C. Taylor, F. Kienzle, R. L. Robey, A. McKillop, J. D. Hunt, *J. Am. Chem. Soc.* **1971**, *93*, 4845-4850.
7. G. A, Olah, I. Hashimoto, H. C. Lin, *Proc. Natl. Acad. Sci. U.S.A.* **1977**, *74*, 4121.